



concentration of surfactant. Two types of microPCMs were then synthesized using emulsion techniques, and the synthesis parameters were manipulated to enhance the thermophysical properties of the microPCMs and suppress the supercooling of encapsulated PCMs. To enhance their thermal conductivity, microPCMs with large latent heat capacity and suppressed supercooling were coated with a metal layer. The as-synthesized phase changeable and thermal conductive microPCMs were applied in a heat transfer fluid to enhance the heat transfer performance.

This work was focused on the following aspects. The first aspect is the thermophysical properties of colloidal solutions, such as thermal conductivity, at low surfactant concentrations around the critical micelle concentration (CMC). The second aspect is the synthesis of microPCMs in the colloidal systems with solid-solid PCM neopentyl glycol and liquid-solid PCM n-octadecane as the core material. The third aspect is the enhancement of thermophysical properties (e.g., heat capacity, supercooling,) of the microPCMs, which was achieved by manipulating the parameters of the environment of chemical synthesis. The fourth aspect is the elevation of the thermophysical properties of the microPCMs, such as thermal conductivity, after the microPCMs were produced. The fifth and final aspect is the applications of the as-produced microPCMs, e.g., to enhance the heat transfer in bulk solid materials for latent heat storage and heat transfer fluids for heat dissipation with the aid of microPCMs, with or without coating with thermal conductive silver layer.

MICROENCAPSULATED PHASE CHANGE MATERIALS FOR ENERGY STORAGE  
AND THERMAL MANAGEMENT

By

Fangyu Cao

Dissertation submitted to the Faculty of the Graduate School of the  
University of Maryland, College Park, in partial fulfillment  
of the requirements for the degree of  
**Doctor of Philosophy**  
2014

Advisory Committee:

Dr. Bao Yang, Chair/Advisor  
Dr. Ashwani K. Gupta  
Dr. Yunho Hwang  
Dr. John Cumings  
Dr. Oded Rabin  
Dr. Chunsheng Wang (Dean's Representative)

© Copyright by  
Fangyu Cao  
2014

## **Dedication**

To my fiancée Yifan.

## **Acknowledgements**

I would like to thank my advisor, Dr. Bao Yang for his guidance, support, and encouragement during my study at the University of Maryland. I would also like to thank Dr. Ashwani Gupta, Dr. Yunho Hwang, Dr. John Cumings, Dr. Oded Rabin, and Dr. Chunsheng Wang for serving on my dissertation committee, reviewing my dissertation and giving me valuable suggestions.

I would like to thank Dr. Xinan Liu for aiding me during thermal conductivity measurements, Dr. Jiajun Xu for helping me conduct SANS experiments, Dr. John Lawler and Dr. Paul Kalinowski for the help in conducting the fluid heat transfer measurement, Dr. Zenghu Han and Dr. Von Cresce for aiding me during the DSC experiments, Dr. Li-Chung Lai for helping me during SEM and TEM imaging, and Dr. Juchen Guo for the help during the sample preparation of various polymers. I also would like to thank Mr. Dale Huang, Mr. Zhi Yang, and Dr. Yanting Luo for valuable discussions on my research.

# Table of Contents

ABSTRACT.....	i
Dedication.....	ii
Acknowledgements.....	iii
Table of Contents.....	iv
List of Tables .....	x
List of Figures.....	xi
Nomenclature.....	xvii
Acronyms and Abbreviations.....	xvii
Symbols.....	xviii
Greek Letters .....	xix
Subscripts .....	xx
Chapter 1.    Introduction.....	1
1.1    Thermal Management with Phase Change Materials .....	1
1.1.1 Methods for Energy Storage.....	1
1.1.2 Thermophysical Energy Storage .....	3
1.1.3 Phase Change Materials and Supercooling Phenomena.....	4
1.1.4 Thermochemical Energy Storage .....	7
1.2    Microencapsulated Phase Change Materials .....	9
1.2.1 Background of MicroPCMs .....	10
1.2.2 Synthesis Approaches of MicroPCMs .....	11
1.2.3 Applications of MicroPCMs .....	13
1.3    Motivation and Rationales of Improving MicroPCMs.....	14
1.3.1 Motivation to Improve the Fluidic Heat Transfer Performance.....	14

1.3.2 Rationales behind MicroPCMs .....	15
1.4 Objectives of Research .....	19
1.4.1 Production Methods of MicroPCMs .....	19
1.4.2 Supercooling Suppression .....	20
1.4.3 Thermal Conductivity Enhancement .....	21
1.4.4 Applications in Heat Transfer Fluids .....	22
Chapter 2. Literature Review .....	24
2.1 Ternary Colloidal Systems of Surfactant-Water-Oil .....	24
2.1.1 Amphiphile / Surfactant .....	25
2.1.2 Emulsion.....	28
2.1.3 Microemulsion .....	29
2.1.4 Thermodynamic Stability of Emulsion and Microemulsion Systems .....	32
2.2 Synthesis of MicroPCMs in Colloidal Systems .....	34
2.2.1 Sol-Gel Process for MicroPCM Synthesis .....	35
2.2.2 In-Situ Polymerization .....	36
2.3 Supercooling Suppression of MicroPCMs .....	38
2.4 Enhancement of Thermal Conductivity for MicroPCMs .....	41
2.5 Applications of MicroPCMs in Heat Transfer Fluids.....	41
2.6 Summary.....	42
Chapter 3. Characterization Methods for Structures and Properties .....	44
3.1 Determination of Elemental Composition and Molecular Structure .....	44
3.1.1 Energy Dispersive X-Ray Spectroscopy .....	44
3.1.2 Fourier Transform Infrared Spectroscopy .....	45
3.2 Investigation of Morphology and Crystal Structure .....	45
3.2.1 Small-Angle Neutron Scattering .....	45

3.2.2	Scanning Electronic Microscopy.....	46
3.2.3	Transmission Electronic Microscopy.....	46
3.3	Characterization of Thermophysical Properties .....	47
3.3.1	Differential Scanning Calorimetry .....	47
3.3.2	Thermal Conductivity Measurement of Solid Materials.....	48
3.4	Measurements of Thermophysical Properties of Fluids .....	49
3.4.1	Viscosity.....	49
3.4.2	Stability .....	49
3.4.3	Thermal Conductivity Measurement of Fluids.....	49
Chapter 4.	Thermal Conductivity of Dilute Colloidal Solutions.....	52
4.1	Introduction .....	52
4.2	Preparation of the Colloidal Solutions.....	54
4.3	Determination of the CMC with SANS.....	55
4.4	Thermal Conductivity of the Colloidal Solutions.....	56
4.5	Analysis of the Minimum Thermal Conductivity at the CMC .....	57
4.6	Summary.....	60
Chapter 5.	Microencapsulated Solid-Solid PCMs.....	61
5.1	Introduction .....	61
5.2	Synthesis of the Solid-Solid MicroPCMs.....	62
5.2.1	Materials.....	62
5.2.2	Synthesis of the MicroPCMs.....	63
5.3	Characterization of the Solid-Solid MicroPCMs.....	64
5.3.1	Morphologies of the MicroPCMs.....	64
5.3.2	Chemical Composition of the MicroPCMs .....	65
5.3.3	Phase Change Behavior the MicroPCMs .....	67

5.3.4	Specific Heat of Fluids Containing the MicroPCMs.....	69
5.3.5	Viscosity of PAO Fluids Containing the MicroPCMs .....	71
5.4	Summary.....	72
Chapter 6.	Microencapsulated Liquid-Solid PCMs.....	73
6.1	Introduction .....	73
6.2	Synthesis of the Liquid-Solid MicroPCMs .....	75
6.2.1	The Selection of PCM Material.....	75
6.2.2	The Selection of Shell Material.....	75
6.2.3	Synthesis of the Paraffin/MFR MicroPCMs .....	77
6.3	Characterization of the Liquid-Solid MicroPCMs .....	81
6.3.1	Morphology and Microstructure of the MicroPCMs.....	81
6.3.2	Thermophysical Properties of the MicroPCMs.....	82
6.4	Supercooling Suppression by Shell Optimization.....	84
6.4.1	Effect of the Ratio of Precursors .....	84
6.4.2	Effect of pH Values in the Pre-Polymerization Process.....	87
6.4.3	Effect of Acid Concentration in the Polymerization Process.....	88
6.4.4	Specific Heat Elevation by Supercooling Suppression .....	89
6.5	Summary.....	90
Chapter 7.	Thermal Conductivity Enhancement of the MicroPCMs .....	92
7.1	Introduction .....	92
7.2	Preparation of the Thermal Conductive PCM-Ag Microcapsules.....	93
7.3	Characterization of the PCM-Ag Powder and Pellets .....	95
7.3.1	Morphology of the PCM-Ag Particles .....	95
7.3.2	Thermal Conductivity Analysis of the PCM-Ag Pellets .....	96
7.3.3	Trade-off between Heat Capacity and Thermal Conductivity .....	98

7.4	Summary.....	99
Chapter 8.	Application of MicroPCMs in Heat Transfer Fluids .....	100
8.1	Introduction .....	100
8.2	Characterization of the Phase Changeable Heat Transfer Fluids .....	101
8.2.1	Materials.....	101
8.2.2	Thermal Conductivity and Viscosity of the Heat Transfer Fluids.....	102
8.2.3	Specific Heat Capacity of the Heat Transfer Fluids.....	104
8.3	Fluidic and Heat Transfer Performance of the Heat Transfer Fluids .....	105
8.3.1	Pressure Drop .....	107
8.3.2	Heat Transfer Results .....	109
8.3.3	Stability of the Heat Transfer Fluids .....	112
8.4	Uncertainty Analysis .....	114
8.5	Summary.....	115
Chapter 9.	Conclusions and Future Directions.....	116
9.1	Conclusions of Experimental and Analytical Work .....	116
9.2	Limitation and Future Works .....	118
9.3	Contribution.....	120
9.3.1	Journal Papers .....	120
9.3.2	Book Chapters .....	121
9.3.3	Patent Applications .....	121
Appendices.....		122
A.1	Techniques for Characterization of Heat Transfer Fluids .....	122
A.1.1	The $3\omega$ – Wire Method.....	122
A.1.2	Differential Scanning Calorimetry .....	124
A.2	Theories of Thermal Conductivity .....	125

A.2.1 Effective Medium Theory (EMT): the Maxwell Model.....	125
A.2.2 Hashin-Shtrikman (H-S) Model .....	127
Bibliography .....	128

## List of Tables

Table 1-1. List of selected phase change materials and their thermophysical and chemical properties [4-6, 17-20]. M.P.: melting point; hPCM: latent heat of fusion; $\rho_s$ : density of PCM in solid phase; ks: thermal conductivity in solid phase. ....	5
Table 1-2. Summary of materials for thermochemical energy storage [7, 28-31, 33, 37, 38]..	9
Table 2-1. Summary of supercooling suppression of microPCMs based on paraffin.....	40
Table 5-1. Pros and cons of three types of liquid-solid and solid-solid PCMs [4-6, 10, 18, 48, 57, 58, 192-195].....	61
Table 5-2. Index of the absorption peaks in the FT-IR spectra of silica [198-200], NPG [199, 201, 202], and the NPG/silica microPCMs.....	66
Table 6-1. List of melamine-resin-shelled microPCM samples [65].....	79
Table 8-1. Properties the latent functional heat transfer fluids with addition of microPCMs and PCM-Ag particles [67, 226]. Thermal Conductivity, Viscosity, and Latent Heat Capacity of the heat transfer fluids were all measured from a 20 wt% suspension of the PCMs in PAO. ....	103
Table 8-2. Uncertainties of the measured and calculated properties of the fluids [226].....	114

## List of Figures

Figure 1-1. Types of energy storage and typical techniques [1-3].....	2
Figure 1-2. Thermal energy storage in forms of sensible heat and latent heat. ....	4
Figure 1-3. A demonstration of an open sorption storage system based on dehumidification with liquid desiccant during water vapor sorption (thermal energy discharge) and desorption (thermal energy storage). ....	8
Figure 1-4. Micro-structures of microPCMs.....	11
Figure 2-1. Photos of samples of (from left to right) immiscible oil-water mixture, oil-in-water emulsion, and microemulsion. ....	25
Figure 2-2. Basic structure of micelles in O/W emulsion and reverse micelles in W/O emulsions. A typical surfactant molecule is schemed with an orange colored hydrophobic tail and a gray-blue colored hydrophilic head [108]. ....	26
Figure 2-3. Different structures inside micelle systems [122]. ....	30
Figure 2-4: Winsor structure models of microemulsions [125]. ....	31
Figure 2-5. Schematic diagram of Gibbs free energy of microemulsion and nanoemulsion systems compared to the phase separated state. The emulsion/microemulsion and the separated oil-water phases are transferable with an activation energy $\Delta G^*$ . ....	32
Figure 2-6. The general process of in-situ polymerization for the synthesis of microPCMs. ....	37
Figure 3-1. The steady state method for thermal conductivity measurement based on the Fourier heat transfer equation. ....	48
Figure 4-1. Schematic representation of surfactant concentration dependence of several physical properties for surfactant solutions, including surface tension, fluorescence, electrical conductivity, etc. The red solid line corresponds to the curve of thermal conductivity based on this research, in which a minimum occurs at the CMC [169]. ....	53

Figure 4-2. Molecular structure of AOT [178]. .....	55
Figure 4-3. SANS scattering spectra from AOT/n-octane solutions. The curves are labeled by the mass fraction of AOT in the solution. Insert: average radius of the solvated AOT molecules or micelles versus mass concentration of AOT in n-octane.....	55
Figure 4-4. Dimensionless thermal conductivity change $k_{AOT/octane}$ versus surfactant mass fraction in the AOT/n-octane solutions, where $k_{AOT/octane} = k_{solution} - k_{octane} / k_{octane}$ . Inserted is the expansion of selected part of the curve.....	56
Figure 4-5. Dimensionless thermal conductivity change $k_{AOT/PAO}$ versus surfactant mass fraction in the AOT/PAO solutions, where $k_{AOT/PAO} = k_{solution} - k_{PAO} / k_{PAO}$ . Inserted is the expansion of selected part of the curve. ....	57
Figure 4-6. Scheme of thermal conductivity of AOT/n-octane solution at AOT concentration a) below and b) above the CMC. The red arrows show the direction of heat flow. ....	59
Figure 5-1. Molecular structure of neopentyl glycol (NPG) [178]. .....	63
Figure 5-2. Molecular structure of tetraethyl orthosilicate (TEOS) [178]. .....	63
Figure 5-3. Molecular structure of polysorbate 80 (Tween <sup>®</sup> 80) [178]. .....	63
Figure 5-4. Images of as-synthesized microcapsules of NPG in silica shell: a) SEM, c) TEM, and wrinkled silica shell after NPG is removed: b) SEM, and d) TEM. Inserted in a) is a histogram of the particle size distribution from 0 to 4 $\mu\text{m}$ [66]. .....	65
Figure 5-5. FT-IR spectra of sample a) silica, b) NPG, and c) microcapsules as synthesized [66]. .....	66
Figure 5-6. DSC heating and cooling curves of samples, a) pure, bulk NPG, b) dispersions of 20 wt% pure NPG micro-particles without encapsulation in PAO, and c) dispersions of 20 wt% NPG/silica microPCMs in PAO [66]. .....	68

Figure 5-7. Estimated effective specific heat capacity of the PAO-based heat transfer fluids with pure NPG particles and NPG/silica microPCMs in various $x_{PCM}$ [66].	70
Figure 5-8. Dynamic viscosities of pure PAO and the dispersion of 20 wt% microcapsules in PAO vs temperature [66].	71
Figure 6-1. Molecular structure of melamine and formaldehyde, and the polymeric structure of melamine-formaldehyde resin. Two types of bridges (etheric bridge (-C-O-C-) and methylene bridge (-C-), as circled) in the figure can be formed between two melamine rings, depending on the reaction environment of the polymerization [206].	76
Figure 6-2. The chemical route for the fabrication of paraffin/MFR microPCMs [65].	77
Figure 6-3. SEM and TEM images of the microcapsules with octadecane encapsulated in the melamine-formaldehyde resin shell [65]. a) SEM image of the sample produced with 50 g/L SDS. b) SEM and TEM (inserted) image of the sample prepared with 10 g/L SDS. The insert is a TEM image showing the shell thickness. c) micro/nanoparticles in filtrate.	80
Figure 6-4. DSC curves of a) pure n-octadecane and b) powder of sample MC01, the “raw” microPCMs before suppression of supercooling [65]. Heating and cooling rate of the DSC is 10 °C/min.	82
Figure 6-5. Complete DSC curve of sample MC01, dispersed in PAO [65]. Significant supercooling can be found in the curve, from which a degree of supercooling of 13.6 °C can be calculated.	83
Figure 6-6. DSC freezing curves of samples MC01-04 with various F:M ratio in precursors [65]. Curves are shifted along Y axis.	84
Figure 6-7. a) DSC freezing curves of samples MC04-09 [65]. Curves are shifted along Y axis. b) Relative latent heat of phase transition peaks for various pH values of pre-condensation solution [65].	87

Figure 6-8. a) DSC freezing curves of samples MC10-15 [65]. Curves are shifted along Y axis. b) Relative latent heat of phase transition peaks for various HAc concentrations in the emulsion [65]. .....	89
Figure 6-9. Calculation of apparent specific heat increase by the latent heat of microPCMs corresponding to different operation temperature ranges [65]. The horizontal line shows the increase at an operation temperature range of 13.6 °C. ....	90
Figure 7-1. A strategy of producing thermal responsive energy storage materials. Step a): microencapsulation of paraffin in MFR shell; b): coating microPCMs with thermal conductive layer; and c): tableting of the powder of thermal conductive microPCMs to bulk TES material. ....	93
Figure 7-2. Sample PCM-Ag pellets with various thickness and composition. The diameter of each cylindrical pellets is ½ inch.....	94
Figure 7-3. SEM images of the PCM-Ag microcapsules [67, 226]. a) and b) typical SEM images of the PCM-Ag particles with different silver ratio. c) and d) elemental (Ag and C, correspondingly) distribution in the PCM-Ag microcapsule. ....	95
Figure 7-4. Experimental and theoretical thermal conductivities of different models of metal-PCM composites with different metal ratio. ....	96
Figure 7-5. The change of thermal conductivity and heat capacity of silver-coated PCM-Ag versus the mass and volume fraction of silver. ....	98
Figure 8-1. The strategy of synthesizing PCM-Ags by coating microPCMs with thin coating of silver [67].....	101
Figure 8-2. SEM and EDS of the microPCMs with rough silver coating and smooth silver coating [67]. The EDS yellow images show the distribution of silver on the surface of the above microPCM, and the red ones correspond to that of carbon. ....	102

Figure 8-3. Average specific heat enhancement of the latent functional thermal fluids with addition of 20 wt% PCM-Ag3 microcapsules [67].....	104
Figure 8-4. Schematic diagram (left) of the experimental set-up for heat transfer measurement and a photograph of the microchannel (right) with size [67, 226].....	105
Figure 8-5. Photograph of the experimental setup for heat transfer measurement [226].....	106
Figure 8-6. Pressure drop (Y axis) in the cold plate at different inlet temperatures versus flow rate (X axis) of the heat transfer fluids comparison of PAO, PAO with 20 wt% paraffin/MFR microPCMs(without silver coating), and PAO with 20 wt% PCM-Ag3 [67, 226]. .....	107
Figure 8-7. Friction factor (Y axis) versus Reynolds number (X axis) comparison of PAO, PAO with 20 wt% paraffin/MFR microPCMs(without silver coating), and PAO with 20 wt% PCM-Ag3 [67, 226]. .....	108
Figure 8-8. Heat transfer coefficient (Y axis) versus flow rate (X axis) of the heat transfer fluids PAO, PAO with 20 wt% paraffin/MFR microPCMs(without silver coating), and PAO with 20 wt% PCM-Ag3 at different inlet temperatures [67, 226].....	110
Figure 8-9. Nusselt number (Y axis) versus Reynolds number (X axis) of PAO, PAO with 20 wt% paraffin/MFR microPCMs(without silver coating), and PAO with 20 wt% PCM-Ag3 at different inlet temperatures [67, 226]. .....	111
Figure 8-10. Thermal resistance comparison at different inlet temperatures of PAO, PAO with 20 wt% paraffin/MFR microPCMs(without silver coating), and PAO with 20 wt% PCM-Ag3 [226]. .....	112
Figure 8-11. Extended duration pressure drop of a PCM-Ag3 enhanced fluid [226].....	113
Figure 8-12. Pressure drop in idel experiments with 10 minutes break [226]. .....	113
Figure A-9-1. Setup of the 3 $\omega$ - wire method for thermal conductivity measurement of heat transfer fluids [167].....	122

Figure A-9-2. Scheme of the setup of a DSC cell [236]. ..... 125

# Nomenclature

## Acronyms and Abbreviations

BF	base fluid
CMC	critical micelle concentration
DSC	differential scanning calorimetry
EDS	energy dispersive spectroscopy
F:M	formaldehyde : melamine ratio in mass
FT-IR	Fourier transform infrared spectroscopy
HLB	hydrophilic-lipophilic balance
HTF	heat transfer fluid
LFTF	latent functional thermal fluid
LHS	latent heat storage
M. P.	melting point
MFR	melamine-formaldehyde resin; melamine resin
microPCM	microencapsulated phase change material
NPG	neopentyl glycol
O/W	oil in water
PCM	phase change material
PAO	poly-alpha olefin
SDS	sodium dodecyl sulfate
SEM	scanning electron microscopy

SHS	sensible heat storage
TEM	transmission electron microscopy
TEOS	tetraethyl orthosilicate
TES	thermal energy storage
W/O	water in oil

### **Symbols**

<i>A</i>	area
<i>B</i>	coefficient of homogeneous nucleation
<i>C</i>	specific heat
<i>c</i>	concentration
<i>D</i>	diameter
<i>G</i>	gas substance
<i>h</i>	heat transfer coefficient
<i>I</i>	intensity
<i>J</i>	probability of homogeneous nucleation.
<i>K</i>	constant
<i>k</i>	thermal conductivity
<i>L</i>	length
<i>l</i>	length
<i>M</i>	molar mass
<i>m</i>	mass

$Nu$	Nusselt number
$O$	oil phase
$P$	pumping power; packing parameter
$p$	pressure
$Q$	heat, i.e. thermal energy
$q$	heat storage per mass
$R$	thermal resistance
$Re$	Reynolds number
$S$	surfactant
$T$	temperature
$W$	aqueous phase
$wt$	weight ratio
$V$	molar volume
$v$	volume
$\dot{V}$	volumetric flow rate
$x$	fraction, percentage

### **Greek Letters**

$\alpha$	liquid-rotator phase transition peak of n-octadecane on DSC
$\beta$	rotator-solid phase transition peak of n-octadecane on DSC
$\gamma$	supercooled liquid-solid phase transition peak on DSC
$\lambda$	wavelength
$\rho$	density

$\theta$	angle
$\mu$	viscosity
$\omega$	frequency
$\Delta G$	Gibbs free energy
$\Delta H$	latent heat of phase transition
$\Delta h$	latent heat of phase transition per mass
$\Delta P$	pressure drop
$\Delta T$	temperature difference

### **Subscripts**

$C$	cubic phase of neopentyl glycol
$f$	fraction model
$in$	inlet flow
$M$	monoclinic phase of neopentyl glycol
$MC$	microchannel
$m$	melting
$max$	maximum
$l$	liquid
$O$	oil phase
$p$	particle
$R$	thermal resistance
$S$	surfactant
$SC$	supercooling

<i>s</i>	solid phase
<i>suf</i>	surface of the heater
<i>W</i>	water or other aqueous phase

# Chapter 1. Introduction

## ***1.1 Thermal Management with Phase Change Materials***

Human civilizations have always coupled with the utilization of various sources of energy. From the invention of fire and the storage of ice thousands years ago, the growth and development of our society has been well witnessed, as well as the serious impacts of damage and pollution back to nature such as the overuse of natural resources and greenhouse emissions due to the huge demand for energy. The continuous increase of greenhouse gas emissions and the climb in fuel prices are the main driving forces behind efforts to utilize various sources of energy more effectively. Hence, a rational strategy for the sustainability of energy system is necessary, particularly through advanced technologies and systems of energy storage and thermal management.

### **1.1.1 Methods for Energy Storage**

Researchers worldwide continue to search of new and renewable energy sources that are cost efficient to energy store and utilize. One of the options is to develop energy storage devices, which are as important as developing new sources of energy. It is a great challenge to store energy in suitable forms that can be converted into the required form conveniently. Energy storage leads to saving of fossil fuels and makes more cost effective utilization, not only reducing the mismatch between supply and demand but also improving the performance of energy systems and playing an important role in energy conservation [1, 2]. To date, various technologies have been developed and applied in energy storage from grid scale to portable devices [1-3]. These technologies are summarized in Figure 1-1. Among the technologies, thermal energy storage (TES) is an important technology with widespread applications which

may contribute to avoiding environmental problems and increasing the efficiency of energy utilization.

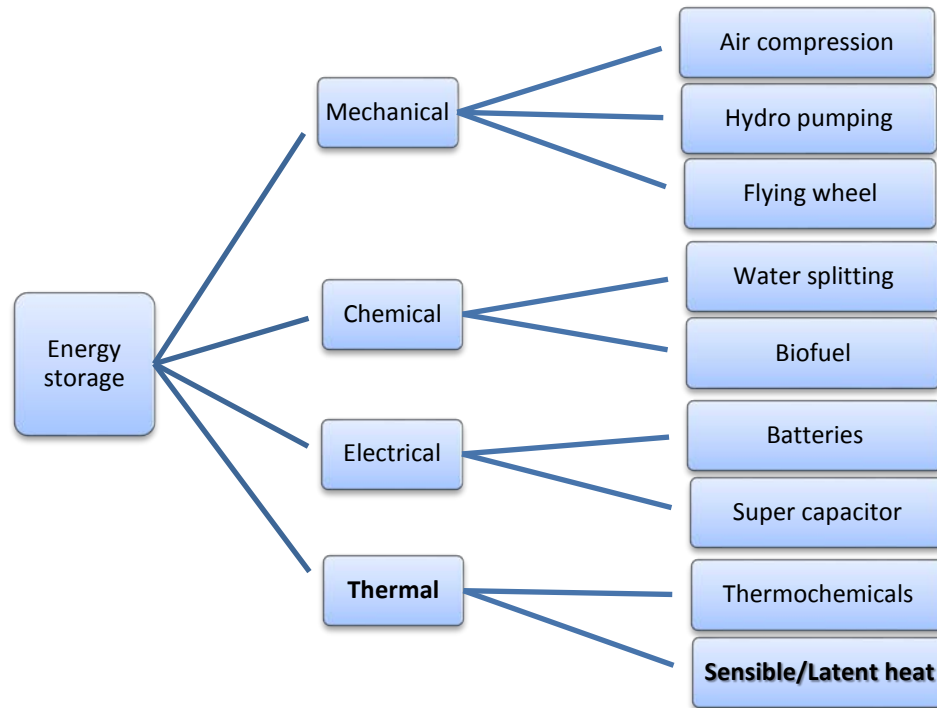


Figure 1-1. Types of energy storage and typical techniques [1-3].

TES is a type of technologies that temporarily holds thermal energy for later utilization. It is a significant technology in systems involving multiple energy resources as it can make the operation more efficient, particularly by bridging periods when energy is supplied and periods when it is demanded [4-7]. Thus, TES may play an important role in increasing the contribution of various types of energy, especially the renewables such as solar energy and wind, on the energy map of the world.

Various TES technologies are available for different applications. The selection of a TES system for a particular application depends on factors including storage duration, temperature requirements, thermal insulation, storage capacity, available space, economics, etc. Generally speaking, thermal energy can be stored using either physical or chemical processes, described correspondingly as follows.

### 1.1.2 Thermophysical Energy Storage

Two main types of thermophysical energy storage are commercially available: sensible heat storage (SHS) and latent heat storage (LHS). The most common way of heat storage is as sensible heat, in which heat transfer to the medium of sensible heat storage leads to a phase transition temperature increase directly. The heat storage medium can be water, brine, rock, soil, etc. Heat storage in a SHS medium  $Q_{SHS}$  is related to the mass and temperature increase of the storage medium when heating from  $T_{low}$  to  $T_{high}$ :

$$Q_{SHS} = m_{SHS} \int_{T_{low}}^{T_{high}} C_{p,SHS} dT \quad (\text{Equation 1-1})$$

where  $m_{SHS}$  and  $C_{p,SHS}$  are the mass and specific heat capacity of the storage material.

LHS systems store energy through phase transition, mainly liquid-solid and/or solid-solid phase transition processes in cyclic applications. A substance used for LHS is called a phase change material (PCM), examples of which are water/ice, salt hydrates, paraffin, polyalcohols, etc. Latent heat stored in a LHS medium  $Q_{LHS}$  is related to the mass of the storage medium:

$$Q_{LHS} = m_{PCM} \Delta h_{PCM} \quad (\text{Equation 1-2})$$

where  $m_{PCM}$  and  $h_{PCM}$  are the mass and enthalpy of phase transition of the PCM. Due to the high enthalpy change during phase transition, thermal energy stored in a LHS unit is usually greater than a SHS one in similar scale. In addition, heat is transferred to or from the LHS medium while the temperature remains at the phase transition point during a phase transition, thus LHS can also be used for thermal management to maintain a small temperature range.

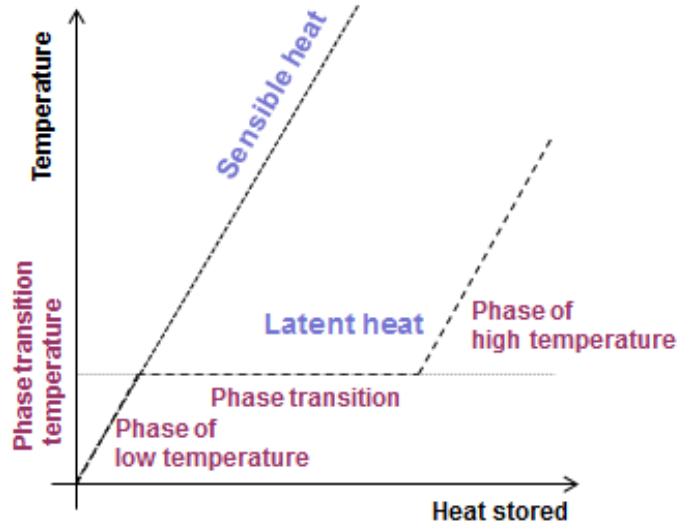


Figure 1-2. Thermal energy storage in forms of sensible heat and latent heat.

### 1.1.3 Phase Change Materials and Supercooling Phenomena

As described above, a PCM is a substance with a high latent heat and is thus capable to store and release large amounts of thermal energy during phase transition at a certain temperature. Thermal energy is absorbed or released in the form of latent heat when the material changes from one solid phase to another or from solid to liquid and vice versa. Shown in Table 1-1, a lot of candidates have been discovered and used as PCMs, most of which are inorganic salt hydrates such as  $\text{CaCl}_2 \cdot 6\text{H}_2\text{O}$  (i.e., Glauber's salt),  $\text{Na}_2\text{SO}_4 \cdot 10\text{H}_2\text{O}$ ,  $\text{Na}_2\text{HPO}_4 \cdot 12\text{H}_2\text{O}$ , etc.; organic PCMs such as paraffin and fatty acids; and solid state PCMs including neopentyl glycol (NPG) and pentaerythritol [4-6, 8-12].

It should be pointed out that all of the commercially available PCMs with reasonably high latent heat are poor thermal conductors. Thermal conductivity of salt hydrates is in the scale of 1 W/mk, and that of paraffin is even lower at around 0.2~0.3 W/mK. In practical applications, lots of efforts have been doing to increase the thermal conductivity of PCMs while maintaining the rest thermophysical properties [13-16].

Table 1-1. List of selected phase change materials and their thermophysical and chemical properties [4-6, 17-20]. M.P.: melting point;  $h_{PCM}$ : latent heat of fusion;  $\rho_s$ : density of PCM in solid phase;  $k_s$ : thermal conductivity in solid phase.

Material		M.P. (°C)	$h_{PCM}$ (J/g)	$\rho_s$ (g/cm <sup>3</sup> )	$k_s$ (W/mk)		
Inorganics	Salt hydrate and eutectics	CaCl <sub>2</sub> · 6H <sub>2</sub> O	29	192	1.8	1.0	
		NaSO <sub>4</sub> · 10H <sub>2</sub> O	30	254	1.5	-	
		NaS <sub>2</sub> O <sub>3</sub> · 5H <sub>2</sub> O	48	209	1.6	-	
		Ba(OH) <sub>2</sub> · 8H <sub>2</sub> O	78	280	2.1	0.65	
	Other inorganic	H <sub>2</sub> O	0	333	0.91	2.2	
		Ga	30	80	5.9	40.6	
		In	157	29	7.3	81.8	
		NaNO <sub>3</sub>	307	199	2.3	-	
	Organics	Paraffin	n-Dodecane, C <sub>12</sub> H <sub>26</sub>	-12	216	0.75	0.21
			n-Octadecane, C <sub>18</sub> H <sub>38</sub>	27	245	0.81	0.35
n-Eicosane, C <sub>20</sub> H <sub>42</sub>			37	247	0.91	0.21	
n-Octacosane, C <sub>28</sub> H <sub>58</sub>			61	255	0.91	0.21	
Fatty acid		Caprylic acid	16	148	1.1	-	
		Capric acid	32	153	0.88	-	
		Palmitic acid	64	185	0.85	-	
Poly-alcohol		Neopentyl glycol	43	130	1.1	0.43	
		Pentaerythritol	185	303	1.4	-	

The history of using PCMs is quite old. Before the modern mechanical refrigeration system was introduced, people used ice to cool food, medicine, and the indoor environment. It is recorded that ice blocks collected in the winter from frozen lakes or rivers were stored in “ice houses” and used for relieving summer heat thousands of years ago in ancient China [21]. More recently, ice was also placed in duct systems to cool and dehumidify warm air blown by fan in the early nineteenth century [7]. Also in the 1800s, The “cold accumulators”, a type of flat metal container filled with frozen low-melting point salt mixtures, were used to transport dairy products and other perishables [22]. Since the 1970s, long-term and large-scale storage of latent heat by utilizing ice and snow has involved the seasonal storage of winter’s cold for

use in cooling buildings during summer in areas of long cold winters with brief hot summers, such as in Canada and Sweden [7]. As an example, the Sundsvall Hospital snow cooling plant, located in central Sweden where the annual mean temperature is 6 °C, is designed for a cooling load of 1,000 MWh, which requires 30,000 m<sup>3</sup> of snow [23].

In addition to cold storage, PCMs have also been used for various heating applications over the last century. They have been utilized in ‘hot bottle’ applications for direct warmth to the human body, hot plates, coffee pots, etc. Salt hydrates such as hydrated sodium acetate, sodium sulfate, and magnesium nitrate were commonly employed, though their performance was erratic in the beginning because of the supercooling [24-27]. The major thrust of the research of PCMs in last century including building heating and cooling, energy efficiency, off-peak electricity storage, and thermal control with PCMs in NASA’s space program. In daily life, an example of industrial products of PCMs is hand warmers using sodium acetate trihydrate (CH<sub>3</sub>COONa·3H<sub>2</sub>O) to store thermal energy.

In large-scale industrial application of PCMs, supercooling, i.e., the melting-freezing hysteresis, remains a major obstacle. Supercooling, also known as undercooling or subcooling, is the process of lowering the temperature of a PCM below its phase transition point without the occurrence of phase transition phenomenon. For example, water below its melting point crystallizes in the ideal condition or in the presence of seed crystals or nuclei. Lacking any such nuclei in real conditions, the supercooled water can remain liquid at a temperature much lower than the melting point until homogeneous nucleation occurs.

Taking liquid-solid phase change as an example, the supercooling  $\Delta T_{sc}$  of a PCM can be evaluated by

$$\Delta T_{sc} = T_m - T_f \quad (\text{Equation 1-3})$$

where  $T_m$  and  $T_f$  are the measured melting and freezing temperature, respectively. In purpose of utilizing the latent heat of PCMs, the operation temperature should at least cover the range from  $T_m$  to  $T_f$  so as to complete the cycle of phase transition, i.e., the hot temperature limit  $T_{high} > T_m$ , and the cold temperature limit  $T_{low} < T_f$ . Giving an operation temperature range  $\Delta T = T_{high} - T_{low}$ , having both LHS and SHS considered, the overall thermal energy stored in a PCM  $Q_{PCM}$  can be estimated by

$$Q_{PCM} = m_{PCM} \left[ \Delta h_{PCM} + \int_{T_{low}}^{T_f} C_{p,s} dT + \int_{T_m}^{T_{high}} C_{p,l} dT \right] \quad (\text{Equation 1-4})$$

while the apparent specific heat of PCMs  $C_{PCM}$  can be estimated by

$$C_{PCM} = \left[ \Delta h_{PCM} + \int_{T_{low}}^{T_f} C_{p,s} dT + \int_{T_m}^{T_{high}} C_{p,l} dT \right] / \Delta T \quad (\text{Equation 1-5})$$

in which  $\Delta h_{PCM}$ ,  $C_{p,s}$ , and  $C_{p,l}$  are the latent heat of fusion in the condition of supercooling, specific heat of solid phase, and that of liquid phase of the corresponding PCM. Due to the large latent heat of PCMs in a reasonably small operation temperature range,  $\Delta h_{PCM}$  is usually the major contribution to the apparent specific heat  $C_{PCM}$ . Based on Equation 1-5, the larger  $\Delta T$ , the smaller is the elevation of  $C_{PCM}$  owing to latent heat. As  $\Delta T > \Delta T_{sc}$  is required, an increase of  $\Delta T_{sc}$  can dramatically affect the ability of thermal energy storage and management of the PCMs.

#### 1.1.4 Thermochemical Energy Storage

Different from thermophysical energy storage that involves no chemical process, thermochemical energy storage uses chemisorption or solid-gas chemical reaction to store and release thermal energy. In thermochemical energy storage, energy can be stored with a dissociation reaction and recovered with the reverse chemical reaction of combination.

Generally speaking, there are two types of thermochemical energy storage that have been discussed and demonstrated in literature, in which sorption processes and thermochemical reactions are involved correspondingly. Sorption, including adsorption and absorption, is considered thermochemical as they are based on surface and/or solution chemistry processes. An adsorption process occurs when a gas accumulates on the surface of a sorbent and shapes a molecular or atomic layer, while in an absorption process the gas molecules enter into the bulk phase of corresponding sorbent. A sorbent used in thermochemical energy storage can either be solid or liquid.

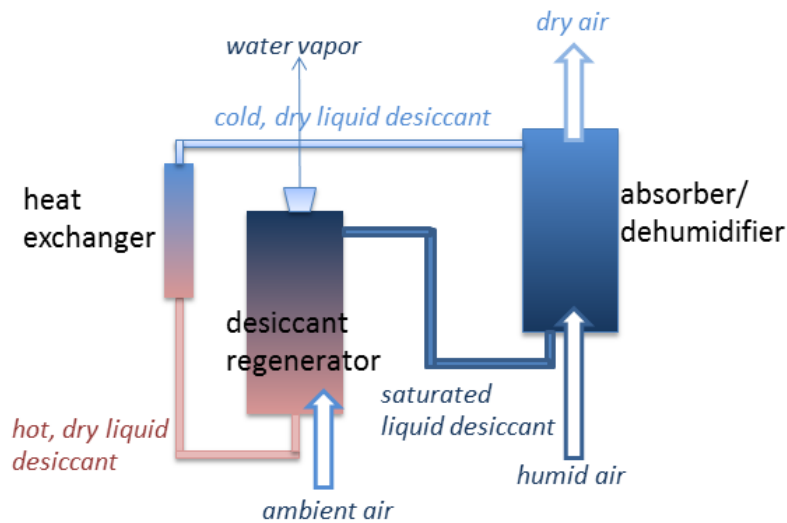


Figure 1-3. A demonstration of an open sorption storage system based on dehumidification with liquid desiccant during water vapor sorption (thermal energy discharge) and desorption (thermal energy storage).

Comparing with other TES methods, thermochemical energy storage has a higher storage density, which allows large quantities of energy to be stored using small amounts of storage substances. In addition, energy storage based on chemical reactions is particularly appropriate for long-term storage applications such as seasonal storage of solar heat, because the process involves almost no energy losses during the storing period, and the storage is usually done at ambient temperatures. Even though, no commercial technique based on

thermochemical energy storage is available, mainly due to the issues of heat and mass transfer, cyclic efficiency, and durability of materials and systems induced by solid reagents or liquid sorbents [28, 29]. On the other hand, as a related research realm using similar thermochemical processes for thermal management, liquid desiccant enhanced air conditioning and water vapor recovery has been extensively explored recently [30-36]. For both thermochemical energy storage and liquid desiccant air conditioning, much work remains to be done on the complex chemical and mechanical systems.

Table 1-2. Summary of materials for thermochemical energy storage [7, 28-31, 33, 37, 38].

Type of reaction/sorption		Reagent / sorbent	
Chemical reaction	Hydration	MgO, CaO	
	Carbonization	PbO, CaO	
Sorption	Ammonia sorption	BaCl <sub>2</sub> , MnCl <sub>2</sub> , NiCl <sub>2</sub> , MgCl <sub>2</sub> , NH <sub>4</sub> Cl, NaBr, etc.	
	Water sorption in solid sorbents and desiccants	Sorbents	Zeolites Silica gel
		Metal hydrides	ZrMnFe, ZrTiCrFe, LmNiSn, LaNi, etc.
		Salt hydrates	MgSO <sub>4</sub> , CaCl <sub>2</sub> , BaBr <sub>2</sub> , NaS, LiBr, etc.
	Water absorption in liquid desiccants	Salt solutions	Saturated CaCl <sub>2</sub> solution, Saturated LiBr solution, etc.
Glycols		Ethylene glycol, Triethylene glycol, etc.	

## 1.2 *Microencapsulated Phase Change Materials*

Despite the considerable potential of thermophysical energy storage, applications of PCMs suffer from inherent disadvantages such as low thermal conductivity, considerable change in volume on phase transition, corrosiveness, decomposition, leakage, and/or large supercooling. Each of the disadvantages affects phase change properties of PCMs and further the efficiency of TES. In order to overcome these problems, a technique utilizing microencapsulated phase change materials (microPCMs) in TES systems has recently been

developed and extensively investigated, by which PCMs are encapsulated in an inorganic/polymeric shell or matrix to maintain the shape and chemical stability, meanwhile preventing the PCM core from leakage to and reaction with surrounding [17, 39-53].

Since the invention of microPCMs, various applications had been found in textiles, building materials, heat transfer fluids, and etc. In textiles and building materials, utilizing microPCMs increase the thermal mass without much increase of the weight of the media [5, 6, 17, 19, 48, 54, 55]. For heat transfer fluid applications, both emulsions of PCMs and slurries of microPCMs are fabricated by dispersing PCMs into the carrier fluids to produce latent functional thermal fluids (LFTFs) that are potentially applicable to refrigeration loops and air conditioning for improving thermal efficiency and reducing required quantity of refrigerant [40, 43, 48, 56]. In this section, basic structures and fundamental properties of microPCMs are introduced.

### **1.2.1 Background of MicroPCMs**

There are limitations to employ PCMs for TES directly. For example, it requires special latent heat devices or heat exchangers for heat transfer in the storage media, which increase costs and thermal resistance between PCMs and surroundings. It has been comprehensively investigated for new forms of PCMs with stabilized shapes and structures, which can be prepared by mixing PCMs with supporting materials such as polymer and graphite[48, 57, 58]. These composites can be applied directly for TES and thermal management with no extra devices required. However, PCMs in these composites tends to diffuse away and loose from the supporting materials gradually during solid-liquid phase transition, although the shape of the support materials remains [59]. To prevent the leakage of melted PCMs during the phase transition, to increase the heat transfer rate, and to reduce PCM

reactivity with surroundings, microencapsulation of PCMs is probably the best solution [48, 57, 58, 60].

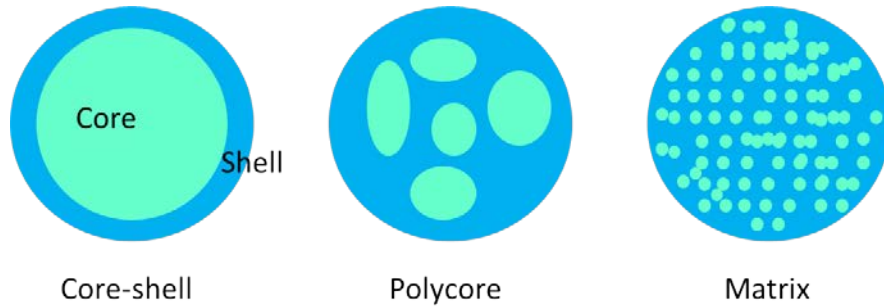


Figure 1-4. Micro-structures of microPCMs.

Microencapsulation is a process of coating or embedding particles or droplets within a shell or matrix to produce micro-sized capsules. All three states of materials can be microencapsulated, though it is rare to encapsulate a gas. By microencapsulation, it is as easy to handle liquid and gas phase materials as to handle solids. Microencapsulation also provides a physical barrier to protect microencapsulated materials from reacting to surroundings.

A microPCM usually has a regular shape (e.g., spherical, oval, or tubular), but it can also be made in an irregular shape. Depending on the physic-chemical properties of the core and shell composition as well as the application, microPCMs with different structures can be synthesized, as shown in Figure 1-4. Generally speaking, a capsule of microPCMs is composed of two parts: a PCM as a core or filler, and an inorganic or polymer shell or closed frame as a container. In addition, it may contain one PCM core or multiple cores in a microcapsule.

### 1.2.2 Synthesis Approaches of MicroPCMs

A microencapsulation process is designed based on the physical and chemical properties of the core and shell materials to be used. Microencapsulation processes can be

categorized into three groups: chemical processes, physical processes, and physical-chemical processes, listed as follows:

Physical processes:

Centrifugal extrusion,

Aerosol coating,

Vibrational nozzle,

Spray drying;

Physical-chemical processes:

Solvent evaporation,

Coacervation;

Chemical processes:

Sol-gel,

In-situ polymerization,

Interfacial polymerization,

Emulsion polymerization.

The use of some methods has been limited due to regulatory affairs, the cost of processing, and the use of organic solvents which can be a concern for environmental problems [48, 55].

Physical processes and physical-chemical processes of microencapsulation are mainly spray drying, centrifugal, and solution evaporating processes, size of as-produced microPCMs from which is inherently large ( $> 100\mu\text{m}$ ) [48]. To produce microPCMs with size smaller than  $100\mu\text{m}$ , chemical processes are often applied. The chemical processes, including sol-gel, in-situ polymerization, interfacial polymerization, and emulsion polymerization processes,

generally involve bringing together two immiscible liquids, e.g. water and an organic solvent, respectively. Precursors of shell are dissolved either in each of the immiscible liquids as direct-acting intermediates that react to establish a solid pre-condensate, or in one of the liquids that react with each other and condense on the interface ignited by parameters such as pH value and/or temperature [40, 44, 48, 57, 61-64]. Most microPCMs are fabricated by the chemical methods due to their properties and applications [48]. In this work, chemical processes are involved to synthesize microPCMs in emulsion systems [65-67]. Details of the state-of-the-art of chemical syntheses of microPCMs can be found in Section 2.2, and the methods of synthesis used in this dissertation research can be found in Section 5.2 and 6.2.

### **1.2.3 Applications of MicroPCMs**

MicroPCMs may be used in form of powder in textiles or buildings to enhance their heat capacity and capability to store thermal energy, or dispersed in carrier fluids to enhance heat transfer efficiency of the fluids for the purpose of heat dissipation. In textile industries, microPCMs are used in flame retarded cotton to resist heat and flame since they can absorb thermal energy and prevent quick temperature increase and burning of cloth [68, 69]. Both paraffin such as n-hexadecane, n-octadecane, n-nonadecane and inorganic PCMs such as phosphates have been used as PCMs in textiles. It has been found that a combination of microcapsules containing different types of PCMs are better than those including a mixture of these PCMs, as thermophysical properties may change due to the mixing of the PCMs [55, 68-70].

PCMs has also been widely studied as a potential aid to building materials for enhancement of thermal comfort and energy saving in buildings [19, 59, 71-73]. There are limitations in using bulk PCMs as building materials, such as that they may interact with building structure and change properties of both PCMs and structure materials, and that the

leakage problem of PCMs can be significant during the life time of the buildings. In addition, PCMs have poor thermal conductivity, which limits heat transfer in building materials and also the performance of PCMs in controlling in-door temperature in the buildings. In order to overcome these problems, microPCMs instead of bulk PCMs have been integrated into conventional building materials so as to prevent the leakage problems and the interaction between PCMs and other building materials [74]. In addition, heat transfer rate of the building materials raises significantly due to a much larger heat transfer area across the shells of the microPCMs. A comprehensive review of microPCMs in building applications has been given by Tyagi et al. [74].

PCMs have also be applied in heat transfer fluids to enhance heat capacity of the fluids as a heat transfer media [9, 40, 45, 48, 57, 75-77]. There are two types of PCM-containing heat transfer fluids, i.e., PCM emulsions and microPCMs slurries. An appropriate amount of surfactant (or dispersant) may be used to help making a PCM emulsion or slurry more stable and better dispersed in the carrier fluid. Water, engine oils, and fluorocarbon are normally used carrier fluids, depending on specific requirements of different applications. In comparison of conventional heat transfer fluids, the microPCM-enhanced fluids have larger heat capacity and are able to work as the media for TES and heat transfer simultaneously, and thus an improvement of performance can be expected.

### ***1.3 Motivation and Rationales of Improving MicroPCMs***

#### **1.3.1 Motivation to Improve the Fluidic Heat Transfer Performance**

It has recently been eye-witnessed an explosive development of communication, electronics, auto-computing industries, and energy utilization, all of which are indisputably continuing to develop fast in visible future. Heat dissipation from mechanical, electrical, and electronic components has become a serious problem that may obstacle these fast-growing

technologies. Heat generated by and required to be rejected from these devices is continually increasing due to the trend toward more power output from engines, faster speed and smaller size for microelectronic devices, and brighter beams by light sources in optical devices.

Though all three heat transfer modes can be used for heat dissipation, utilization of heat transfer fluids by taking advantage of the large heat flux of convection is one of the most common and effective choices. Heat transfer fluids have found many industrial applications in automotive, energy supply, air-conditioning, electronic cooling, and etc. However, the low thermal conductivity and heat capacity of conventional heat transfer fluids is a limiting factor in the design of heat dissipation systems. The increasing power density of equipment in various industries calls for innovative thermal management technologies. Generally speaking, there are two ways to meet the increasing requirements for heat dissipation: 1) designing new heat exchangers, such as increasing surface area by fins and microchannel and integrating spot cooling and miniaturized cryo-devices, and 2) improving heat transfer capability of heat transfer fluids. The effectiveness of updating the design of cooling devices as a conventional method to enhance heat transfer, however, has almost reached a limit [78, 79]. The seeking for new heat transfer fluids with higher heat capacity and thermal conductivity as well as lower viscosity is important now.

### **1.3.2 Rationales behind MicroPCMs**

TES techniques based on the use of PCMs have been raising a great practical interest, motivated by the large thermal energy stored per unit PCM in a small temperature range around its phase transition temperature. The systems for TES with PCMs have been developed for various applications from textiles to fluidic heat transfer enhancements. Specifically, new techniques of using a solid-liquid or liquid-liquid two-phase flow to improve fluidic heat transfer have been proposed and investigated. This type of techniques consists of forming a

two-phase fluid from the mixture of a carrier fluid and a PCM, producing a fluid with considerable capability of LHS. These heat transfer fluids have been cataloged in five types:[80]

- 1) Ice slurries in water;
- 2) PCM emulsions, in which PCMs are dispersed in water with the use of surfactants;
- 3) MicroPCM slurries, in which PCMs are microencapsulated and dispersed in water;
- 4) Salt hydrate PCM slurries; and
- 5) Shape-stabilized PCM slurries, based on shape-stabilized PCMs that consist of paraffin infiltrated in high density polyethylene.

Since PCMs have much higher heat capacity than conventional heat transfer fluids that utilize sensible heat only, it is a straightforward logic to increase the heat capacity of heat transfer fluids by adding PCMs. However, if PCMs are added directly without encapsulation, it may not aid the heat capacity of heat transfer fluids efficiently but cause troublesome problems:

- a) Without protection, PCMs may be soluble or reactive in carrier fluids. That way, PCMs lost their property of phase transition at a certain temperature, which means that no latent heat capacity is available in this condition;
- b) Supercooling can be significant when the scale of PCM particles is small. In this case, phase transition of the PCM tends not to happen until it is supercooled to a considerably low temperature. Among a large temperature range of operation, increase of overall fluid heat capacity as a result of the great amount of latent heat is less significant comparing with accumulated sensible heat over the temperature range;

- c) Large PCM particles are easy to settle out from heat transfer fluids, especially in low-speed circulation. The settling out of PCM particles induces not only losing latent heat capacity but also forming a sediment layer at the surface of containers or pipelines, thus increasing thermal resistance and impairing heat transfer performance of the system. In addition, large size of the PCM particles or the agglomerates of them may cause severe clogging problems, especially in microchannel;
- d) Small PCM particles are not thermodynamically stable in fluid and tend to grow or agglomerate to big ones to reduce overall surface tension;
- e) Erosion of containers or pipelines by PCMs increases rapidly when speed of circulation increases, especially when PCMs are hard or corrosive.

Due to these disadvantages of direct dispersed PCM suspensions, the method of adding PCM directly into heat transfer fluids is not preferred. To avoid these disadvantages, PCMs may be microencapsulated before dispersing into the base fluids. A variety of microPCM structures has been reported, possessing different mechanical and thermal properties from the corresponding bulk materials. The as-synthesized microPCMs are expected to exhibit several beneficial features as follows:

- a) High heat capacity. It has been demonstrated that latent heat energy storage has larger heat capacity than utilizing sensible heat, as shown in Figure 1-2. Due to the high latent heat of PCMs, it requires less amount of energy storage medium than utilizing sensible heat only to achieve the same magnitude of TES. Calculated from averaging the overall heat capacity by a certain operation temperature range, the apparent specific heat of a PCM is also significantly higher than its specific heat without phase transition. In microPCMs, though overall latent heat is smaller

than that of bulk PCMs due to the mass fraction of shell material, the fraction of PCM in a microPCM should be large enough to achieve a sufficient amount of heat capacity.

- b) Suppressed supercooling. Most PCMs have a certain amount of supercooling during homogeneous nucleation processes. This phenomenon is more significant in microPCMs, as the probability to generate a homogeneous nucleation site in a confined volume of a microcapsule is smaller than that in bulk PCMs [81]. To suppress supercooling of microPCMs, various additives have been used as nucleate agents, which introduce heterogeneous nucleation sites into microcapsules and decrease the potential barrier of corresponding phase transition.
- c) Elimination of leakage. Encapsulation of a PCM in rigid shells prevents it from leakage during phase transition processes. In applications to heat transfer fluids and building materials, for example, mechanical strength of the shells determines the sustainability of the microPCM from leakage. It has been found that with melamine-formaldehyde resin (MFR) as the shell material, microcapsules can survive under a deformation up to 68% [82], which ensure the little leakage probability of PCMs from microcapsules.
- d) Elimination of agglomeration and clogging. The microPCMs are micro-sized, shape stable, and well dispersible in fluids. Due to the stable shell structure, encapsulated PCMs are protected from attaching each other and forming agglomerations. As a result, using of microPCMs cause little clogging problems in pipelines.
- e) Reduction of erosion. Common materials used to produce shells for encapsulating PCMs are polymers and inorganic materials such as silica. Comparing with the

hard particles, microPCMs make less damage to the walls of pipelines, pumps, and heat exchangers. In addition, corrosive PCMs are encapsulated and prevented from wall materials, and thus potential chemical reactions that induce erosion can be eliminated.

## **1.4 Objectives of Research**

There are four objectives in this work. Listed step by step, they are: 1) developing a new production method of microPCMs; 2) solving the problem of large supercooling that occurs in microPCMs with large PCM loading; 3) elevating thermal conductivity of the microPCMs; and 4) applying microPCMs in conventional heat transfer fluids to develop a type of phase changeable heat transfer fluids so as to improve both thermal conductivity and heat capacity of the fluids simultaneously.

### **1.4.1 Production Methods of MicroPCMs**

Two types of methods of chemical synthesis of microPCMs have been developed in literature, i.e. the sol-gel methods and the in situ polymerization methods, as described in previous sections [40, 44, 48, 57, 61-64, 83-85]. The first type of methods involves a one-step process of hydrolysis of precursors, and thus is suitable in microencapsulation of hydrophobic PCMs with inorganic shells. The second one has all precursors of polymer contained in continuous water phase, so that through the synthesis the hydrophobic PCM droplets can be protected from contamination. That way, pure PCM cores with predictable thermophysical properties in microPCMs can be obtained. This method is widely used in encapsulation with urea-formaldehyde and melamine-formaldehyde resin.

However, neither of these methods is suitable for mass production of microPCMs with proper thermophysical properties, especially for hydrophilic PCMs that are miscible in aqueous phase. In addition to the problem of miscibility, there are other issues induced by

microencapsulation, such as large supercooling of the microencapsulated PCMs due to the lack of nucleate sites in microcapsules. To deal with these issues, suitable production methods are developed in this work for microencapsulation of hydrophilic PCMs based on wet-chemical techniques.

#### **1.4.2 Supercooling Suppression**

One of the most common problems in both bulk PCMs and microPCMs is supercooling, i.e., hysteresis of phase transition despite thermodynamic preference. This problem is more serious in microPCMs than that in bulk PCMs, because homogeneous nucleation in the confined volume of a microcapsule randomly happens in a less preferred probability. As a result, the hysteresis of nucleation in microPCMs is more significant, which represents as larger supercooling macroscopically.

Researches have been working on controlling the supercooling of microPCMs since 1990s [86]. The most common and practically applicable method for supercooling suppression is to add nucleation agents to promote heterogeneous nucleation during melt crystallization. This effort has been done for supercooling suppression in bulk PCMs such as salt hydrates for decades [4, 5, 19] and recently applied on microPCMs [44, 86-88]. Unfortunately, the additives cause additional problems, not only by decreasing heat capacity of microPCMs due to the large mass fraction of the nucleate agents, but also by affecting other thermophysical properties of microPCMs, e.g., melting point.

The aim in this section is to suppress the inherent supercooling of PCMs confined in microcapsules without the use of additives as nucleate agents, meanwhile maintaining other pros of thermophysical properties such as large heat capacity. Instead of additional nucleate agents, shells of microPCMs are optimized so as to decrease the surface tension between the

shell and the encapsulated PCM, and thus provide nucleate sites to promote heterogeneous nucleation and suppress supercooling of encapsulated PCMs.

### **1.4.3 Thermal Conductivity Enhancement**

Heat transfer fluids suffer not only from low heat capacity but also low thermal conductivity [45, 53, 89-92]. On one hand, heat capacity of conventional fluids are relatively low, which can be elevated by utilizing microPCMs; on the other hand, thermal conductivity of microPCMs are as low as common heat transfer fluids and thus contributes little on the elevation of thermal conductivity of heat transfer fluids. Most PCMs, especially commonly used organic PCMs, have relatively low thermal conductivity as shown in Table 1-1, and so the commonly used shell materials such as silica, CaCO<sub>3</sub>, and polymers. As a result, by adding microPCMs into heat transfer fluids, heat capacity of the fluids can be elevated while thermal conductivity of the fluids remains low, which is a drawback to achieve better heat transfer performance. It is highly desirable to combine the advantages of high heat capacity with high thermal conductivity in heat transfer fluids for better performance.

Adding conductive particles are proven to be able to elevate thermal conductivity of a heat transfer fluid [13, 79, 93]. Meanwhile, comparing with sensible heat capacity of conventional heat transfer fluids, latent heat of the PCMs are significantly larger [4, 8]. As a combination of both advantages, utilizing the large amount of latent heat along with modification for enhanced thermal conductivity in heat transfer fluids is a possible route to meet current requirements from the fast-growing industry. In our previous work[53], a new class of phase change nanofluids with improved heat capacity as well as thermal conductivity was developed, which are synthesized by dispersing thermally conductive phase changeable indium nanoparticles into base fluids. The high thermal conductivity of indium nanoparticles increases thermal conductivity of heat transfer fluids just as common nanofluids; meanwhile,

phase change process of indium nanoparticles is reversible, and large amount of latent heat is absorbed or released during the phase transition, resulting an increase of heat capacity of the fluids. However, the elevation of heat capacity was not pushed to the limit because of the supercooling of indium nanoparticles, and contamination to pipelines and containers can be significant without encapsulation of this PCM.

A different way to combine high heat capacity and high thermal conductivity based on microPCMs are demonstrated in this dissertation. MicroPCMs provide base fluids high heat capacity; in addition, a metal layer is coated on the surface of the microPCMs to accomplish the improvement of thermal conductivity. That way, microPCMs with both high heat capacity and high thermal conductivity can be prepared.

#### **1.4.4 Applications in Heat Transfer Fluids**

Interest in engineered suspensions of micro/nanoparticles in liquids has increased in recent years, particularly due to the potential for higher fluid thermal conductivities, resulting in smaller and more compact heat exchangers [9, 45, 53, 75, 78, 79, 90, 92]. It has also been reported that convective heat transfer of heat transfer fluids can be significantly enhanced by using thermal conductive nanofluids [18, 45, 53, 78, 79, 93-102]. However, heat capacity of these nanofluids is generally as low as, if not lower than, conventional heat transfer fluids. On the other hand, microPCMs has also been applied in heat transfer fluids to enhance heat transfer, and the main enhancement provided by PCMs is a significant increased TES density due to latent heat. However, thermal conductivities of most PCMs are relatively low. For example, the paraffin/PAO heat transfer fluid have comparable thermal conductivities of around 0.14 W/mK.

In this section, the as-synthesized microPCMs, with and without elevation of thermal conductivity by metal coating, are applied in PAO-based heat transfer fluids in purpose of

improving their heat transfer properties. The influence of the microPCMs on the fluidic and thermal properties of the modified heat transfer fluids are investigated and compared with that of original PAO-based heat transfer fluids.

## Chapter 2. Literature Review

MicroPCMs have great potential to improve heat transfer properties of heat transfer fluids more effectively than bulk PCMs and PCM emulsion without encapsulation. Proper microencapsulation of PCMs not only maintains large latent heat capacity, but also introduces other useful properties such as suppressed supercooling, elevated thermal conductivity, stabilized shape and structure, and less probability of leakage and agglomeration. As a result, microPCMs have great potential in applications to various heat transfer fields.

In this chapter, a comprehensive review of microPCMs related to this work are given, including the contents of background, synthesis, properties modification, and applications. First, theories and properties of colloidal solutions and emulsion systems for the synthesis of microPCMs are reviewed. Later on, methods of the microPCM synthesis are discussed, including recent developments of supercooling suppression and thermal conductivity enhancement of microPCMs. At last, the state-of-the-art applications of microPCMs in heat transfer fluids are summarized.

### ***2.1 Ternary Colloidal Systems of Surfactant-Water-Oil***

Old proverb says that “oil and water don’t mix.” However, by using surfactants or dispersants, oil and water can be mixed to form a stable colloid system either kinetically or thermodynamically. A liquid colloidal system consists of a dispersion of one component, liquid or solid, within a liquid medium. Known as emulsion and microemulsion, liquid colloidal systems show interesting physical and chemical properties which have led to wide applications including foods, cosmetics, pharmaceuticals, energy, and etc. Based on their thermodynamic stability, colloidal systems can be classified as emulsion and microemulsion

[103-107]. It is useful to begin the understanding of colloidal systems with making the distinction between these two terminologies.



Figure 2-1. Photos of samples of (from left to right) immiscible oil-water mixture, oil-in-water emulsion, and microemulsion.

### **2.1.1 Amphiphile / Surfactant**

Molecules with both hydrophilic and hydrophobic moieties are called amphiphiles [108]. By definition, an amphiphilic molecule consists of two well-defined moieties: one of which is oil soluble (i.e., oleophilic or hydrophobic), and the other is water soluble (i.e., oleophobic or hydrophilic). Because of this dual nature, amphiphile molecules have the ability to self-assemble into ordered structures in solution and accumulate at water-air interface, thus decrease the surface tension compared to that of pure water. They can also reduce the interfacial tension between organic solvent and water by adsorbing at the liquid-liquid interface. As amphiphiles can work as surface active agents, they are also called surfactants.

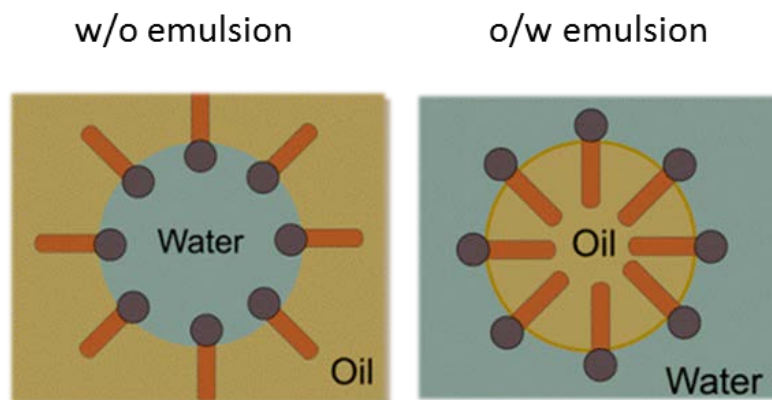


Figure 2-2. Basic structure of micelles in O/W emulsion and reverse micelles in W/O emulsions. A typical surfactant molecule is schemed with an orange colored hydrophobic tail and a gray-blue colored hydrophilic head [108].

Various microstructures may form by self-assembly of surfactants in solutions [104, 108, 109]. In aqueous solutions, the tendency of hydrophobic moiety to avoid contacting with water is the basis of the association of molecules in micelles. Micelles are formed spontaneously when the concentration of surfactant exceeds a certain value, namely the critical micelle concentration (CMC). The CMC, which represents a fundamental micelle quantity to study the self-aggregation of amphiphilic molecules in solution, appears to be the most important property in the study of the micellization of amphiphilic molecules. On the contrary, in organic solutions, hydrophilic region tends to avoid contact with organic solvents, and thus forming reverse micelles.

Due to the initiation of structure change over the point of CMC, the amphiphilic solutions go through a notable change in physical properties such as electrical conductivity, surface tension, osmotic pressure, solubility, or fluorescence. Each of the properties monotone increases or decreases with the concentration of surfactant, with an abrupt change of first-order derivative at the point of CMC [110-116]. The CMC of a surfactant in a solution can be determined by the intersection of the two straight lines of solution properties above and below.

Based on the types of their hydrophilic heads, surfactants can be divided into ionic ones and nonionic ones [108]. The category of ionic surfactants includes cationic ones and anionic ones, on the basis of the charge of their head groups. Specifically, amphoteric surfactants change their nature from cationic to anionic with increasing pH value. On the other hand, nonionic surfactants are not charged. Their hydrophilic head is, for instance, a short polyethylene oxide chain or a polyhydroxyl chain. Different from ionic surfactants, nonionic are not sensitive to hard water or pH solutions, and are usually compatible with other types of surfactants.

The behavior of a surfactant is influenced by hydrophilic-lipophilic properties, geometrical shape of the molecules, and spontaneous curvature of the surfactant films at the interface of aqueous phase and oil phase. The hydrophilic-lipophilic balance (HLB) is an empirical number which was defined [117] as the ratio of hydrophilic and lipophilic moieties in a surfactant molecule. Reflecting the affinity of surfactant partitioning between oil and water, a HLB number can roughly be calculated according to the following equation [117]

$$\text{HLB} = 20 \times \frac{M_{\text{hydrophilic}}}{M_{\text{molecule}}} \quad (\text{Equation 2-1})$$

where  $M_{\text{hydrophilic}}$  is the molar mass of the hydrophilic moiety, and  $M_{\text{molecule}}$  is that of the whole surfactant molecules. Apparently, HLB is a value ranging between 0 and 20. Generally speaking, a surfactant with  $\text{HLB} > 10$  is more affinity to water and that with  $\text{HLB} < 10$  more to oil.

An alternative prediction of the structure of an aggregate of surfactant molecules can be done considering the molecular geometry of the surfactant, described by the packing parameter  $P$  [118]:

$$P = \frac{v_{molecule}}{A_{molecule} l_{hydrophobic}} \quad (\text{Equation 2-2})$$

where  $v_{molecule}$  is the molecular volume,  $l_{hydrophobic}$  is the length of the extended hydrophobic chain, and  $A_{hydrophilic}$  is the effective area of the hydrophilic head resulting from the balance between the attraction of hydrophobic chains and the repulsion between heads, taking hydration into account. Practically, the actual area of hydrophilic head and consequently  $P$  changes with concentration and thus vary the curvature of the aggregate. The self-assembly of surfactant molecules in solution, which may be spherical micelles, cylindrical micelles, and patterns of cubic, hexagonal, and lamellar, is directly related to the  $P$  value.

Adopted by a surfactant film in the absence of constraints, the surfactant film bends spontaneously towards the medium where it is more soluble [107]. This phenomenon occurs due to that surfactant film possesses bending elasticity, which is governed by properties of surfactant heads and tails [119]. In a ternary system of surfactant/oil/water, if the polar head is bulkier than the hydrophobic tail, the film curves towards water, which is defined as positive mean curvature by convention, oil-in-water (O/W) structure is favored. In contrast, a negative mean curvature favors water-in-oil (W/O) structure, which forms when the head is less bulky than the tail. If heads and tails have more or less the same form, a zero mean curvature is obtained.

### **2.1.2 Emulsion**

A mixture of two immiscible liquids plus a surfactant that lowers the interfacial tension between the two liquids may result in the formation of an emulsion or a microemulsion. The main differences between an emulsions and a microemulsion are their microstructure, size of droplets, and thermodynamic stability [120], which are discussed as follows.

A number of definitions of the word “emulsion” were presented in literature [103-105, 107, 109, 119-123]. Generally speaking, an emulsion is a heterogeneous system that consists

of one or more immiscible liquids dispersed in another in form of droplets. Usually prepared by applying a shear force onto the system, such an emulsion system retains a minimal stability against creaming or sedimentation [120]. For example, when water (W) is dispersed in an oil (O) phase with proper amount of surfactant (S), a water-in-oil (W/O) emulsion can be formed, while an oil-in-water (O/W) emulsion is obtained when oil is dispersed in water. The usage of the terms O/W and W/O continuous from traditional terminology, even though it is understood that water phase may in fact contain dissolved or pure electrolyte, alcohols, acids, glycols, and so on, whereas oil phase can be any liquid insoluble in water, such as silicones and fluorocarbons.

Size of emulsion droplets may vary from microns to nanometers. Specifically, when droplets size is in nano-scale, the corresponding emulsions is called nanoemulsion (or miniemulsion) [109, 121]. Even though heterogeneous as emulsions in general, a nanoemulsion appears transparent or translucent in visible light and usually possesses significantly higher stability than normal emulsions, due to the characteristic size range of droplets.

### **2.1.3 Microemulsion**

The term “microemulsion” is generally refer to homogeneous and thermodynamically stable isotropic liquids formed by mixing water, oil, and surfactants together by a proper ratio [104]. For example, an O/W microemulsion is a thermodynamically stable colloidal dispersion consisting of small spheroid particles or microstructures that comprised of oil, surfactant, and possibly co-surfactant dispersed within an aqueous medium. The surfactant molecules in an O/W microemulsion are organized so that their non-polar tails associate with each other to form a hydrophobic core, since this reduces the thermodynamically unfavorable contact area between non-polar functional groups and water. On the contrary, the hydrophilic head groups

of surfactant molecules protrude into surrounding aqueous phase. Oil molecules may be incorporated into the hydrophobic interior of a micelle as separate cores or between the surfactant tails in forms of lamellar layers. If the oil molecules have some polar groups, these groups may be incorporated into the micelle in such a way that they interact with polar groups on surfactant head groups or protrude some distance into water.

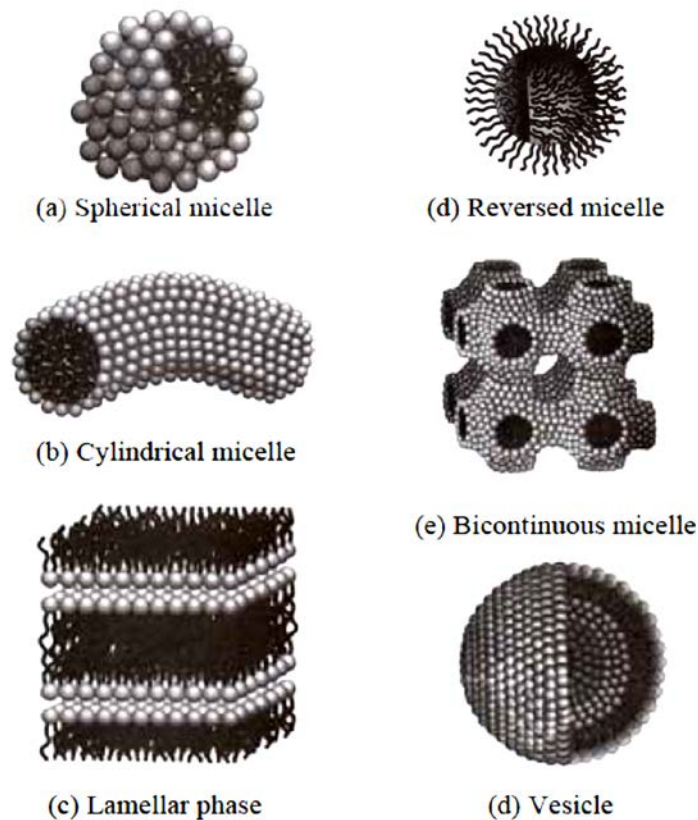


Figure 2-3. Different structures inside micelle systems [122].

Depending on the composition of water, oil, and surfactant and the environmental conditions, it can be formed within a microemulsion system with different microstructure (or phase) or their equilibrium, such as spheroid (e.g., micelles or reverse micelles), cylindrical (e.g., rod micelles or reverse rod micelles), lamellar, or sponge-like structures. As a result, these phases may be oil-continuous, water-continuous, or bicontinuous.

A well-known classification of microemulsions was developed by Winsor [124, 125], who identified four general types of phase equilibria in a W-O-S ternary system:

- Type I: the surfactant is preferentially soluble in water and O/W microemulsion forms (Winsor I). The surfactant-rich water-based microemulsion phase coexists with the oil phase where surfactant is only present as monomers at small concentration.
- Type II: the surfactant is mainly in the oil phase and W/O microemulsion forms. The surfactant-rich oil-based microemulsion phase coexists with the surfactant-poor aqueous phase (Winsor II).
- Type III: a three-phase system where a surfactant-rich middle-phase coexists with both excess surfactant-poor water and oil phases (Winsor III).
- Type IV: a single-phase (Winsor IV) micellar solution, that forms upon addition of a sufficient quantity of surfactant.

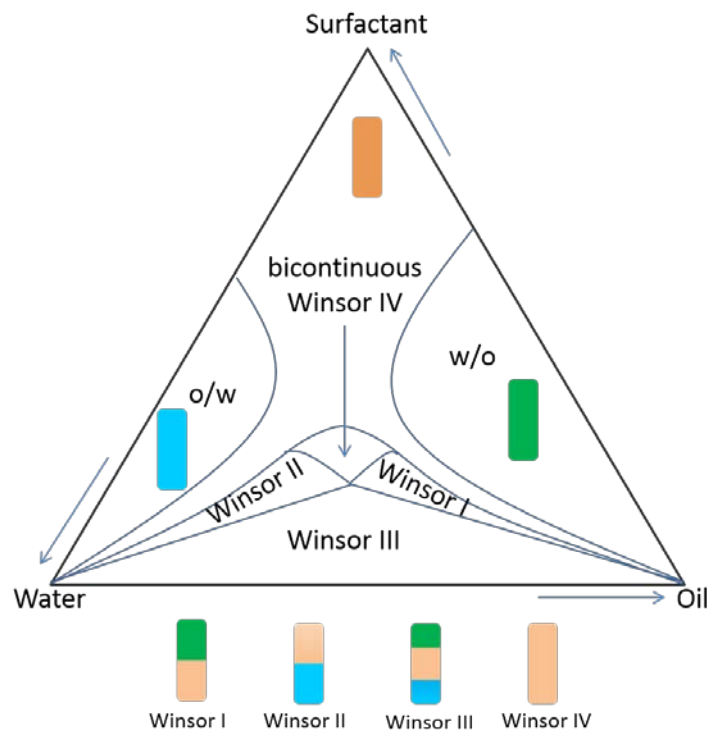


Figure 2-4: Winsor structure models of microemulsions [125].

Preferentially depending on the type of surfactants and environmental conditions, types I, II, III or IV may form in a colloidal systems where the dominant type is related to the molecular arrangement at the interface. Phase transitions may be brought about by manipulating the parameters such as electrolyte concentration (in the cases of ionic surfactants) and temperature (for non-ionic ones).

### 2.1.4 Thermodynamic Stability of Emulsion and Microemulsion Systems

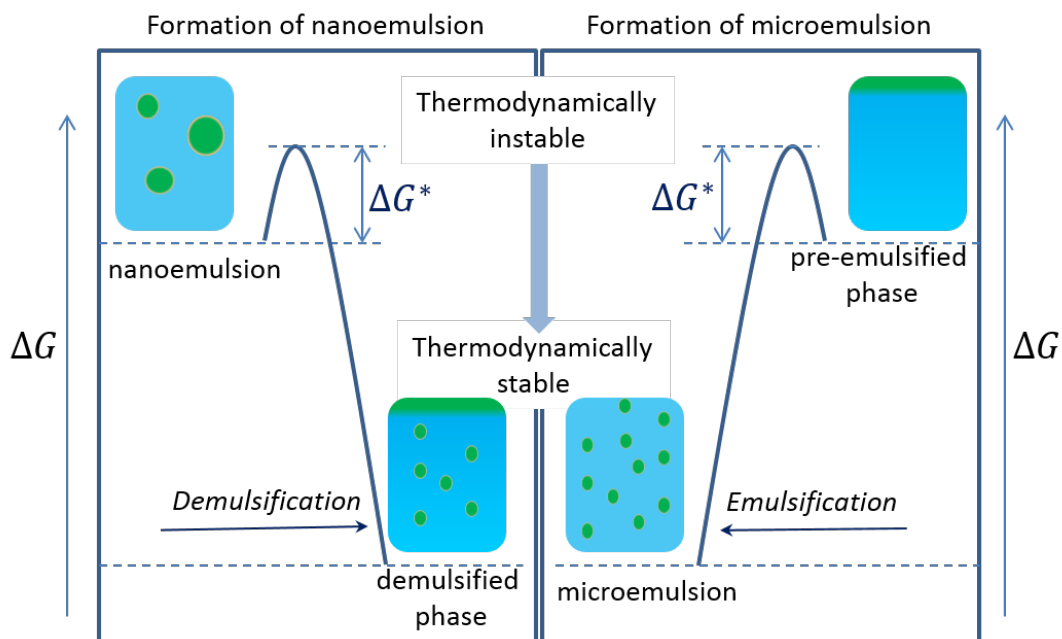


Figure 2-5. Schematic diagram of Gibbs free energy of microemulsion and nanoemulsion systems compared to the phase separated state. The emulsion/microemulsion and the separated oil-water phases are transferable with an activation energy  $\Delta G^*$ .

The most fundamental way of distinguishing an emulsion and a microemulsion is in terms of their thermodynamic stabilities: emulsions are thermodynamically unstable, whereas microemulsions are thermodynamically stable. Figure 2-5 schematically compares Gibbs free energy of colloidal dispersions to that of separate oil-water phases before emulsification, taking a case of O/W system for example. It is assumed that water phase consists of surfactant

molecules dispersed within water in the form of either monomers or micelles, depending on the total concentration and the CMC of corresponding surfactant.

The thermodynamic stability of a colloidal dispersion is determined by the difference in Gibbs free energy between the dispersion and the separate oil-water phases. Thermodynamically, a system always tends to revert to the state with the lowest free energy given specified conditions (e.g., composition, temperature). For a microemulsion, the free energy of the colloidal dispersion is lower than the free energy of the separate oil-water phases, which means that a microemulsion is thermodynamically stable. A microemulsion is thermodynamically stable under a particular range of conditions, and hence it should form spontaneously when the S, O, and W are brought together, and then it should remain stable indefinitely provided the initial conditions remain unaltered. However, a microemulsion may not form spontaneously in practice. Such a pre-microemulsion system may persist in a metastable state for a considerable period of time if it is kinetically stable. In general, the kinetic stability is governed by two major factors: energy barriers and mass transport. On one hand, the conversion of one state to another are slowed down if there is a potential barrier (activation energy) separating two states. On the other hand, the rate at which a system changes from one state to another state is determined by the speed at which the materials present can rearrange themselves into the new configuration. Consequently, it may be necessary to mechanically agitate or heat the system in order to prepare a microemulsion from S, O, and W ingredients. The physicochemical origin of the energy barrier in microemulsion systems is not well understood, but it may be related to the free energy associated with moving a nonpolar molecule from an oil phase to a water phase [103, 104]. When a non-polar molecule comes into contact with water, there is a thermodynamic penalty associated with the hydrophobic effect, which increases as the contact area between the non-polar groups and water increases. The magnitude of this term partly determines the water solubility of the oil molecules: the

larger the Gibbs free energy penalty, the lower the water solubility. The kinetics of microemulsion formation also depends on the speed that oil molecules move from the oil phase, through the water phase, and into the micelles, which is governed by their translational diffusion coefficients.

In contrast, for an emulsion, the free energy of the colloidal dispersion is higher than the free energy of the separate oil-water phases, which means the emulsion is thermodynamically unstable. An emulsion can be made to be kinetically stable or metastable by ensuring that there is a sufficiently large energy barrier between the two states. It breaks down essentially given sufficient time, the rate of which depends on the height of any energy barriers between the emulsion and the separated oil-water phases as well as on specific mass transport processes involved. The height of the energy barrier determines the kinetic stability of an emulsion: the higher the energy barrier, the longer the emulsion persists [103, 126]. The height of the energy barrier is mainly determined by physicochemical phenomena that prevent droplets from coming into close proximity, such as repulsive hydrodynamic and colloidal (e.g., steric and electrostatic) interactions operating between droplets. The rate at which an emulsion reverts back to the separated phases is also determined by the frequency that the oil droplets come into contact with each other, which depends on the primary mechanism responsible for particle–particle contacts, such as Brownian motion, applied shear, and/or gravitational forces [103, 109].

## **2.2 *Synthesis of MicroPCMs in Colloidal Systems***

As described in Chapter 1, microencapsulation processes can be categorized into three groups: chemical processes, physical processes, and physical-chemical processes. To produce microPCMs with size smaller than 100  $\mu\text{m}$ , chemical processes are more often applied. Chemical processes, including sol-gel, in-situ polymerization, interfacial polymerization, and

emulsion polymerization processes, generally involve bringing together two immiscible liquids, e.g. water and organic solvent, respectively, and one or more surfactant and co-surfactant to make durable emulsion so as to carry on the microencapsulation process. Generally, a process of microPCMs synthesis involves two stages. In the first stage, a dispersion of PCM is formed in a continuous medium. In the second one, this dispersion is transformed and finally stabilized and solidified to make a firm structure around each PCM droplets. Thus, emulsifying techniques are the simplest way and widely extended for the obtaining of microPCMs. In this section, two of the methods applied in this work research for microPCMs synthesis are briefly reviewed.

### **2.2.1 Sol-Gel Process for MicroPCM Synthesis**

The sol-gel process may be described as the polycondensation reaction, during which a molecular precursor in a liquid phase forms a colloidal solution (so called “sol”) and subsequently converts to a solid network (“gel”). In this reaction, precursors of shell materials, usually inorganic silicate or silicate esters, are mixed in aqueous solution to make the sol. The sol then evolves gradually towards the formation of a gel-like diphasic system. The morphologies of the solid products range from discrete particles to continuous polymer networks. Removal of the remaining liquid phase requires a drying process, which is typically accompanied by a significant amount of shrinkage and densification.

Microencapsulation methods in silica or other inorganic media have been intensively studied by utilizing the sol-gel method through an O/W emulsion route, due to its easy control over spherical morphology and size distributions. For example, it has been used to prepare microPCMs with silica shell and stearic acid core, which is a saturated fatty acid with the melting point of 56 °C [73]. Another study shows that paraffin wax can be microencapsulated with silica shell, with melting point at 58 °C and latent heat of 156.9 J/g [127]. With a

combination of O/W emulsion technique and sol-gel process, the inorganic encapsulation of PCM n-pentadecane with silica shell was also studied, and SEM results confirmed the production of micro-sized spherical microcapsules [85]. Encapsulation of PCMs using sol-gel methods with polymer precursor such as poly(methyl methacrylate) network-silica hybrid as the shell material has also been developed [84].

### 2.2.2 In-Situ Polymerization

The most important wet-chemical technique used to synthesize microPCMs is the in-situ polymerization. This technique involves the formation of PCM-in-water emulsions using hydrophobic PCMs such as paraffin. In in-situ polymerization, the precursors of the microPCM shells are dissolved in water phase, and polymer shell are formed as a result of the process of polymerization at the interface (i.e., the surfactant layer) in O/W emulsion. This technique is specifically important for urea-formaldehyde and melamine-formaldehyde encapsulation system [62, 63, 128-139].

Figure 2-6 shows the processes of the in-situ polymerization processes. Different from the other polymerization methods, no reactants are included in the core material. All polymerization occurs in the continuous water phase rather than on both sides of the interface in interfacial polymerization and in the core material in emulsion polymerization. As a result, there is no contamination to the core PCM during the reaction, thus pure PCM cores in the microcapsules with predictable thermophysical properties can be expected.

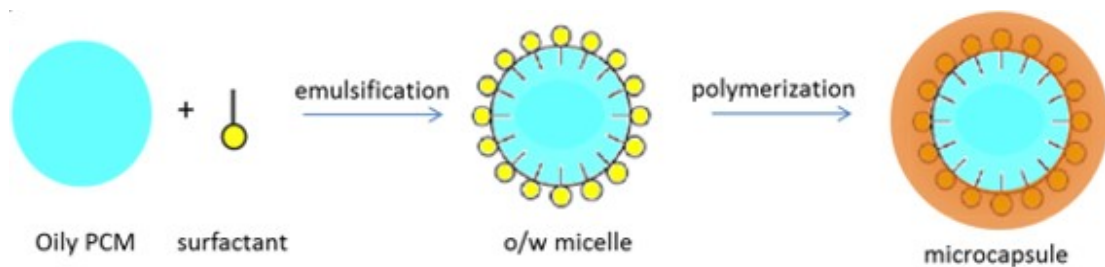


Figure 2-6. The general process of in-situ polymerization for the synthesis of microPCMs.

Due to its good chemical stability and mechanical strength, melamine formaldehyde resin [62, 128-137] and urea formaldehyde resin [63, 133, 138, 139] has been widely used as the shell material of microcapsules. Hong and Park [137] fabricated melamine resin microcapsules with long self-life using fragrant oil as core material and melamine formaldehyde as shell material by in-situ polymerization. The size of all the resulted particles is below 10  $\mu\text{m}$ , and their size distribution is narrow. The microencapsulation efficiency is about 87% and the loading amount of fragrant oil in the microcapsules is about 53 wt%. Zhang et al. [41, 140, 141] fabricated microcapsules and nanocapsules using 70 wt% octadecane with melamine formaldehyde shell. The stirring rate, emulsifier content and cyclohexane content have effects on the diameters and morphology of the microencapsulated octadecane. The diameter distribution becomes narrower with the increase of stirring rate and emulsifier content. The diameters have no effects on the melting behaviors of microcapsules; however, they have significant effects on the crystallization behaviors. They also demonstrated that thermal stability of the microcapsules can be improved using different molar ratios of urea-melamine-formaldehyde copolymers as shell. Song et al. [142] prepared microcapsules with aminoplast as the shell and bromo-hexadecane ( $\text{BrC}_{16}$ ) as the core. The results shows that the use of silver nanoparticles significantly increases strength and solves the common problem of particle agglomeration. In addition, new microcapsules demonstrate higher thermal stability performance and capable of enduring higher temperature. Shin et al. [132] prepared melamine-formaldehyde resin microcapsules containing eicosane for textile materials. Their results suggest that microcapsules with higher core/shell ratios need to be made to improve the thermal-regulating efficiency of fabrics. A treated fabric with 22.9% microPCM add-on is capable of absorbing 4.44 J/g of heat if the microcapsules on the fabric undergo a melting

process, yet no information of supercooling at a freezing process was given. Boh et al. [143] fabricated microcapsules using higher hydrocarbon phase change material as the core and amino-aldehyde resins as the shell. The high molecular weight of emulsifier is better than low molecular weight and by increasing the amount of emulsifier. Su et al. [144] prepared a series of melamine formaldehyde microcapsules containing composite PCMs as core material, in which the surface morphologies and the shell structure of microcapsules are crucial to thermal properties, the melt point of PCM in the shell does not change and the heat transfer is obvious. Rao et al. [75] used n-docosane as the core material with MFR as the shell material to fabric microPCMs. To get a better microencapsulation efficiency of the core material in the preparation experiment, the core mass fraction in a single particle is lower than 70%. DSC thermal analysis shows that the prepared microPCMs with a core mass fraction of 60% has a high heat of fusion up to 150 J/g.

Various other effort has been applied by different researchers [41, 57, 61, 88, 128-131, 133, 134, 145, 146]. However, similar problems occur among these studies, which are the potential issue of leakage, low thermal conductivity of the microPCMs, and significant supercooling of the core material. Most of the microcapsules are also defected with low PCM content, which results in low heat capacity. These problems and possible solutions are discussed in the following sections.

### **2.3 *Supercooling Suppression of MicroPCMs***

One of the common problems in both bulk PCMs and microPCMs is the supercooling, i.e., the hysteresis of phase transition. In homogeneous nucleation where no additional nucleate agent is used, an energy barrier occurs in the formation of initial nucleus of a crystal. The rate of homogeneous nucleation is determined by the rate of formation of nuclei. After the formation of nuclei, further growth of low-temperature phase becomes energetically favorable.

A random fluctuation of energy in PCMs is necessary to overcome the energy barrier and form nuclei. The probability to overcome energy barrier and form nuclei depends on the temperature difference between current temperature and ideal phase transition temperature. In homogeneous nucleation, to initialize the nucleation, a significant temperature difference is required.

To avoid the large supercooling induced by homogeneous nucleation, nucleate agents are added to introduce heterogeneous nucleate sites. For example, salt hydrates are a type of inorganic liquid-solid PCMs with great potential in application, but supercooling is a big trouble for this type of PCMs due to the potential barrier of homogeneous nucleation. Researchers have found various nucleate agents for salt hydrate PCMs, which can be divided into two types: iso-structural nucleate agents and epitaxial nucleate agents [4]. The iso-structural nucleate agents are salt hydrates with nearly identical crystal structures and lattice parameters to the PCM. This type of nucleate agents are usually quite effective yet lack of durability, due to their dehydration, solubility, and difficulty to be uniformly distributed in PCMs. Epitaxial nucleate agents, in another hand, have no evident structural fit with the PCM and less effective nucleation ability than the iso-structural ones. Only ex post facto explanations of the mechanics of these epitaxial nucleate agents are suggested, and the reported effects of same agents are often different from each other [5, 6, 8, 10, 147-149].

The supercooling problem is more serious in microPCMs, because homogeneous nucleation in the confined volume of a microcapsule randomly happens in a less preferred probability [81, 150]. As a result, the hysteresis of nucleation and phase transition from high-temperature phase to low-temperature phase is more significant, which is represented as larger supercooling of microPCMs macroscopically.

Similar as in bulk PCMs, the most common and practically applicable method to deal with the supercooling problems in microPCMs is also adding nucleation agents to promote

heterogeneous nucleation during melt crystallization. Lee [42] found that derivatives of paraffin, such as 1-octadecylamine and 1-octadecanol, are suitable for reducing supercooling of octadecane microcapsules. Fan et al. [41, 88] reported that paraffin with melting point 60~65 °C (20 wt% of the core materials) is able to eliminate supercooling of n-octadecane in microcapsules without affecting morphology and dispersity of the microcapsules. However, the PCM content in the microcapsules is relatively small. Alvarado et al. [44] selected to use 6 wt% tetradecane and 6 wt% tetradecanol for supercooling suppression of microencapsulated tetradecane. These nucleating additives are miscible with PCM alkanes at elevated temperature, but they precipitate from the solution when temperature drops below the freezing point of the additives and thus promote heterogeneous nucleation. This way, supercooling is successfully suppressed and the heat capacity is also maintained. Xie et al. [151] studied the crystallization behavior of octadecane confined in small (1.5 μm) microcapsules, which yields separated freezing peak and supercooling as small as 0.3 °C. In all these methods, however, one drawback is that the effective latent heat of the PCM microcapsules is reduced due to the large amount of additive, which meanwhile changes other thermophysical properties of the PCMs.

Table 2-1. Summary of supercooling suppression of microPCMs based on paraffin.

Author (first)	Year	Diameter (μm)	Shell	PCM	PCM ratio (wt%)	Supercooling (°C)
Fan [41]	2004		UMFR <sup>I</sup>	octadecane	20%	2.5
Zhang [88]	2005	0.3-6.4	UMFR	octadecane	70%	~8 <sup>II</sup>
Alvarado[44]	2007	5	gelatin	tetradecane	88.3%	0.7
Xie [151]	2008	1.5	MFR	octadecane	~12% <sup>III</sup>	0.3

I: urea-melamine-formaldehyde resin.

II: supercooling based on the onset temperature of the main peak of freezing.

III: calculated from given data in the reference.

## **2.4 *Enhancement of Thermal Conductivity for MicroPCMs***

There is an emerging requirement of high thermal conductive microPCMs to enhance their heat transfer performance for thermal energy storage and thermal management. In bulk PCMs, thermal conductivity can be enhanced by high-thermal-conductive fillers. Common filler such as copper, aluminum, nickel, and carbon foams have been used to increase the thermal conductivity of PCMs [152]. However, the improvements are limited in microPCMs due to the confined volume.

In microPCMs, a more effective way is to use thermal conductive materials as shells. Using organic-inorganic hybrids as shell materials have attracted substantial attention because of the potential of combining advantages of both components within a molecular scale composite. Organic materials such as melamine-formaldehyde resin can offer structural flexibility and convenient processing, while inorganic compounds provide potential for higher thermal conductivity and mechanical stability. In addition, chemical stability and flame retardancy of inorganic materials such as silica are better than that of organics as well. As a result, choosing an appropriate inorganic material as a part of the shell for the microPCMs is a promising idea for enhancing their thermal conductivity. Wang et al. [83] synthesized a types of microPCMs with octadecane as the core PCM and silica as the shell, which have higher thermal stability and good phase change performance, meanwhile have significantly enhanced thermal conductivity than microPCMs with organic shells. However, due to the limited thermal conductivity of current inorganic shell materials such as silica and  $\text{CaCO}_3$ , the increase of thermal conductivity of microPCMs is also limited.

## **2.5 *Applications of MicroPCMs in Heat Transfer Fluids***

Applications of microPCMs in heat transfer fluids include the use in TES and heat dissipation. Examples of these applications include two-phase flow in cooled ceiling system,

secondary loop for refrigeration and air conditioning, and PCM-embedded heat sink [9, 153-155]. A study [153] of the performance of PCM in an annular space were carried out by using both bulk PCMs and microPCMs. It was found that the heat transfer rate of microPCMs is about 25% higher during the charging period and 20% higher during the discharging period, which indicates that microPCMs could significantly increase the ability of thermal energy storage. Similar research [154] has been done with commercially available microPCMs as both TES and heat transfer media, which concludes that 40 wt% microPCMs could reduce flow rate while maintaining the constant cooling temperature effectively and thus reduce the total pumping power comparing to conventional heat transfer fluids. Another research using commercial microPCMs was processed by Gschwander et al. [155]. The microPCMs were dispersed in water to form a slurry and pumped for several weeks continuously. This long-term test indicates that a centrifugal pump is suitable for pumping microPCMs enhanced heat transfer fluids. MicroPCMs may be broken when transported through pump, but this can be tackled by increasing the thickness of shell and reducing the diameter, which meanwhile results in less latent heat provided by microPCMs. The measurement of temperature and pressure drop shows that microPCMs are especially advantageous for the applications within a small temperature difference during the operation.

## **2.6 Summary**

For applications in TES and heat dissipation, an ideal microPCMs should have high heat capacity, good chemical and thermal stability, small supercooling, and sufficient thermal conductivity. Many research has been done on developing microPCMs with optimized properties for various applications. In these literatures, most researches were reported to produce stable microPCMs with sufficient heat capacity and to suppress supercooling of microPCMs. There are also literatures [83] reporting the enhanced thermal conductivity of

microPCMs, though the improvements are not significant comparing with other thermal conductive materials. Commercial microPCMs products [156-158] are also available, though their supercooling and low thermal conductivity are still troublesome for direct applications. Nevertheless, it is still necessary to improve the thermophysical properties and performance of microPCMs in TES and heat dissipation, so as to promote their applicability to industrial scale.

## Chapter 3. Characterization Methods for Structures and Properties

Characterization of heat transfer fluid systems is a combination of characterization of particles and characterization of fluids. Characterization of particles includes investigation of elemental compositions, determination of particle morphology, and characterization of particle crystal structure and microstructures. Characterization of fluids covers fluid stability, thermal conductivity, heat capacity, viscosity, and heat transfer coefficients. These chemical and physical properties are very important for deepening understanding of the mechanisms to elevate heat capacity and thermal conductivity of heat transfer fluids. In this chapter, an introduction of related characterization methods and instruments are given. Additional information can be found in Appendix.

### ***3.1 Determination of Elemental Composition and Molecular Structure***

#### **3.1.1 Energy Dispersive X-Ray Spectroscopy**

Elemental compositions of nanoparticles can be determined by Energy dispersive X-ray spectroscopy (EDS, or EDX), a common accessory of an Electron Microscope. EDS is an analytical tool used mainly for characterization of chemical compositions of materials. The fundamental principle of EDS is based on that each element in the periodic table possesses a unique electronic structure. When a material is bombarded by accelerating incident electrons, the response of each element to these electromagnetic waves, e. g., the wavelength of output characteristic X-rays, are unique. Information of characteristic X-rays can thus be used for chemical analysis. In this work, elemental composition in solid materials are determined by EDS, with a deviation of  $\pm 0.1\%$ .

### **3.1.2 Fourier Transform Infrared Spectroscopy**

Fourier Transform Infrared Spectroscopy (FT-IR) is one of the most powerful tools for identifying types of chemical bonds and functional groups in a molecule. In FT-IR, infrared radiation is passed through a sample, during which some of the infrared radiation is absorbed by the sample. The rest of the radiation passes through the sample and is then detected with a sensor. The spectrum represents the molecular absorption and transmission and creates a molecular fingerprint of the sample. By interpreting an FT-IR spectrum, chemical bonds in the molecule can be determined. In this work, FT-IR is taken with a Thermo Scientific Nicolet IR200 spectrometer. The deviation of wavelength is  $\pm 0.1 \text{ cm}^{-1}$ .

## **3.2 *Investigation of Morphology and Crystal Structure***

### **3.2.1 Small-Angle Neutron Scattering**

Small-Angle Neutron Scattering (SANS) is a technique using elastic neutron scattering at small scattering angles to investigate nanosized or submicro-sized structure at mesoscale. During a SANS experiment, a beam of neutron is directed at a substance, which can be a solution, a powder, or a crystal. The neutrons are elastically scattered by interaction with nuclei or magnetic momentum of unpaired electrons in the sample.

As one of the ideal tools to study colloidal systems with dimensions in the range 0.5 ~ 30 nm, SANS has been carried out to clarify the formation of micelles and the microstructure of micelle solutions [159-165]. In this work, SANS measurements are conducted on the NG-3(30 m) beamline at the NIST Center for Neutron Research (NCNR) in Gaithersburg, MD. Samples are prepared with deuterated solvent to achieve the needed contrast between the droplets and solvent. The scattering intensity  $I$  is measured versus the scattering vector  $q =$

$4\pi \sin(\theta/2) / \lambda$ , where  $\lambda$  is the wavelength of incident neutrons and  $\theta$  is the scattering angle.

The approximation  $q = 2\pi\theta/\lambda$  is used due to the small angle  $\theta$ .

### **3.2.2 Scanning Electronic Microscopy**

Scanning Electronic Microscopy (SEM) can be used to obtain better resolution and higher useful magnification than conventional optical microscopy. In addition to surface topography, SEM also provides the crystal structure, chemical composition, and electrical behavior of the top microns of specimen. In SEM, a fine probe of electrons with energy typically up to 40 keV is focused on a specimen, which is mounted on an electrically conductive substance in a vacuum chamber.

In this work, all SEM images were taken at room temperature using a Hitachi SU-70 Scanning Electronic Microscope. Most of the samples in this work are poor electrical conductor. To make it suitable for SEM imaging, a sputter coating process is required to coat a thin layer of gold on the surface of non-conductive samples.

### **3.2.3 Transmission Electronic Microscopy**

Transmission Electronic Microscopy (TEM) is a straightforward method to observe dimensions and geometry of nanoparticles, which also use a probe of electron to detect the structure of a sample. Different from SEM, TEM collect information from transmitted electrons. The main limitation of TEM observation is that the viewing field of TEM is relatively small, which potentially raise the possibility that the region to be analyzed may not be characteristic of the whole sample. Several (more than 6) different places are observed and averaged information is obtained and analyzed in order to overcome this drawback. In this work, all TEM images were taken using a JEOL JEM-2100 Transmission Electronic Microscope.

### 3.3 *Characterization of Thermophysical Properties*

#### 3.3.1 Differential Scanning Calorimetry

Differential scanning calorimetry (DSC) is a powerful tool to measure specific heat and heat capacity of PCMs. The difference in the amount of heat flow required for heating up the sample pan and the reference pan are measured as a function of temperature. The sample and reference pans are maintained at nearly the same temperature throughout the experiment. By measuring the difference in heat flow, specific heat and heat capacity of the sample is obtained. For example, if there is a phase transition in the sample pan, because of the release or absorption of sensible and latent heat, different amount of heat is needed to flow into the two pans to maintain both pans at the same temperature. As a result, endothermic or exothermic peaks present on measured DSC curves, corresponding to the phase transition. Phase transition temperatures, latent heat, and specific heat before and after phase transition can be determined according to DSC curves.

In case of utilizing latent heat to increase heat capacity of heat transfer fluids, a thermophysical quantity to reflect the increase more straightforwardly is the average specific heat, i.e., the effective specific heat. An average specific heat of a latent system at a certain operation temperature range is calculated by averaging overall heat capacity over the temperature range.

In this work, all DSC curves were measured using a TA Q100 Differential Scanning Calorimeter in nitrogen atmosphere, with a deviation of  $\pm 0.02$  K for temperature, and  $\pm 0.05$  J/g for heat capacity.

### 3.3.2 Thermal Conductivity Measurement of Solid Materials

Thermal conductivity of solid samples were measured with a steady state method based on Fourier's heat transfer equation:

$$Q = kA \frac{dT}{dx} \quad (2-1)$$

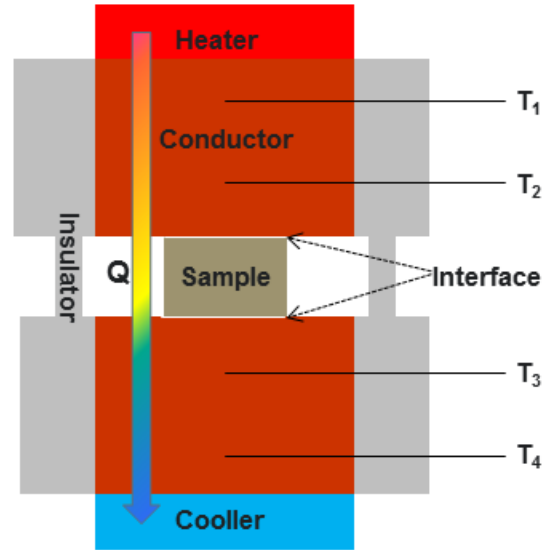


Figure 3-1. The steady state method for thermal conductivity measurement based on the Fourier heat transfer equation.

The Scheme of this method is shown in Figure 3-1. Temperature at both sides of the sample are calculated based on measured temperatures, from which  $k$  is calculated. Major error of this measurement comes from the interface resistance, which is usually suppressed by using high thermal conductivity thermal interface materials. In this work, the measurement is taken with a P. A. Hilton H112 Heat Transfer Service Unit. The deviation of thermal conductivity is  $\pm 0.2$  W/mK.

### **3.4 *Measurements of Thermophysical Properties of Fluids***

#### **3.4.1 Viscosity**

Viscosity of a heat transfer fluid is an important indication to evaluate heat transfer properties of the fluid. In this work, viscosity of heat transfer fluids are measured with a Brookfield DV-I prime viscometer, with different particle loadings in the heat transfer fluids at different temperatures and different rotor RPMs. The deviation of viscosity is  $\pm 0.1$  cP.

#### **3.4.2 Stability**

As the dispersion of particles in a heat transfer fluid is not thermodynamically stable, the particles tend to sediment from the fluid eventually. It depends on the material properties of the particles, the dispersion technique used in preparation, and the surfactants used to make a kinetically stable fluid. Although stability of a heat transfer fluid is very important in order for practical application, the methods are limited on the measurement of this property. It has been reported [166] that UV-vis spectrometry was used to quantitatively determine the colloidal stability of the dispersions. Another method for the estimation of the stability of fluids is to measure the volume of sediment versus the sediment time.

In this work, the stability of our heat transfer fluids is investigated using the second method. A vial of fluid sample is mounted onto a horizontal and stable surface. After a pre-set period of time, the liquid is carefully decanted, and the weight of the sediment is measured.

#### **3.4.3 Thermal Conductivity Measurement of Fluids**

The hot-wire method is a transient dynamic technique for simultaneously measuring thermal conductivity and thermal diffusivity of materials. This method is based on the measurement of time-dependent temperature rise in a heat source, i.e. a hot wire, which is immersed in the material to be tested to serve simultaneously as an electrical resistance heater

and a resistance thermometer. The hot wire is fabricated as small as several microns in diameter to approximate a simple one dimensional transient line-source of heat in an infinite medium as closely as possible in order to minimize the necessity of making corrections for its actual geometry. However, the influence of convection on hot-wire measurement is not negligible. To avoid this problem, the  $3\omega$  - wire method was employed to measure thermal conductivity of liquids.

The  $3\omega$  - wire method combines the advantages of both the  $3\omega$  method and the hot-wire method. Similar to the hot-wire method, a metal wire with a length of  $L$  and a radius of  $r$  is suspended in a liquid to act as both a heater and a thermometer. Superposition of a DC source, a sinusoidal AC current at frequency  $\omega$  is passed through the metal wire as heating. Heat generated in the metal wire is also related to the resistance of the wire, which is a function of temperature. The corresponding temperature rise in the sample to be measured is a  $2\omega$  superposition of a DC component, and so as the resistance of the wire. By calculation (see A.1.1), the voltage across the wire contains the voltage drop due to the DC resistance of the wire at  $1\omega$ , and two new components proportional to the temperature rise in the wire at  $3\omega$  and  $1\omega$ . The  $3\omega$  voltage component can be extracted by using a lock-in amplifier and is then used to deduce the temperature rise amplitude at  $2\omega$ , which is used to determine the thermal conductivity of the fluid.

The  $3\omega$  - wire method is more accurate than traditional hot-wire transient methods. On one hand, the temperature oscillation can be kept small enough (below 1 K [52, 92], compared to about 5 K for the hot-wire method) within the test liquid to retain constant liquid properties. On the other hand, background noises such as temperature variation have much less influence on the measurements due to the use of the lock-in technique. These advantages make the  $3\omega$  - wire method ideally suited for measuring the thermal conductivity of fluids.

In this work, we used a Labview-based homemade system to measure thermal conductivity of heat transfer fluids with applying the  $3\omega$  - wire method [167]. A TSI 1240-T1.5 metal wire is used as the heater and sensor. A Stanford SR850 OSP Lock-in Amplifier are used in the system for data collection.

## Chapter 4. Thermal Conductivity of Dilute Colloidal Solutions

### 4.1 *Introduction*

Colloidal solutions and emulsion systems constitute an important role in various sectors of modern science and industry. In this work for example, microPCMs were synthesized in an emulsion system, the processes of which are discussed in the following chapters. The dispersion of microPCMs in heat transfer fluids may also related to colloidal systems, using surfactant as stabilizer. It is important to have a better understanding of the colloidal system for the design and applications of microPCMs.

In emulsion systems, surfactant molecules orient themselves according to their amphiphilic molecular structure and hence adsorb at oil-water interfaces, with the polar groups towards water and nonpolar groups towards non-aqueous phase. As a result, one of the fundamental properties of surfactants is their self-association into organized molecular structures such as micelles, vesicles, microemulsion, and so on [123]. The simplest class of the association colloids is micelles, i.e., spherical clusters of surfactants in solvent. Micellization characteristics of a surfactant in a colloidal solution are understood by determining the values of its micellization parameters, such as the CMC.

The CMC of a surfactant in a solution represents a fundamental micelle quantity to study the self-aggregation of amphiphilic molecules in solution. According to its definition, the CMC is the concentration of a surfactant in a solution at which the molecules start to self-associate into micelles instead of accumulating at surfaces or interfaces. As a result, surface tension of a colloidal solution does not reduce further with the addition of surfactant above the CMC. Due to the initiation of structure change at this point, the surfactant solution goes through a notable change in physical properties such as electrical conductivity, surface tension, osmotic pressure, solubility, and fluorescence, each of which monotone increases or decreases

with the concentration of surfactant, with an abrupt change of its first-order derivative at the CMC [110-116].

The CMC can be determined by finding the intersection of the two straight lines of a solution property above and below. For example, with a pure surfactant, the surface tension is linearly dependent on the logarithm of the concentration over a large range below the CMC, while extensively independent to the concentration when above the CMC [168]. This independence is called surface tension isotherm. Using the data of surface tension, the CMC can be read at the intersection of the straight line passing through the plateau and the regression straight line of the linearly dependent region. This determination can be applied to all colloidal solutions without been affected by the type, concentration, and impurities in the solution.

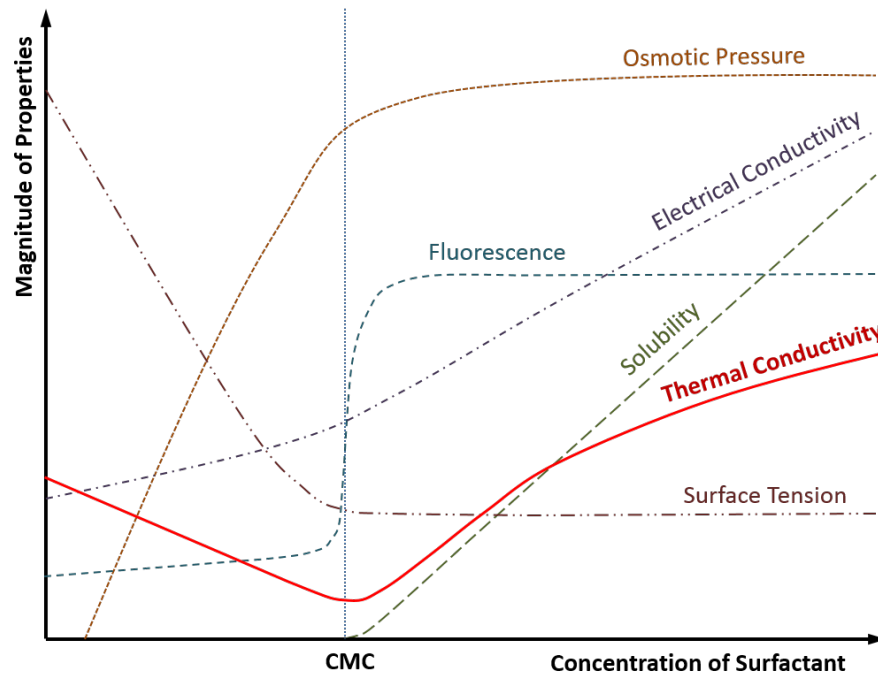


Figure 4-1. Schematic representation of surfactant concentration dependence of several physical properties for surfactant solutions, including surface tension, fluorescence, electrical conductivity, etc. The red solid line corresponds to the curve of thermal conductivity based on this research, in which a minimum occurs at the CMC [169].

Other methods based on various solution properties have also been developed to measure the CMC. The William method [170-172] suggests to measure the CMC based on electrical conductivity of the surfactant solution. This method is sensitive to salt solved in the solution, and can only applied to ionic surfactant solutions. The methods using UV absorption, light scattering, and fluoresce spectroscopy are sensitive to small particles and clusters in colloidal systems, and thus require a clean and pure solution [115, 171, 172]. SANS can also be used to measure the CMC using neutron beam as the light source [168].

Though thermal conductivity of colloid solutions have long been interested [98, 100, 173-177], the performance of thermal conductivity of a surfactant solution below or around the CMC value has not been investigated, to the best of our knowledge. In this chapter, we investigated thermal conductivity of diluted surfactant solutions with ionic surfactants in organic solvents. For the first time, a minimum thermal conductivity of the surfactant solution has been discovered at the CMC of the surfactant in the solution. This phenomenon is significantly different from other physical properties that monotone increase or decrease with the concentration of surfactant. We believe this minimum thermal conductivity method for obtaining the CMC offers a simple and straightforward alternative for measuring the CMC.

## ***4.2 Preparation of the Colloidal Solutions***

Dioctyl sulfosuccinate sodium salt (98%) (AOT), n-octane (>99%), and deuterated n-octane (98 atom% D) were all purchased from Sigma-Aldrich. Polyalphaolefin (PAO, 2 cSt) were purchased from Chevron Phillips Chemical Company. The AOT/n-octane colloidal systems are spontaneously formed by self-assembly of AOT molecules in the liquid of n-octane. Solutions of AOT in n-octane are transparent, but they scatter light at higher AOT concentration due to the Tyndall effect.

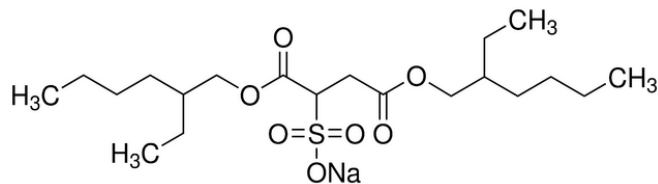


Figure 4-2. Molecular structure of AOT [178].

### 4.3 Determination of the CMC with SANS

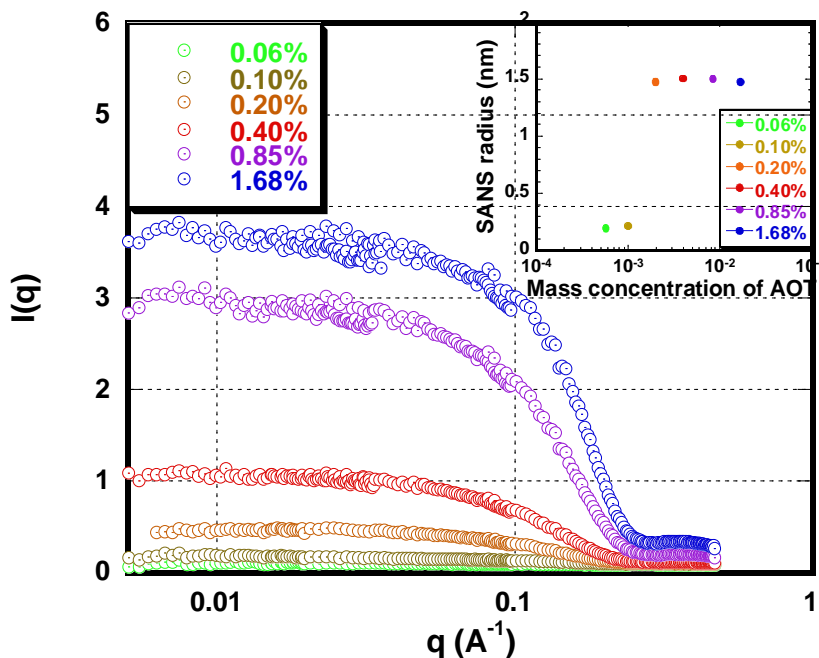


Figure 4-3. SANS scattering spectra from AOT/n-octane solutions. The curves are labeled by the mass fraction of AOT in the solution. Insert: average radius of the solved AOT molecules or micelles versus mass concentration of AOT in n-octane.

AOT/n-octane samples for SANS measurements were prepared in deuterated n-octane to achieve the needed contrast between scatters and solvent. Figure 4-3 shows SANS spectra ( $I(q)$  vs  $q$ ) for the samples. Each of the spectra clearly rises above the base line at higher AOT concentration, signaling the formation of AOT micelles. Further analysis of the SANS data shows that an abrupt increase of the size of the binary system occurs in the AOT mass concentration range from 0.001 to 0.002, which indicates the formation of micelles. The CMC

of AOT in n-octane solution is located in the range of [0.001, 0.002]. By fitting the SANS data using the IGOR PRO software under the protocol from NCNR NIST with the hard-sphere model [90, 163, 179, 180], the radii of the AOT micelles are found to be around 1.47 nm, indicating that each of the micelles consists of 20-30 monomers.

#### 4.4 Thermal Conductivity of the Colloidal Solutions

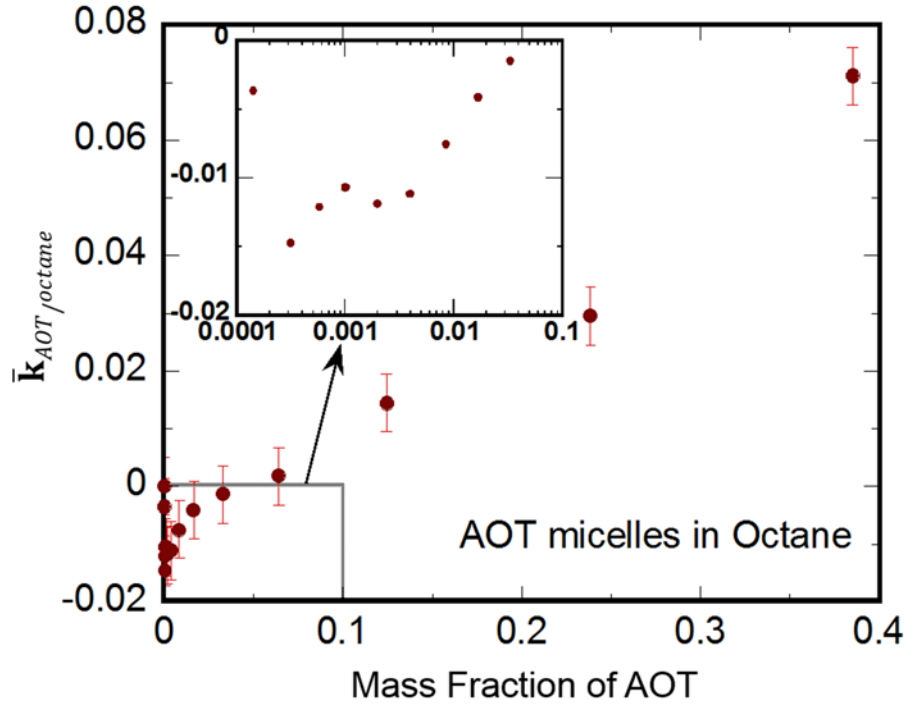


Figure 4-4. Dimensionless thermal conductivity change  $\bar{k}_{AOT/octane}$  versus surfactant mass fraction in the AOT/n-octane solutions, where  $\bar{k}_{AOT/octane} = (k_{solution} - k_{octane})/k_{octane}$ . Inserted is the expansion of selected part of the curve.

Thermal conductivity of AOT/n-octane solutions is measured using the  $3\omega$ -wire method [92]. As shown in Figure 4-4, the dimensionless thermal conductivity change of the AOT/n-octane solutions decreases in the beginning as the AOT loading increases from zero, then goes through a minimum and starts to increase. The inflexion occurs when AOT mass fraction is around 0.002, identical to the CMC of AOT in n-octane determined with SANS. A

similar colloidal system of AOT/PAO solution was also investigate by the same method and shown in Figure 4-5. A minimum of thermal conductivity at around 0.0015 of AOT mass fraction occurs in the AOT/PAO system. This non-monotone trend in the colloidal solutions is significantly different from normal binary solution system, in which thermal conductivity increases or decreases with the concentration of the solute monotonously. The existing theories, such as effective medium theory [181], apparently fail to explain the observed minimum in the binary solution system solely.

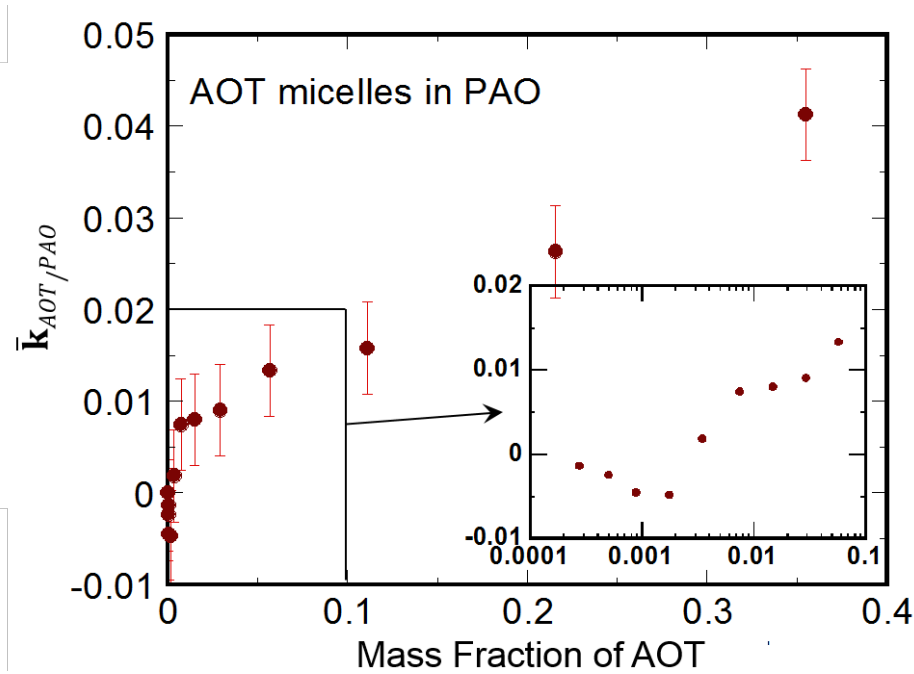


Figure 4-5. Dimensionless thermal conductivity change  $\bar{k}_{AOT/PAO}$  versus surfactant mass fraction in the AOT/PAO solutions, where  $\bar{k}_{AOT/PAO} = (k_{solution} - k_{PAO})/k_{PAO}$ . Inserted is the expansion of selected part of the curve.

#### 4.5 Analysis of the Minimum Thermal Conductivity at the CMC

When AOT concentration in a solution is lower than the CMC, it distributes in the solution like normal solutes, except that a layer of surfactant molecules forms at the surface of the solution. As AOT concentration increases above its CMC in n-octane, the oleophobic

sulfonate head groups associate together to form micelles, from which the nonpolar n-octane molecules are excluded. In these micelles, AOT molecules arrange radially with the sulfonate head group surrounding the hollow center, while the oleophilic tails of alkane chain penetrates into the solution.

The mass action model is commonly employed in theoretical thermodynamic treatment of micelles [123, 182-184], which regards micelle as a chemical species. That way, the colloid system can be treated as a ternary solution system, the three components of which are n-octane, the surfactant monomers with concentration  $c_{AOT}$  lower than or equal to the CMC, and the surfactant micelles that occurs only above the CMC. When  $c_{AOT} < \text{CMC}$ , no micelle formed in the solution, and the monotone decreasing  $\bar{k}$  in this range shown in Figure 4-4 and Figure 4-5 fits the effective medium theory when the solute molecules in the solution has lower thermal conductivity than the solvent. As  $c_{AOT}$  increase above the constant CMC, AOT micelles occurs, meanwhile  $\bar{k}$  increases with the increase of micelle concentration. This increase indicates that the effective thermal conductivity of AOT micelles is surprisingly higher than that of the solvent, on the contrary to that of AOT monomers in the solution. This dramatic change must be analyzed with molecular dynamics rather than ordinary heat conduction models.

When  $c_{AOT} < \text{CMC}$ , there is no micelle formed in the solution, and the oleophobic sulfonate head directly contact with the bulk n-octane solvent. Dutta et al. [185] found that due to the inter-molecular force, low-density region occurs in surfactant solution at the hydrophobic-hydrophilic interface. In this work, density at the contact interface of oleophobic head and the bulk octane may be lowered due to the inter-molecular force [185, 186]. It is reasonable that the low-density gap also accompanied with a range of low thermal conductivity, and thus obstruct heat transfer. This effect leads to a thermal conductivity decrease with increasing AOT concentration below CMC.

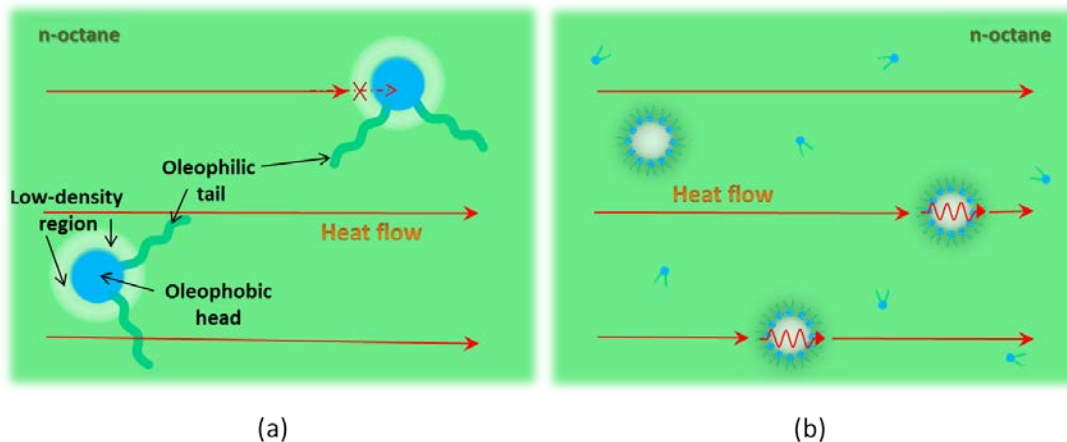


Figure 4-6. Scheme of thermal conductivity of AOT/n-octane solution at AOT concentration a) below and b) above the CMC. The red arrows show the direction of heat flow.

On the other hand, when  $c_{AOT} > CMC$ , it forms AOT reverse micelles in the solution. The oleophobic sulfonate heads curl up in the micelles to avoid direct contact with the n-octane solvent. As a result, no low-density gap occurs between the surfactant molecules and the solvent and obstructs heat transfer. In addition, the reverse micelle structure may further enhance the thermal energy transport in the fluid [177, 187]. It is well-known that the formation of reverse micelles in organic solvent requires at least trace amount of water [105]. Confined in the reverse micelles, the trace amount of absorbed water molecules form hydrogen bond network together with the hydrophilic head of surfactant molecules [188], i.e. the sulfonate head of AOT. As a much stronger intermolecular interaction, hydrogen bond has been reported to be able to enhance heat transfer at the interface [189-191]. Due to the vibrational matching of O-H bonds and O $\cdots$ H hydrogen bonds in a micelle of AOT, the vibrational energy transferring through this rapid route of hydrogen bond network is more efficient than the ordinary heat transfer in n-octane, hence thermal conductivity of solution is higher. That way, the heat transfer performance of the colloidal solutions with an inflexion at the CMC can be explained.

#### **4.6 Summary**

The CMC is one of the key properties of surfactants. In this section, it is found that there is a minimum thermal conductivity occurs in both the AOT/n-octane solution and the AOT/PAO solution with an AOT loading of around 0.1 ~ 0.2 wt% in both experiments. The existing theories such as effective medium theory apparently fail to explain the fact of the minimum thermal conductivity. To analyze this phenomenon, hypothesis of inter-molecular low-density region and hydrogen bond network enhanced energy transfer was introduced. Based on this discovery, we brought out a method of obtaining the CMC of a surfactant in a solution by measuring thermal conductivity of the solution. Comparing with the change of slope at the CMC in ordinary methods, the inflexion at the minimum thermal conductivity is obvious and easy to be determined.

## Chapter 5. Microencapsulated Solid-Solid PCMs

### 5.1 Introduction

Table 5-1. Pros and cons of three types of liquid-solid and solid-solid PCMs [4-6, 10, 18, 48, 57, 58, 192-195].

	Salt Hydrates	Paraffin	Polyalcohol
Phase transition	Solid-liquid	Solid-liquid	Solid-solid
Density	1.44 – 2.19 g/cm <sup>3</sup>	0.75 – 0.93 g/cm <sup>3</sup>	0.91 – 1.15 g/cm <sup>3</sup>
Latent heat	108 – 370 J/g	189 – 255 J/g	27 – 264 J/g
Melting temperature	8 – 137 °C	-12 – 71 °C	22 – 86 °C
Tunable melting point	Discrete	N.A.	Continuous
Thermal conductivity	0.49 – 0.65 W/mK	0.15 – 0.23 W/mK	0.03 – 0.21 W/mK
Volume change	Small	Large	Very small
Corrosion to metal	Corrosive	Non-corrosive	Non-corrosive
Corrosion to plastic	Corrosive	Swelling/soften	Reactive
Cyclic stability	Poor	Good	Good
Supercooling (bulk)	Large	Small	Large
Flowability	Yes	Yes	No
Sublimation	No	No	Yes

PCMs have been receiving considerable attention in applications to TES and heat dissipation, due to their high energy density [4-6, 8, 10, 17, 19, 49-53, 71, 196]. Among the four types of PCMs, liquid-solid and solid-solid PCMs are the most promising. Both liquid-solid and solid-solid PCMs have advantages and disadvantages comparing with each other. Table 5-1 shows the pros and cons of three types of most widely used PCMs. The salt hydrate

liquid-solid PCMs are inexpensive and present sharp melting point, large latent heat, and small volume change during the phase transition, and relatively high thermal conductivity compared with other PCMs, yet they tend to lose their great phase change properties during operation cycles. Paraffin, another type of liquid-solid PCMs, has great latent heat capacity, proper melting temperature, and small supercooling compared with salt hydrates, but their density and thermal conductivity are generally small. In addition, they suffer from potential issues in the liquid phases such as liquid leakage. Compared with conventional liquid-solid PCMs, the solid-solid PCMs such as polyalcohol do not involve liquid phase during phase transitions, hence freeing them from concerns about liquid leakage and thermal expansion. Additionally, phase transition temperature of polyalcohol PCMs can be tuned continuously by mixing two or more polyalcohol, making them suitable for various applications with certain operation temperatures [18, 192, 193]. However, their latent heat are generally small, supercooling are significant, and sublimation may also be a problem in some applications.

We focus on the polyalcohol solid-solid PCMs in this chapter. Microcapsules comprised of NPG encapsulated in silica microspheres were synthesized with the use of emulsion techniques [66]. Chemical composition and phase change behavior of the NPG/silica microcapsules were investigated. Suspensions of the NPG/silica microPCMs in heat transfer fluid PAO were also prepared, and their effective specific heat capacity was also estimated.

## **5.2 *Synthesis of the Solid-Solid MicroPCMs***

### **5.2.1 Materials**

Neopentyl glycol (NPG, 99%), cyclohexane (99%), ethanol (99.5%), hydrochloric acid (37% aqueous solution), tetraethyl orthosilicate (TEOS, 99%), and polysorbate 80 (Tween 80) were purchased from Sigma-Aldrich. Synfluid polyalphaolefin (PAO, 2cSt) was purchased

from Chevron Philips Chemical Company LLC and distilled water was supplied by the University of Maryland, College Park. All chemicals were used as received.

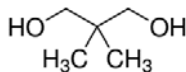


Figure 5-1. Molecular structure of neopentyl glycol (NPG) [178].

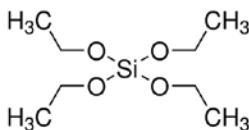


Figure 5-2. Molecular structure of tetraethyl orthosilicate (TEOS) [178].

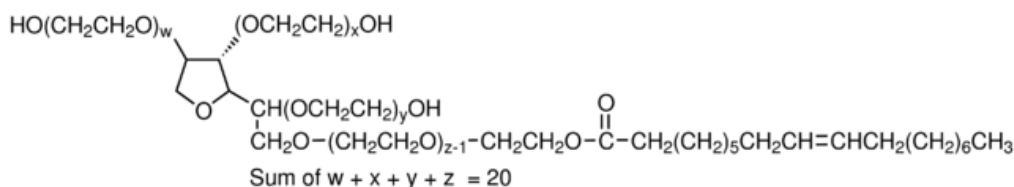
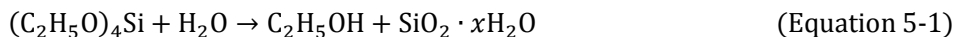


Figure 5-3. Molecular structure of polysorbate 80 (Tween<sup>®</sup> 80) [178].

### 5.2.2 Synthesis of the MicroPCMs

The method of preparing hollow or porous silica microspheres by hydrolysis of TEOS in W/O emulsion has been reported by O'Sullivan et al. [56] and Wang et al. [197]. This method was modified to synthesize NPG/silica microPCMs in this work. Highly concentrated ( $\geq 75$  wt%) NPG aqueous solution with HCl was used as the water phase in W/O emulsions. The silica hollow spheres are formed by the hydrolysis of TEOS, as given by



Due to the hydrophobic precursor TEOS and the hydrophilic product silica, the hydrolysis reaction of TEOS occurs at the interface between aqueous droplets and the bulk cyclohexane. During the reaction, water in the aqueous solution is consumed by the hydrolysis of TEOS. The cores in the as-produced microcapsules are composed of a mixture of NPG, HCl, water, and ethanol, which are later removed.

A typical synthesis procedure is described as follows. An aqueous solution of NPG with hydrochloric acid is used as water phase, while cyclohexane is the oil phase. In a typical preparation procedure, 1.6 g NPG and 0.01 g Tween 80 are dissolved into 0.4 g 20 % HCl aqueous solution, after which the aqueous solution is poured into 250 ml cyclohexane. Vigorous agitation for 10 min is used to create a W/O emulsion, and 1 ml TEOS is then added into the emulsion, which is sealed and stirred for 24 hours at room temperature. The as-produced microcapsules are collected by centrifuge separation, then washed twice with cyclohexane and dried in a vacuum oven to remove residue. The microPCMs are dispersed into PAO later to make phase changeable heat transfer fluids.

To compare with microPCMs, a suspension of micro-sized NPG particles in PAO was also produced. This synthesis was performed by atomizing a mixture of 20 wt% NPG powder in PAO for 1 hour in a sonochemistry equipment, with an atomizer probe controlled by a Sonics VC-750 Ultrasonic Processor. In this preparation, the power of the ultrasonic processor was turned off after 1 minute of atomizing for 30 seconds.

### **5.3 *Characterization of the Solid-Solid MicroPCMs***

#### **5.3.1 Morphologies of the MicroPCMs**

The electron microscope images of NPG/silica microPCMs are shown in Figure 5-4a and c. It can be seen that these microcapsules are spherical in shape with a smooth surface. The diameter of these microcapsules is in the range of 0.2-4  $\mu\text{m}$ , with an average diameter of 1.0  $\mu\text{m}$ . The NPG/silica microcapsules have a relatively larger size distribution than the silica microspheres in literatures [56, 197], due to the high viscosity of the NPG solution as aqueous phase in the emulsion.

The encapsulated NPG can be removed by boiling in water in a sealed autoclave at 150°C for 24 hours. After removing NPG from the microPCMs, silica spheres collapse as shown in Figure 5-4b and d. The shrinkage of the silica spheres is probably due to the thinness of silica layer, as shown in Figure 5-4d.

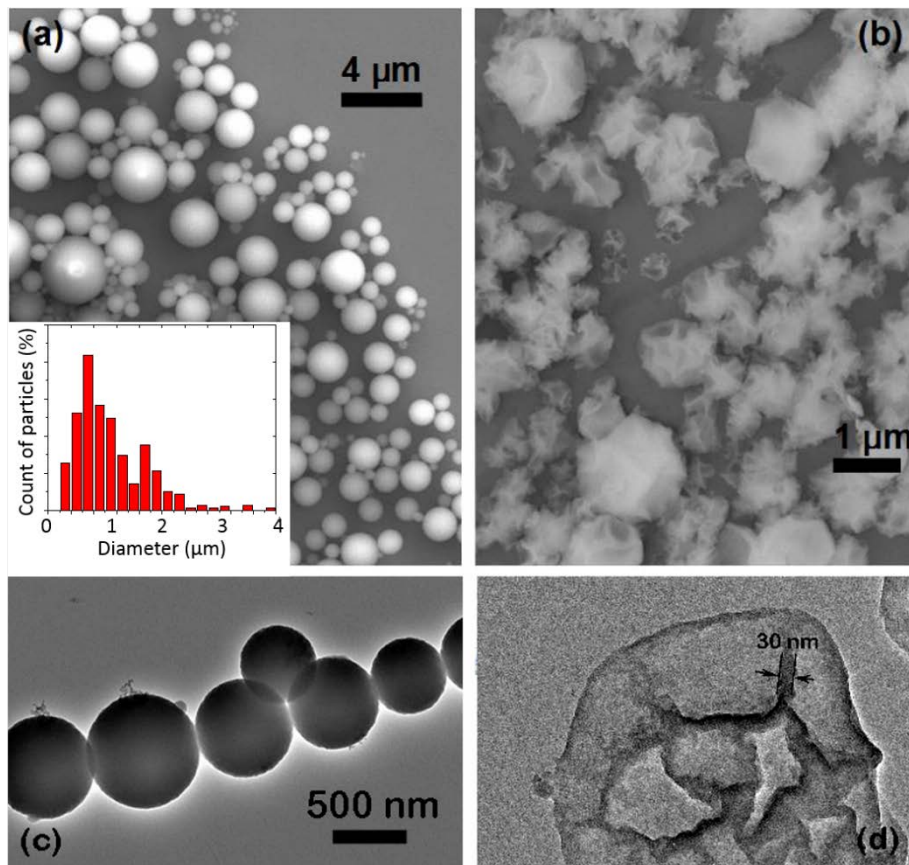


Figure 5-4. Images of as-synthesized microcapsules of NPG in silica shell: a) SEM, c) TEM, and wrinkled silica shell after NPG is removed: b) SEM, and d) TEM. Inserted in a) is a histogram of the particle size distribution from 0 to 4 μm [66].

### 5.3.2 Chemical Composition of the MicroPCMs

FT-IR spectra of NPG/Silica microPCMs were measured to analyze their chemical composition. Figure 5-5 shows the FT-IR spectra of pure silica synthesized by the emulsion method, pure NPG, and the microcapsules comprising NPG encapsulated in silica shell. The FT-IR spectrum of pure silica is characterized by Si-O-Si linkage at 1070, 940, and 800  $\text{cm}^{-1}$ ,

and a broad band around 2850 - 3000  $\text{cm}^{-1}$  due to the O-H stretch of silanol [198]. The peaks in the spectrum of pure NPG correspond to the stretch of C-C, C-H, C-O, and O-H bonds [199]. The spectrum of the microcapsules (curve 5-5c) has all the essential spectral characteristics of both NPG and silica in curves 5-5a and b, respectively.

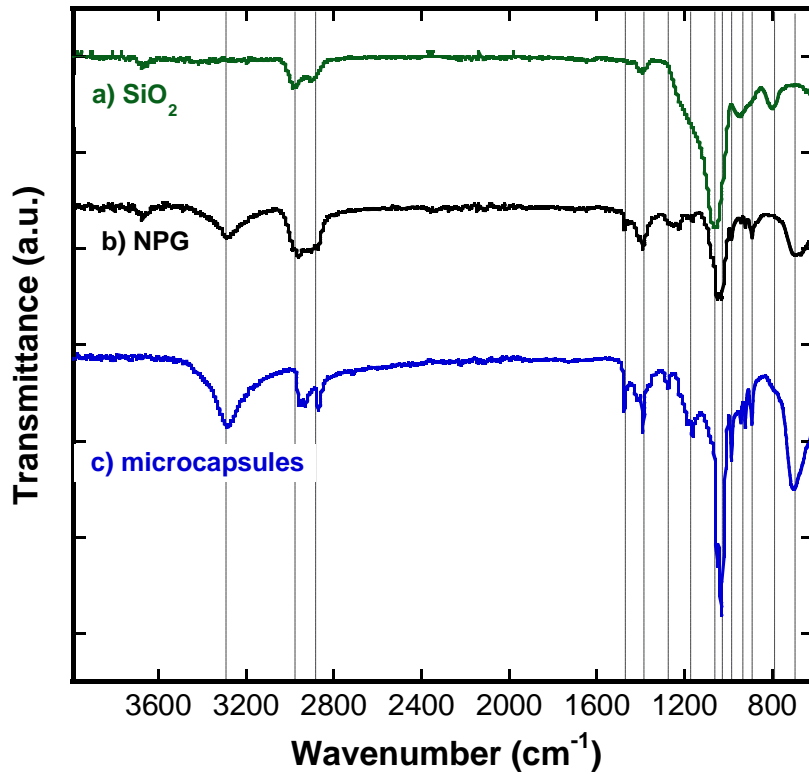


Figure 5-5. FT-IR spectra of sample a) silica, b) NPG, and c) microcapsules as synthesized [66].

Table 5-2. Index of the absorption peaks in the FT-IR spectra of silica [198-200], NPG [199, 201, 202], and the NPG/silica microPCMs.

IR Wavelength (cm-1)	Bond	Appears in FT-IR curves of		
		SiO2	NPG	microPCM
3700	O-H, stretch, absorbed water	√	√	
3300	O-H, stretch, hydroxyl		√	√
3000 - 2850	C-H, stretch, methyl		√	√

1650	H-O-H, bending, absorbed water	√		
1450	H-C-H, bending, methyl		√	√
1350	C-H, bending, methyl	√	√	√
1250	C-O, stretch, hydroxyl		√	√
1180	C-C stretch	√	√	√
1100	Si-O-Si, stretch C-O, stretch, hydroxyl	√	√	√
950	Si-O-H, bending	√		√
900	impurities		√	√
800	Si-O, stretch	√		√
720	H-C-H, bending		√	√

### 5.3.3 Phase Change Behavior the MicroPCMs

Knowledge of the phase change behavior of the solid-solid microPCMs is critical for their applications. Phase change behavior of the PAO-based heat transfer fluids containing pure NPG micro-particles and NPG/silica microcapsules was investigated using DSC. As shown in Figure 5-6, latent heat of bulk NPG is 124.0 J/g and the phase transition initiates at 39.1 °C, in agreement with literature values [192, 203]. Corresponding to the solid-solid phase transition from monoclinic phase to cubic phase, the broad endothermic peak is due to the slow heat transfer rate between in bulk NPG sample. During cooling, the exothermic peak of bulk NPG initiates at  $T_{C-M,bulk} = 27.7$  °C, which corresponds to the cubic-to-monoclinic transition. The supercooling observed in bulk NPG is 11.4 °C.

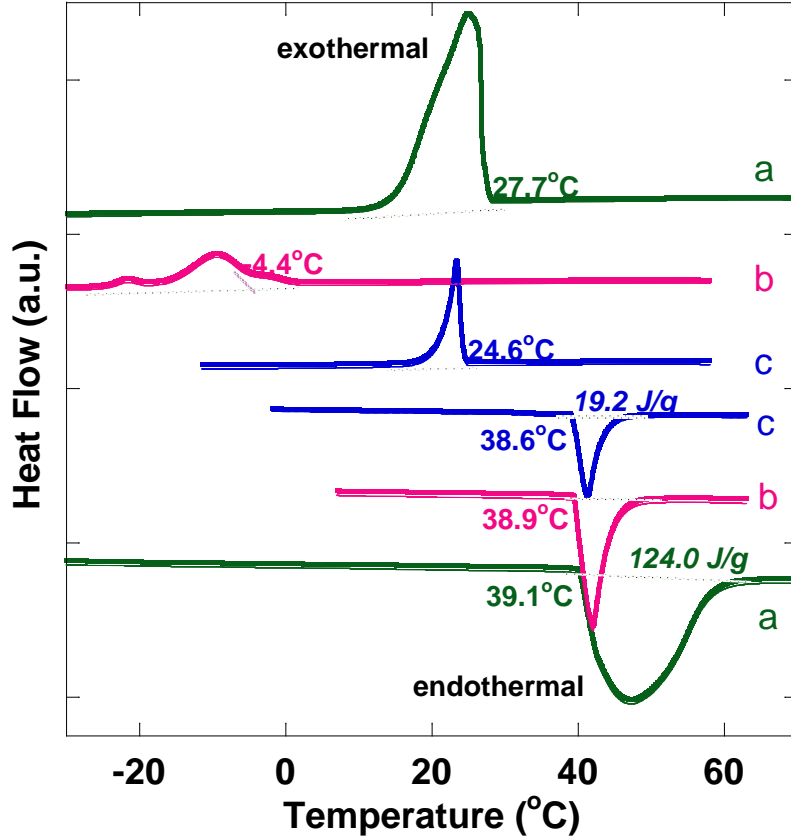


Figure 5-6. DSC heating and cooling curves of samples, a) pure, bulk NPG, b) dispersions of 20 wt% pure NPG micro-particles without encapsulation in PAO, and c) dispersions of 20 wt% NPG/silica microPCMs in PAO [66].

During cooling, NPG micro-particles release the stored thermal energy with the cubic-to-monoclinic transformation at much lower temperature  $T_{C-M,particle} = -4.4\text{ °C}$  than bulk NPG. The supercooling difference observed between bulk and micro-sized NPG can be explained by classical nucleation theory [81, 204]. Probability of homogeneous nucleation to initialize the phase transition,  $J(T)$ , is proportional to PCM volume  $v$ :

$$J(T) = \begin{cases} v\kappa(T) \exp\left(-\frac{B}{T(T-T_{m-c})^2}\right) & \text{for } T < T_{M-C} \\ 0 & \text{for } T \geq T_{M-C} \end{cases} \quad (\text{Equation 5-2})$$

where  $B$  is a coefficient associated with the supercooled substance, and  $T_{M-C}$  is the phase transition temperature of NPG from low temperature monoclinic phase to high temperature

cubic phase. The pre-exponential term  $\kappa(T)$  varies much slower with temperature than the exponential term, and thus can be considered as a constant [81, 205]. For samples with the same chemical composition and crystalline structure, reduction in sample volume leads to smaller probability of homogeneous nucleation and hence larger supercooling. It should be noted that the interface between NPG and PAO provides no heterogeneous nucleation sites for the PCM. The supercooling observed in this dispersion of pure NPG micro-particles in PAO is about 43.3°C, too large relative to the operation temperature range in typical TES and heat dissipation systems.

In contrast, supercooling of NPG was suppressed significantly in NPG/silica microPCMs. It is evident in Figure 5-6 that the supercooling in NPG-silica microcapsules has been reduced to 14.0 °C. Silica provides heterogeneous nucleate sites for the cubic-to-monoclinic phase transition, which reduce the activation energy of nucleation at the inner surface of silica, resulting in the suppressed supercooling.

### 5.3.4 Specific Heat of Fluids Containing the MicroPCMs

By dispersing NPG microcapsules in traditional heat transfer fluids such as PAO, the fluid heat capacity can be significantly increased. Given an operation temperature range  $\Delta T$  ( $\Delta T = T_1 - T_0$ ), the effective specific heat of a heat transfer fluid  $C_{TF}$  can be estimated by [52, 53, 206]

$$C_{TF} = (1 - x_{PCM})C_{BF} + \frac{q}{\Delta T}x_{PCM} \quad (\text{Equation 5-3})$$

in which  $C_{BF}$  is the specific heat of the base fluid,  $q$  is the overall heat capacity per unit mass of the PCM, and  $x_{PCM}$  is the weight ratio of the corresponding PCM in the heat transfer fluid. Measured with DSC, the latent heat capacity of NPG/silica microcapsules was found to be  $\Delta h_{microPCM} = 96.0$  J/g. By comparing  $\Delta h_{microPCM}$  with the latent heat of bulk NPG,  $\Delta h_{NPG} = 124.0$  J/g, the content of NPG in the microPCMs is calculated 77 wt%. Given the minimum

effective operation temperature range  $\Delta T = 14.0\text{ }^{\circ}\text{C}$ , the overall heat capacity  $q$  of the microPCMs is the sum of  $\Delta h_{microPCM}$  and the sensible heat over the operation temperature range.

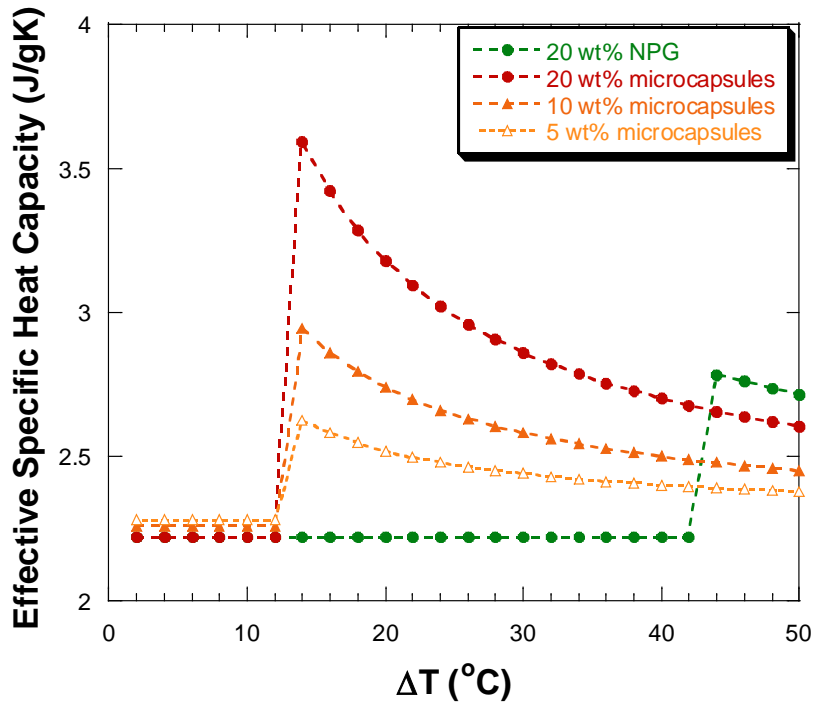


Figure 5-7. Estimated effective specific heat capacity of the PAO-based heat transfer fluids with pure NPG particles and NPG/silica microPCMs in various  $x_{PCM}$  [66].

Effective specific heat of the microcapsules,  $\frac{q}{\Delta T} = 8.8\text{ J/gK}$ , is considerably larger than the specific heat of PAO ( $C_{PAO} = 2.3\text{ J/gK}$ ). Thus, a remarkable elevation of heat capacity can be expected by adding microPCMs in PAO. As shown in Figure 5-6c, with 20wt% of the microcapsules in PAO, the overall heat capacity elevation is 19.2 J/g, and effective specific heat increases by up to 56% from 2.3 J/gK to 3.6 J/gK when the operation temperature range is limited to 14 K. The estimated elevation of effective specific heat of the heat transfer fluids with the addition of microPCMs are shown in Figure 5-7. It should be mentioned that the operation temperature range cannot be decreased without limitation. As described in Chapter

1, to utilize the latent heat of the PCM sufficiently, the lower boundary of the operation temperature range should be lower than the freezing point of the encapsulated PCM, and the upper boundary should be higher than the melting temperature.

### 5.3.5 Viscosity of PAO Fluids Containing the MicroPCMs

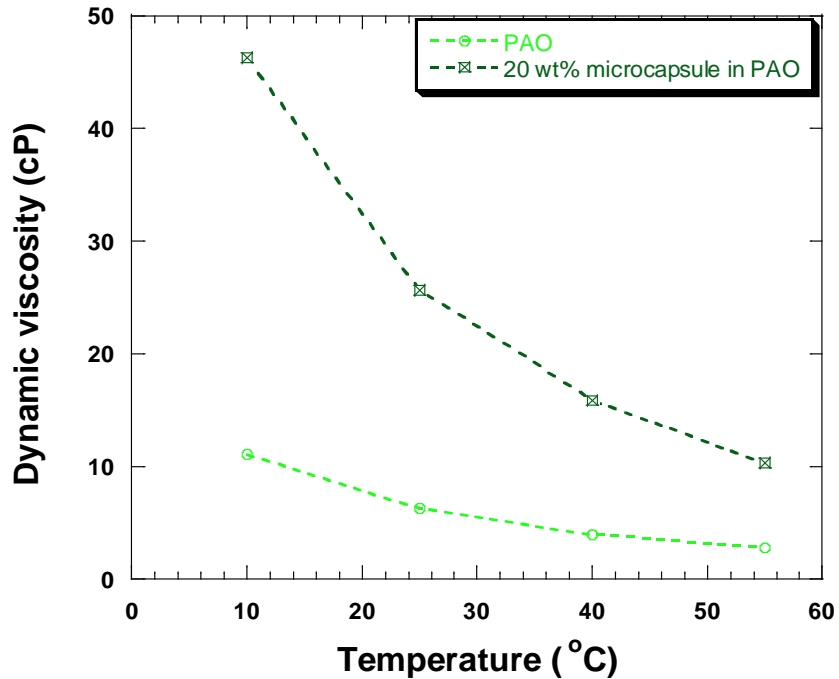


Figure 5-8. Dynamic viscosities of pure PAO and the dispersion of 20 wt% microcapsules in PAO vs temperature [66].

Viscosity of pure PAO and suspension of 20 wt% microcapsules in PAO were measured in the temperature range of 10 - 55 °C. From Figure 5-8, the viscosity of pure PAO was found to decrease with increasing temperature, in good agreement with literature values [207]. Additionally, the viscosity of pure PAO and the phase change fluid were measured at various spindle rotational speeds and exhibited a shear-independent characteristic of Newtonian fluids. It should be noted that in applications to heat transfer systems, a trade-off of

increased pumping power is likely, due to the expected viscosity increase with the addition of particles in heat transfer fluids.

#### **5.4 Summary**

Microcapsules comprised of solid-solid PCM NPG encapsulated in silica were successfully synthesized using an emulsion technique. Size of the microcapsules is in the range of 0.2 - 4  $\mu\text{m}$ . Phase change behavior of the NPG/silica microPCMs as well as pure NPG micro-particles in PAO was investigated with DSC. A large supercooling of about 43.3  $^{\circ}\text{C}$  was observed in pure NPG micro-particles, due to the small volume of the PCM and the associated small probability of homogeneous nucleation. In microPCMs on the other hand, it was found that the silica encapsulation can reduce the supercooling to about 14  $^{\circ}\text{C}$  by providing heterogeneous nucleation sites on the silica frame. Latent heat of the microPCMs is 96.0 J/g, implying a PCM loading of 77 wt% in the composite. The NPG microcapsules can be added to heat transfer fluid to enhance its heat capacity.

It is important to emphasize that the silica-induced heterogeneous nucleation provides an alternative route to the supercooling suppression of microPCMs. Different from conventional supercooling suppression methods, no additional nucleate agent is required as an additive into the PCMs, and thus overall latent heat of microPCMs remains high. In addition, unlike nucleate sites generated by adding nucleate agents in PCMs, the distribution of nucleate sites on the shell or matrix is uniform and stable, and thus better durability can be expected. This method is further applied in another type of microPCMs with manipulable shell polymeric structure in next chapter for the purpose of supercooling suppression.

## Chapter 6. Microencapsulated Liquid-Solid PCMs

### 6.1 Introduction

PCMs have been promising in wide applications because latent heat storage provides much higher energy density comparing with sensible heat storage [5, 6, 8, 17, 53, 57, 91, 196, 208-211]. With their own advantages and disadvantages, different types of PCMs find different industrial applications in various fields from textile to building materials. Paraffin, the n-alkanes ( $C_nH_{2n+2}$ ) with different numbers of carbon atoms in their molecular chain, is a type of PCMs widely used as core material of microcapsules [5, 6, 209, 211-213] because of their appropriate phase transition temperature, large latent heat of fusion, chemical stability, and capability of being microencapsulated, as discussed in the previous chapter.

MicroPCMs have been studied extensively as a route to avoid the possible interaction between PCM and surroundings. Stated in Chapter 1 and 2, one of the common problems microPCMs is the supercooling, i.e., the hysteresis of liquid-solid phase transition. This problem is more serious in microPCMs than in bulk PCMs, because homogeneous nucleation in the confined volume of a microcapsule happens randomly in a less preferred probability. As a result, the hysteresis of nucleation and phase transition from high-temperature phase to low-temperature phase is more significant, which represents as larger supercooling of microPCMs macroscopically.

Based on nucleation theory, supercooling occurs because of the energy barrier of homogeneous or heterogeneous nucleation. The energy barrier of homogeneous nucleation without nucleate agents is much higher than heterogeneous nucleation [150], as shown in Equation 6-1:

$$\Delta G_{heterogeneous} = \Delta G_{homogeneous} \left( \frac{1}{2} - \frac{3}{4} \cos \theta + \frac{1}{4} \cos^3 \theta \right) \quad (\text{Equation 6-1})$$

where  $\theta$  is the contact angle between PCM and nucleate agent, representing their structure similarity. With the addition of similarly structured nucleate agents,  $\Delta G_{heterogeneous}$  can be suppressed approaching zero, hence the supercooling of PCM is eliminated.

Researches have been working on controlling the supercooling of microPCMs since 1990s [41, 42, 44, 88, 151]. The most common and practically applicable method is by using nucleation agents, such as high melting point paraffin or alcohol and solid nanoparticle, to promote heterogeneous nucleation for liquid-solid phase transition. These efforts are summarized and listed in Table 2-1. The main disadvantage of this method is that the effective latent heat of microPCMs is reduced due to the relatively large amount of additives. This additives may also change other thermophysical properties of the PCMs, such as melting point and thermal stability.

In last chapter, we found that supercooling of NPG micro-particles can be suppressed with the encapsulation of silica. In this microPCMs, silica serves not only as structural material to support and protect the PCM encapsulated, but also as nucleate agent to provide heterogeneous nucleate sites for phase transition[66]. That way, supercooling can be suppressed to without using additives as nucleate agents. It is reasonable to apply this method to paraffin-based microPCMs to suppress their supercooling induced by microencapsulation.

In this chapter, a type of paraffin/polymer microPCMs comprising octadecane encapsulated in melamine-formaldehyde resin (MFR) shell is reported. This type of microPCMs was synthesized in an O/W emulsion system through an in-situ polymerization process. Meanwhile, supercooling suppression making use of MFR shell of this type of microPCMs is investigated in this chapter, in which the structure of MFR shell are manipulated to approach the structure of encapsulated paraffin in solid state to provide nucleate sites for the

liquid-solid phase transition. This way, energy barrier to heterogeneous nucleation on the inner wall of the shells can be lowered, and so as to the supercooling.

## **6.2 *Synthesis of the Liquid-Solid MicroPCMs***

### **6.2.1 The Selection of PCM Material**

There are various PCMs commercially available for industrial applications. Among the commercial PCMs, paraffin is the most widely studied for applications to microPCMs, due to the great chemical stability, small supercooling in bulk phase, suitable phase transition temperature, and compatibility for various encapsulation methods [5, 15, 39, 43-47, 54, 61-63, 86-88, 128, 131-133, 139-142, 145, 146, 151, 214-216].

n-octadecane ( $C_{18}H_{38}$ ,  $CH_3(CH_2)_{16}CH_3$ ) is selected as the PCM for this research because of its proper thermophysical and chemical properties [4-6, 29, 31, 48, 57, 217]. Its melting point is around 27 °C, which is proper for the applications of in-door thermal management. It has high latent heat of fusion (241 J/g) and stable phase transition properties, which is essential for PCM applications. In addition, n-octadecane is not soluble in water in either liquid or solid state, which makes it suitable to be encapsulated using the widely used in-situ polymerization process [41, 46, 47, 57, 61-63, 88, 128-134, 139-142, 145, 146]. As a result, n-octadecane is widely used in building materials, textiles, and air-conditioning systems for thermal management in human comfort zone [17, 19, 55, 57, 61, 62, 129, 131, 132, 139-141, 151].

### **6.2.2 The Selection of Shell Material**

MFR is notable for its complex polymeric structure that is widely used in microencapsulation of various materials [135, 136, 218]. The complex structure is determined both by the degree of crosslink among the triazine rings in the polymer molecules and the ratio

of the two different ways of bridging between two neighbor triazine rings, as shown in Figure 6-1. For encapsulated PCMs with MFR, some of the polymeric wall surface structure may fit the requirement of heterogeneous nucleation, i.e., MFR wall may work as nucleate agents to suppress supercooling of encapsulated PCM. Given a certain MFR structure, the larger the interfacial area between MFR inner wall and encapsulated PCM, the larger possibility the proper nucleate sites found on the interface. This is probably the reason of the coincidence between PCM content and supercooling.

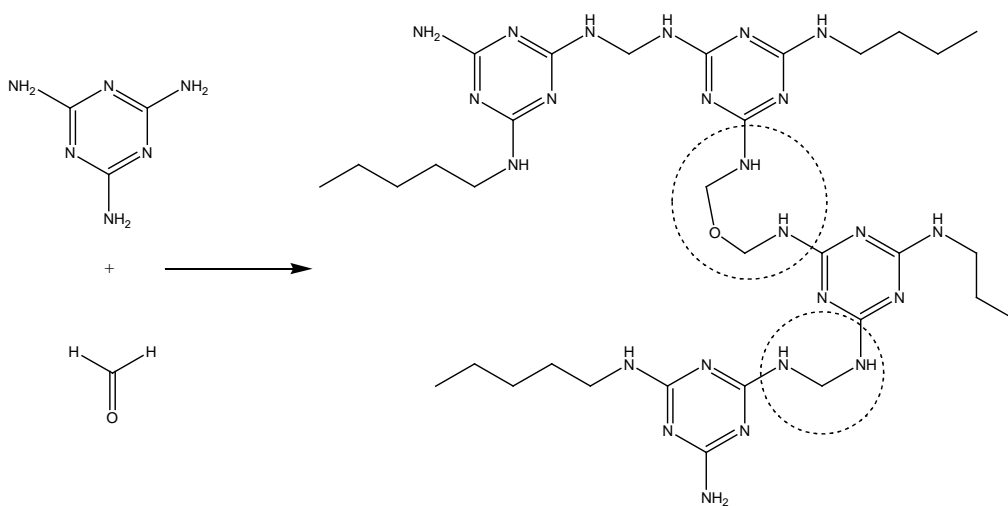


Figure 6-1. Molecular structure of melamine and formaldehyde, and the polymeric structure of melamine-formaldehyde resin. Two types of bridges (etheric bridge (-C-O-C-) and methylene bridge (-C-), as circled) in the figure can be formed between two melamine rings, depending on the reaction environment of the polymerization [206].

The formation of the bridges between melamine rings depends on the reaction environment of polymerization. By manipulating parameters of polymerization and encapsulation, the structure of polymeric wall of microPCMs can be optimized for heterogeneous nucleation of encapsulated paraffin. Meanwhile, by using proper composition of precursors, changing of wall structure hardly decrease the paraffin content in the microPCMs.

This way, the objectives of suppressed supercooling and maintained heat capacity can possibly be achieved mutually.

### 6.2.3 Synthesis of the Paraffin/MFR MicroPCMs

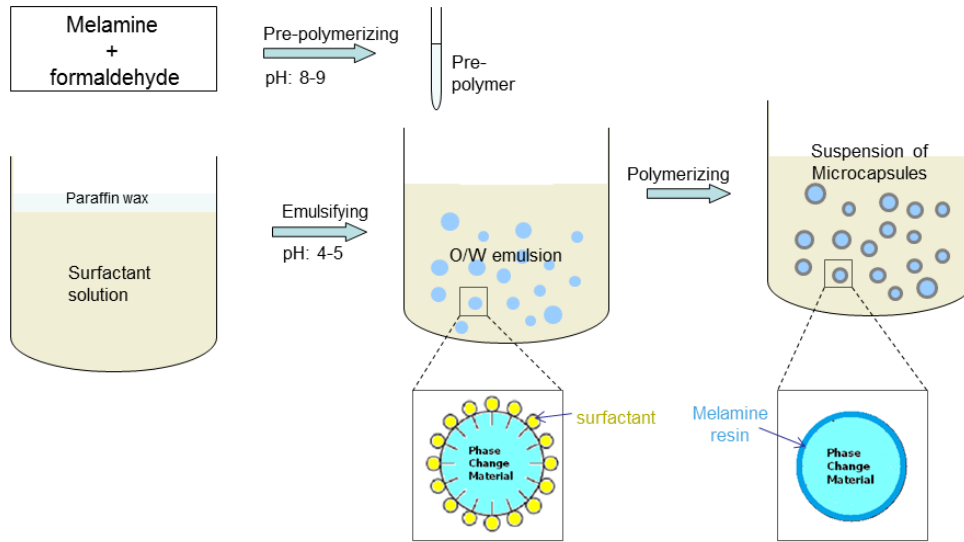
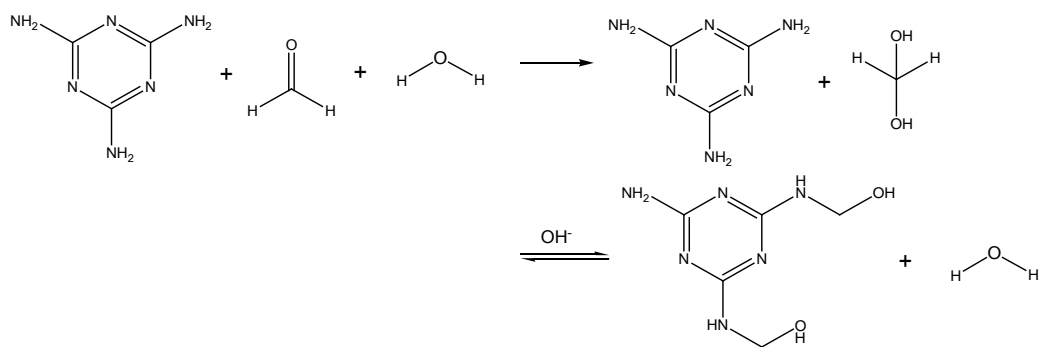


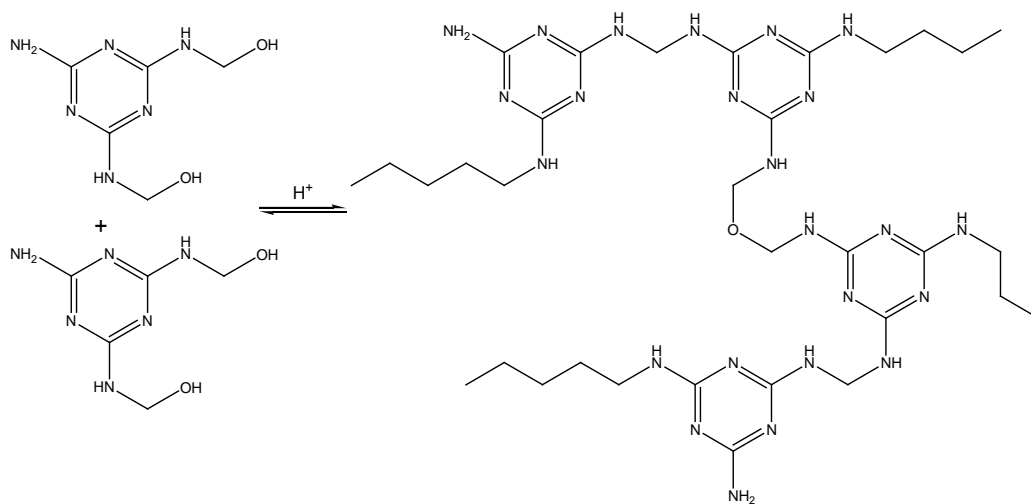
Figure 6-2. The chemical route for the fabrication of paraffin/MFR microPCMs [65].

The paraffin/MFR microcapsules were synthesized following an in-situ polymerization method [41, 57, 61, 88, 128-131, 133, 134, 145, 146]. The chemical route for fabrication of microPCMs is illustrated in Figure 6-2. Typically, to produce pre-polymer for the in-situ polymerization, 1 g of melamine and 1.25 g of 37% formaldehyde are added into 5 ml of distilled water. The pH of the mixture is adjusted to 8.5 with diluted trimethylamine solution. The mixture is kept at 70 °C for 30 minutes until it turns clear and transparent, and the pre-polymer solution is produced after the melamine-formaldehyde pre-condensation reaction shown in Equation 6-2 in a basic environment:



(Equation 6-2)

Meanwhile, 1 g of paraffin is added in 20 ml of distilled water with 0.2 g sodium dodecyl sulfate (SDS) as a surfactant, and then the pH of the aqueous phase is adjusted to 4 with acetic acid (HAc). The mixture is heated to 60 °C to control the reaction rate, emulsified for several minutes, after which 2 g of the as-produced pre-polymer solution is added in. The mixture is stirred at 60 °C for 3 hours to allow the following reaction happen on the interface of paraffin droplets and bulk aqueous phase:



(Equation 6-3)

Microencapsulation undergoes in this process by in situ polymerization of the pre-polymer in an acidic environment, in which MFR shell is formed and condensed on the surface

of n-octadecane droplets. The final fluid is filtered and the solid white product is washed with distilled water and acetone, and then dried at 60 °C overnight.

For preparation of different samples, the parameters of the synthesis may vary. Table 6-1 shows a list of samples with their synthetic parameters.

Table 6-1. List of melamine-resin-shelled microPCM samples [65].

Sample No.	F:M* weight ratio	pH of pre-polymer	Concentration of HAc in emulsion
MC01	2.00	8.30	1.50 ml/L
MC02	1.50	8.30	1.50 ml/L
MC03	1.30	8.30	1.50 ml/L
MC04	1.25	8.30	1.50 ml/L
MC05	1.25	8.00	1.50 ml/L
MC06	1.25	8.25	1.50 ml/L
MC07	1.25	8.50	1.50 ml/L
MC08	1.25	8.75	1.50 ml/L
MC09	1.25	9.00	1.50 ml/L
MC10	1.25	8.50	0.75 ml/L
MC11	1.25	8.50	1.00 ml/L
MC12	1.25	8.50	1.25 ml/L
MC13	1.25	8.50	1.38 ml/L
MC14	1.25	8.50	1.50 ml/L
MC15	1.25	8.50	1.75 ml/L

\*: formaldehyde : melamine

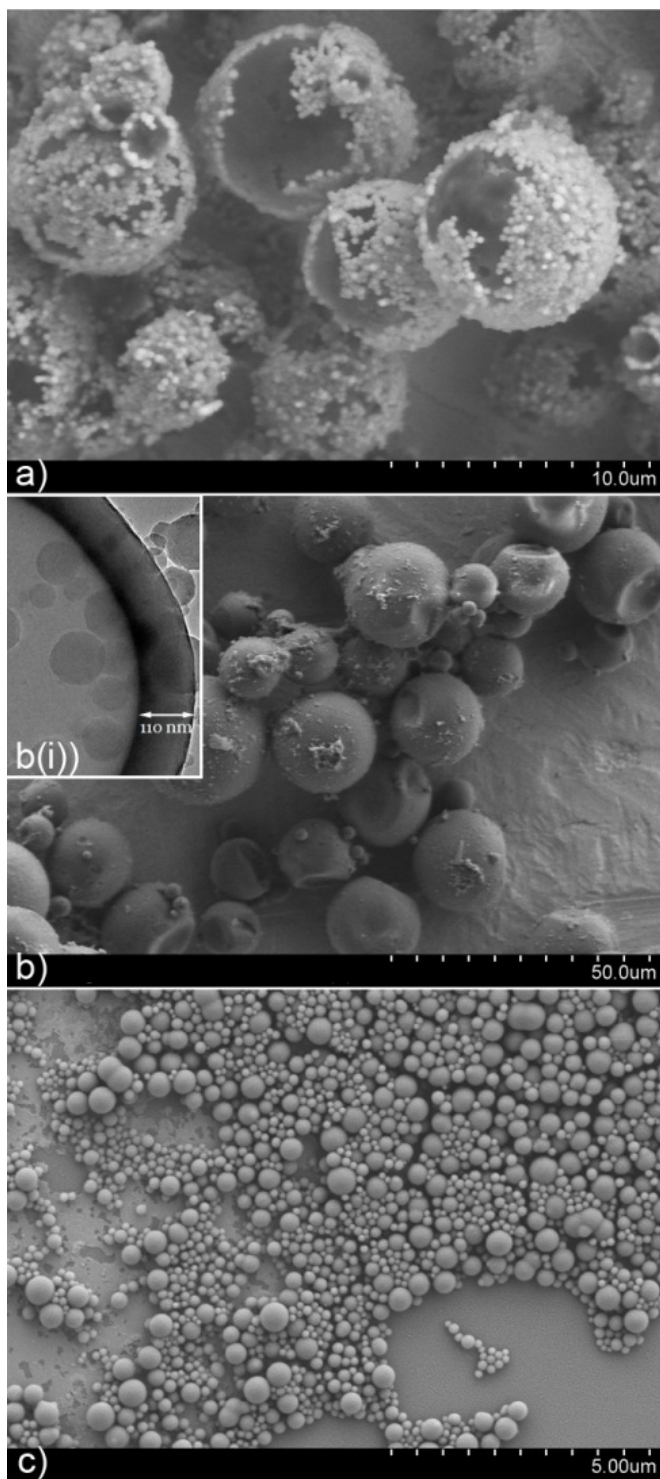


Figure 6-3. SEM and TEM images of the microcapsules with octadecane encapsulated in the melamine-formaldehyde resin shell [65]. a) SEM image of the sample produced with 50 g/L SDS. b) SEM and TEM (inserted) image of the sample prepared with 10 g/L SDS. The insert is a TEM image showing the shell thickness. c) micro/nanoparticles in filtrate.

## 6.3 Characterization of the Liquid-Solid MicroPCMs

### 6.3.1 Morphology and Microstructure of the MicroPCMs

SEM and TEM images of the paraffin/MFR microPCMs are shown in Figure 6-3. It can be found in Figure 6-3a and b that the concentration of surfactant SDS is critical for the formation of microcapsules. Hollow spheres with porous shells, rather than solid resin shell, are formed when the SDS concentration is relatively high, e.g., 50 g/L in emulsion, as shown in Figure 6-3a. The raspberry-like porous shells are made of nanosized spheres grown in the aqueous phase. When SDS concentration drops to 10 g/L, octadecane microcapsules with solid resin shell are formed, as shown in Figure 6-3b. These microcapsules have a diameter ranging from 5  $\mu\text{m}$  to 15  $\mu\text{m}$ , and their resin shell is about 110 nm in thickness. Figure 6-3c shows the submicron resin spheres without octadecane encapsulated, which indicates polymerization reaction occurs not only at the water-oil interface, but also inside the aqueous phase. Thus, excessive amount of melamine-formaldehyde precursors are required in encapsulating octadecane oil in order to compensate the consumption of the polymerization in aqueous phase.

It is interesting that sunk dimples show up on the microcapsules. Origin of these dimples is due to temperature effect on the volume of encapsulated octadecane. The microcapsules are synthesized at a moderate temperature of around 60  $^{\circ}\text{C}$ ; at this temperature as well as other experimental parameters, melamine formaldehyde resin produced in the *in-situ* polymerization process condenses on the surface of octadecane droplets. Due to the effect of surface tension, at the formation of the microcapsules, it should be shaped as microspheres. It is well known that the thermal expansion coefficient of n-octadecane is considerably large (around  $8 \times 10^{-4} \text{ K}^{-1}$ ) during the phase transition [219]. When temperature of the microcapsules drops to room temperature, a volume change of about 3% can be expected on the encapsulated octadecane. As it is not a firm shell of the resin, a volume change of core

material is represented by a shape reformation of the microcapsules, which resulting the occurrence of the dimples on the surface.

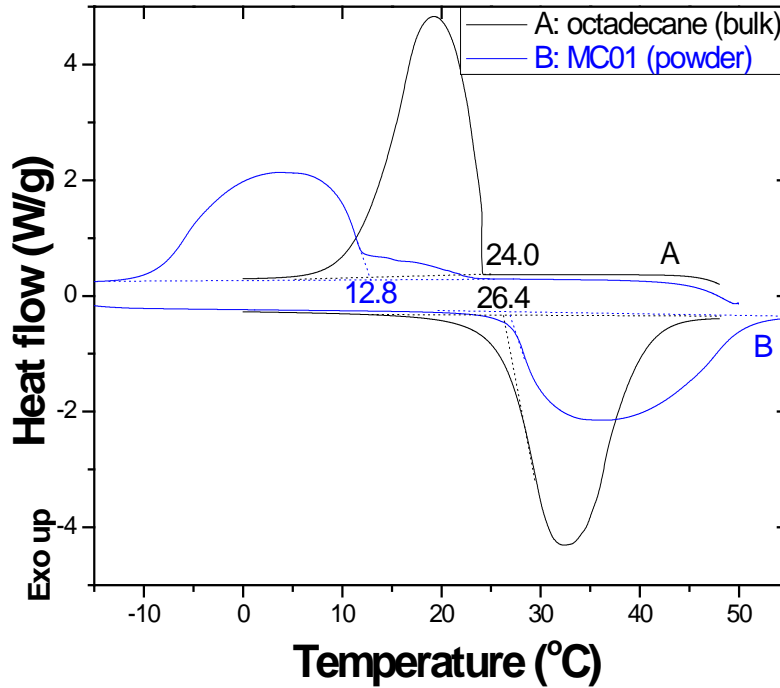


Figure 6-4. DSC curves of a) pure n-octadecane and b) powder of sample MC01, the “raw” microPCMs before suppression of supercooling [65]. Heating and cooling rate of the DSC is 10 °C/min.

### 6.3.2 Thermophysical Properties of the MicroPCMs

Figure 6-4 shows the DSC curves of both pure and microencapsulated n-octadecane. The melting point of pure octadecane is measured as 26.4 °C, while the latent heat of fusion  $\Delta h_{octadecane}$  is 241.0 J/g. The freezing temperature of bulk octadecane is 24.0 °C, by calculation resulting to a small supercooling  $\Delta T_{sc,octadecane} = 2.4$  K is found in pure n-octadecane. For “raw” microPCM sample MC01, however, the freezing temperature is significantly lower at 12.8 °C, resulting to a much larger supercooling  $\Delta T_{sc,MC01} = 13.6$  K.

This value is very close to the homogeneous nucleation temperature of n-octadecane [214]. The reason of this large supercooling is the lack of heterogeneous nucleation site in the confined volume of each microcapsule.

The weight fraction of phase change octadecane can be estimated according to the following equation,

$$\text{PCM}\%_m = \frac{\Delta h_{\text{microPCM}}}{\Delta h_{\text{octadecane}}} \times 100 \quad (\text{Equation 6-4})$$

where  $\Delta H_{\text{octadecane}}$  and  $\Delta H_{\text{microPCM}}$  are the latent heat of fusion of the pure octadecane and the microPCMs, respectively. From the DSC curve of sample MC01, it is read 213 J/g. As a result, the weight fraction of octadecane in the microPCMs is 88.4%.

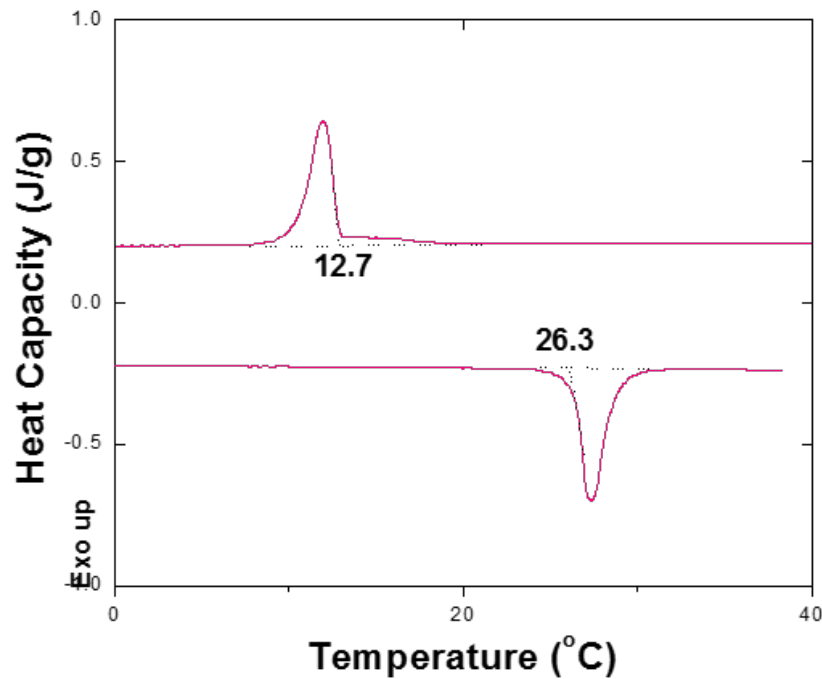


Figure 6-5. Complete DSC curve of sample MC01, dispersed in PAO [65]. Significant supercooling can be found in the curve, from which a degree of supercooling of 13.6 °C can be calculated.

## 6.4 Supercooling Suppression by Shell Optimization

The structure of MFR shell can be manipulated to approach the structure of the encapsulated paraffin in solid state and provide nucleate site for the liquid-solid phase transition. By controlling the parameters of the polymerization and encapsulation, including the ratio of precursors, the pH values of the solutions for pre-polymerization and polymerization, the structure of polymeric wall of the microPCMs made of melamine-formaldehyde resin can be optimized for heterogeneous nucleation of the encapsulated paraffin, and thus suppress the supercooling without extra additives as nucleate agents.

### 6.4.1 Effect of the Ratio of Precursors

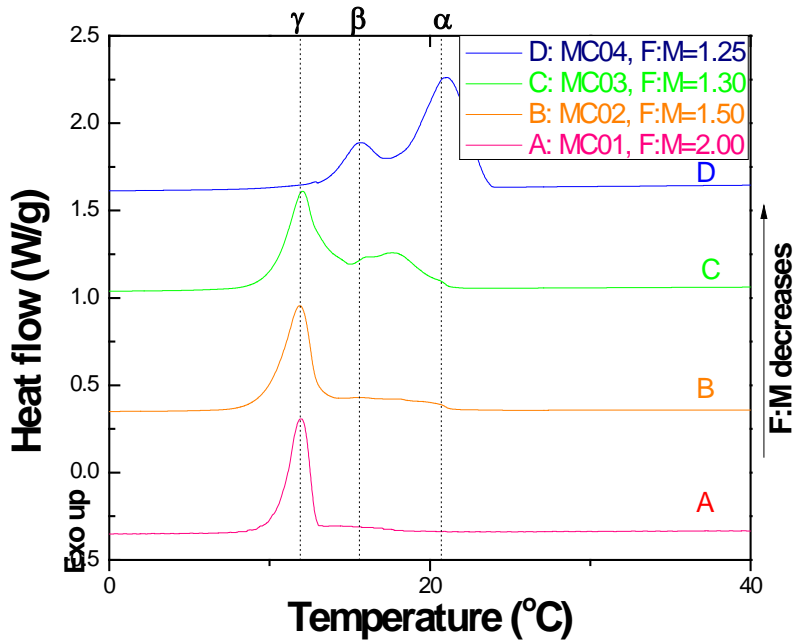


Figure 6-6. DSC freezing curves of samples MC01-04 with various F:M ratio in precursors [65]. Curves are shifted along Y axis.

Figure 6-6 shows the DSC curves of octadecane microcapsules synthesized with various formaldehyde to melamine (F:M) ratio in the precursor. The DSC heating curves are

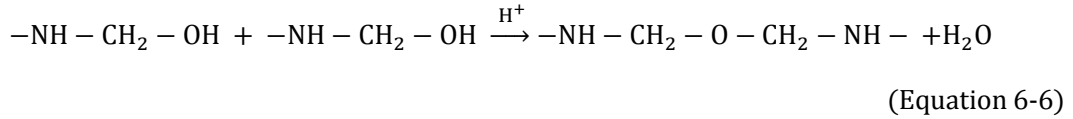
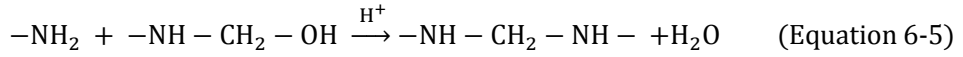
not shown since the melting temperatures of the microencapsulated octadecane are little different in shape from those of the bulk.

Three peaks are observed on the DSC cooling curves of these microcapsules, labeled  $\alpha$ ,  $\beta$ , and  $\gamma$ , from high to low temperatures. Peak  $\gamma$  can be attributed to the transition from liquid octadecane to the thermodynamically-stable triclinic crystal phase based on homogeneous nucleation. The homogeneous nucleation occurs at a supercooling as large as 13.6 °C due to the lack of nucleation sites in the microcapsules. The appearance of peak  $\alpha$  and  $\beta$  implies that the microencapsulated octadecane follows a two-step phase transition mechanism, liquid-rotator phase transition (peak  $\alpha$ ) and rotator-triclinic phase transition (peak  $\beta$ ) [151]. The peak  $\alpha$  also include the contribution from the direct liquid-triclinic phase transition induced by the heterogeneous nucleation at the shell. The rotator phases of alkanes are often observed in confined geometry such as microcapsules, which are weakly-ordered crystalline phases that lack long-range order with respect to rotation about the long axis of the molecules [41, 86, 214, 220, 221].

It can be seen in Figure 6-6 that the homogeneous nucleation, and thus the supercooling, can be efficiently suppressed in the octadecane microcapsule when the F:M ratio in the precursor is fixed at 1.25. Previous studies have found that the F:M ratio has little effect on the microcapsule size, but the molecular structure and composition of the resultant resin shell can be significantly different [135, 222]. As different molecular structures of the wall supply different forms of heterogeneous nucleation sites for the encapsulated PCMs, some of the molecular structures on the inner wall of the resin shell could be more suitable than the others to promote the nucleation of the metastable rotator phase or the triclinic crystalline phase.

Two types of functional groups form on the triazine rings of the pre-polymer molecules, the amino groups and the hydroxylmethylamino groups, as described in Equation 6-2. These two functional groups may undergo two different condensation or polymerization reactions in

the acidic environment to form the resin shell, i.e., the amino-hydroxymethylamino condensation and the hydroxymethylamino-hydroxymethylamino condensation:



Meanwhile, some of the functional groups stay suspended during the reaction process due to steric hindrance. The two parallel reactions produce the MFR shell of the microPCMs jointly, as shown in Equations 6-5 and 6-6. Both of the reaction involve at least one hydroxyl methyl group. Apparently, the more hydroxyl methyl groups produced in pre-polymerization, the more condensation reactions happen between the hydroxyl groups and between hydroxyl methyl and amino groups, and thus the larger completeness the crosslink of the MFR polymer. On the other hand, the hydroxyl methyl groups are produced by the reaction of melamine and formaldehyde, as shown in Equation 6-6. In the case of F:M ratio larger than the stoichiometric F:M ratio of the pre-polymerization (i.e., > 1.5), a large number of hydroxyl methyl groups are produced. With this larger production comparing with that of small F:M ratio, more functional groups (including the hydroxyl methyl groups and the amino groups) on the triazine rings are involved in the polymerization process shown in Equation 6-5 and 6-6, which leads to a higher degree of crosslink in the as-produced MFR shell of the microcapsules.

A large supercooling, associated with the liquid-triclinic crystalline transition induced by homogeneous nucleation, is observed in these microcapsules prepared with larger F:M ratio and larger degree of crosslink of the MFR shells. By contrast, the supercooling of crystallization can be largely eliminated when the F:M ratio reduces to 1.25, where the resin shell has lower cross-linking degree and more free-standing amino groups that are not involved

in the polymerization. It is worth noting that further lowering the F:M ratio ( $<1.25$ ) yields instable pre-polymer and no formation of microcapsules.

According to the aforementioned analysis, we could argue empirically that the resin shell with less degree of crosslink and more free-standing functional groups could promote nucleation of the metastable rotator phase and the triclinic phases and thus suppress the supercooling associated with homogenous nucleation. This empirical conclusion is also proven in the discussions in next sections, even though the crystal structure of the MFR shells and the mechanics of the supercooling suppression are not well understood yet.

#### 6.4.2 Effect of pH Values in the Pre-Polymerization Process

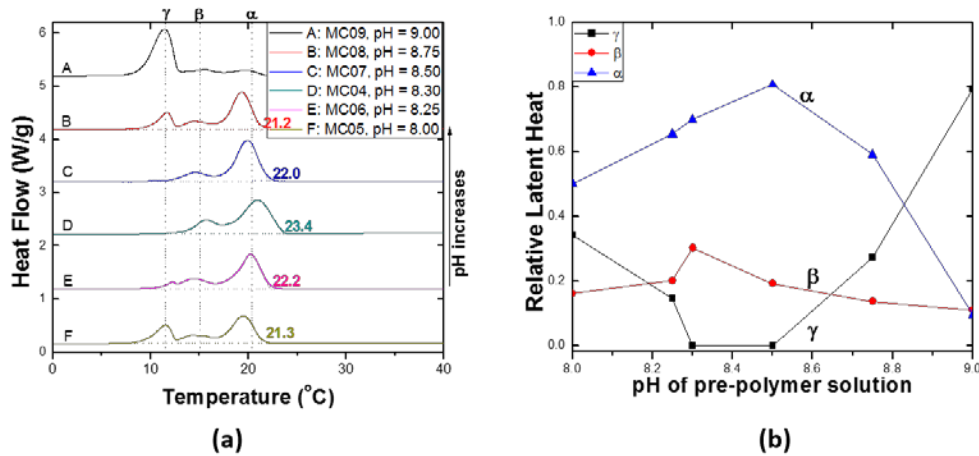


Figure 6-7. a) DSC freezing curves of samples MC04-09 [65]. Curves are shifted along Y axis. b) Relative latent heat of phase transition peaks for various pH values of pre-condensation solution [65].

The pH value in both the pre-polymer solution and the polymerization solution also affects the molecular structure and composition of the melamine formaldehyde resin shells of the microcapsules and thus their phase transition behavior. Both the pH value and F:M ratio control the degree of hydroxylation and the balance between hydroxylated melamine and the precursor melamine and formaldehyde in the pre-polymer solution, as described in Equation 6-

2. Figure 6-7a shows the DSC curves of the octadecane microcapsules prepared with various pH value but constant F:M ratio, and Figure 6-7b lists the relative latent heat of exothermic peaks  $\alpha$ ,  $\beta$ , and  $\gamma$ . The relative latent heat of an exothermic peak is determined as the ratio of its peak area to the total area of three peaks under the DSC curves. It can be seen that the optimum pH value in the pre-polymer is 8.50 where peak  $\gamma$  (and its associated supercooling of homogeneous nucleation) are eliminated and the area of peak  $\alpha$  is maximized. The maximum relative latent heat of phase transition  $\alpha$  is 80.8% while the relative latent heat of peak  $\beta$  is 19.2%, shown in the curve for sample MC07. In addition, the onset temperature of freezing improves from 21.3 °C to 23.4 °C when the pH value tunes from 8.00 to 8.50 at the constant F:M ratio 1.25. This result implies that to minimize the two low-temperature peaks (the homogeneous nucleation freezing peak  $\gamma$  and the rotator-triclinic phase transition peak  $\beta$ ) and so as to maximize the liquid-solid peak  $\alpha$ , a properly cross-linked quasi-linear polymeric structure of MFR is preferred for the nucleation of the solid phase of encapsulated octadecane.

#### **6.4.3 Effect of Acid Concentration in the Polymerization Process**

HAc concentration in the emulsion for polymerization and encapsulation is another parameter that affects the molecular structure and composition of the microcapsule shell and consequently the phase change behavior of n-octadecane. MFR shells are fabricated in this process, as shown in Equations 6-5 and 6-6. The HAc concentration and the resulting pH value in the emulsion have a significant influence on the ratio of these two types of bridges and the polymeric structure of the MF resin shell. The formation of etheric bridges is more preferable than that of methylene bridges in a low pH value (acidic) environment [135]. Figure 6-8a shows the DSC curves of the octadecane microcapsules prepared with different HAc concentration in the emulsion, and Figure 6-8b lists the relative latent heat of exothermic peaks  $\alpha$ ,  $\beta$ , and  $\gamma$ . It can be found in Figure 6-8 that the relative latent heat of peak  $\gamma$  decrease to zero

when the HAc concentration is in the range from 1.38 ml/L to 1.75ml/L with the fixed F:M ratio (1.25) and pH value of the pre-polymer ( $\text{pH}_{\text{prepolymer}} = 8.50$ ), The relative latent heat of peak  $\alpha$  is maximized, reaching 83.7% at the concentration of HAc in the emulsion  $C_{\text{HAc}} = 1.38 \text{ ml/L}$ , while the relative latent heat of peak  $\beta$  is 16.6%. The effective latent heat of these octadecane microcapsules can be as large as  $213 \text{ J/g}$ , and the corresponding weight ratio of the phase change octadecane reaches 88 wt%, which are significantly higher than those in the microcapsules that use additive as nucleating agents[41, 88].

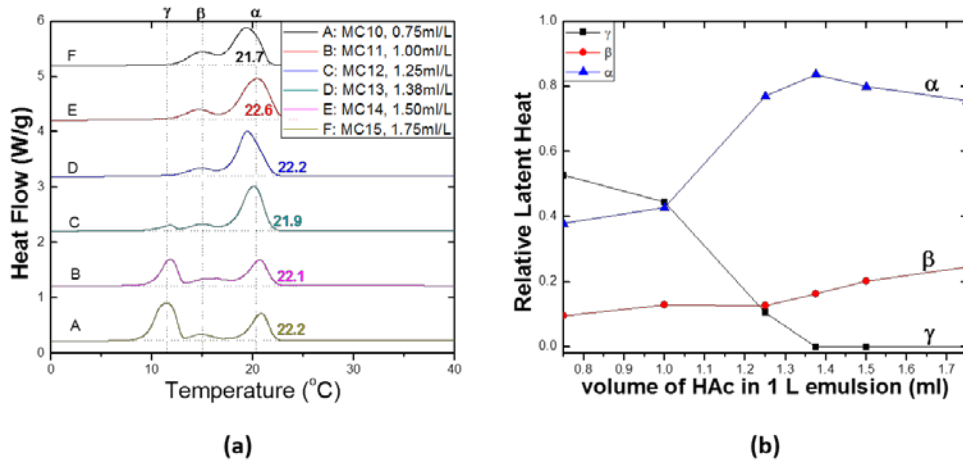


Figure 6-8. a) DSC freezing curves of samples MC10-15 [65]. Curves are shifted along Y axis. b) Relative latent heat of phase transition peaks for various HAc concentrations in the emulsion [65].

#### 6.4.4 Specific Heat Elevation by Supercooling Suppression

Based on latent heat of the microPCMs, the apparent heat capacity enhancements of with various operation temperature ranges of the microPCMs can be calculated by Equation 1-5, which are reproduced accordingly in Figure 6-9. The apparent heat capacity enhancement is reciprocal to the operation temperature range  $\Delta T$ . A significant increase of apparent specific heat has been demonstrated comparing with the increase by microPCMs without shell optimization. For instance, with a reasonable  $\Delta T$  of 5 K and only latent heat of phase transition

$\alpha$  is utilized, the apparent specific heat could be increased to 35.7 J/g, 16.6 times larger as the specific heat of solid octadecane without phase transition. In another case, when the operation temperature range is extended to 10 K to cover both phase transition peaks  $\alpha$  and  $\beta$ , more latent heat can be utilized, though the apparent specific heat increase drops to 21.3 J/g.

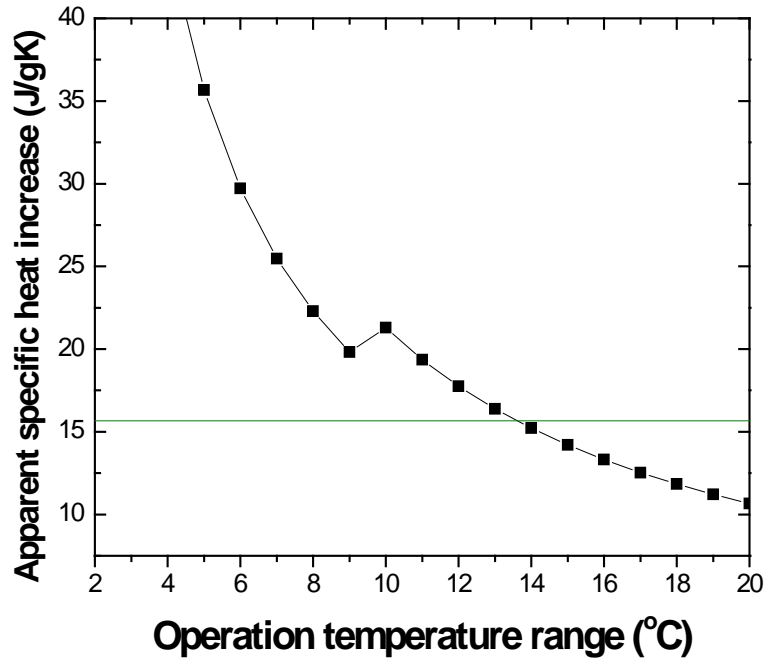


Figure 6-9. Calculation of apparent specific heat increase by the latent heat of microPCMs corresponding to different operation temperature ranges [65]. The horizontal line shows the increase at an operation temperature range of 13.6 °C.

### 6.5 Summary

The supercooling of PCM microcapsules has been suppressed significantly without compromising their effective latent heat of fusion, through optimization of the composition and structure of MFR shell. The octadecane microcapsules are synthesized by using the O/W emulsion technique. The effects of synthesis parameters, such as F:M ratio, pH of pre-polymer,

and pH of the emulsion, on the phase transition properties of the octadecane microcapsules have been investigated systemically. Important observations are listed as follows:

- a. The homogenous nucleation of octadecane triclinic crystal and its associated supercooling can be eliminated by shell-induced liquid-crystal transition. To provide appropriate nucleation sites at the inner wall of the microcapsules, the shell composition and microstructure can be optimized by tuning the synthesis parameters, such as F:M ratio, pH in the prepolymer, and HAc concentration.
- b. Three peaks, labeled  $\alpha$ ,  $\beta$ , and  $\gamma$ , are observed on the DSC cooling curves of the octadecane microcapsules, which are attributed to the shell-induced liquid-rotator and liquid-triclinic transition, rotator-crystal transition, and homogeneously nucleated liquid-triclinic transition, respectively. The relative latent of heat of peak  $\alpha$  can be maximized, reaching 83.7% in the octadecane microcapsules by shell optimization.
- c. The effective latent heat of these octadecane microcapsules can be as large as 213 J/g, and the corresponding weight ratio of the phase change octadecane reaches 88 wt%, which are significantly higher than those in the microcapsules that use additive as nucleating agents.
- d. Hollow spheres with porous, rather than solid resin shell, are formed when the SDS concentration is high, for example, 50 g/L in emulsion. When the SDS concentration drops to 10 g/L, octadecane microcapsules with solid resin shell can be formed.

## Chapter 7. Thermal Conductivity Enhancement of the MicroPCMs

### 7.1 *Introduction*

In last chapters, n-octadecane are microencapsulated to protect them from reacting with or leaking to the environment. Supercooling of the PCMs induced by microencapsulation is also suppressed using optimized MFR shell to provide nucleate sites for heterogeneous nucleation. In addition to supercooling, another vital problem of almost all latent heat based TES systems is the low thermal conductivity of PCMs, which is typically lower than 1 W/mK [6, 8, 10]. Low thermal conductivity restricts heat transfer rate as well as accessibility to thermal energy stored away from heat transfer interfaces. Therefore, there is a need for PCMs with high thermal conductivity in addition to high heat capacity and suppressed supercooling.

To solve this problem, several methods have been investigated to elevate thermal conductivity of PCM systems. The most common way in industry is to introduce highly conductive materials to form a composite of a PCM and a thermal conductivity promoter. The insertion of non-moving metal or graphite parts such as fins, foams, and wools into PCMs has long been practiced and summarized [13]. In microPCMs, however, improvements are limited due to the confined volume. A second option to enhance the thermal conductivity of PCMs is by using nanostructured dispersions in PCMs similar as the dispersion of nanostructures in other liquids to make nanofluids [89]. These emerging materials have only been studied since recently and represent a clear departure from existing practices of utilizing fixed, stationary high thermal conductive structures into PCM. Carbon-based nanostructures, metal oxide nanoparticles, and metallic nanoparticles and nanowires have been explored as the materials of the thermal conductivity promoters. A general problem of this nano-dispersion approach is the instability of the nanostructured dispersion in PCMs after cycles of running.

The third approach, which is rarely reported in literatures, is to coat or encapsulate the PCMs in conductive materials to make thermal conductive microPCMs. In this approach, choosing an appropriate inorganic material as the shell or a part of shell for microPCMs is essential for enhancing their thermal conductivity. For example, Wang et al. [83] synthesized a types of microPCMs with octadecane as core and silica as the shell, which have good thermal stability and good phase change performance, meanwhile enhancing thermal conductivity significantly from microPCMs with organic shells. However, thermal conductivity of silica shell is still low comparing to normal thermal conductive materials such as metals.

In this chapter, an additional layer of silver were coated on paraffin/MFR microPCMs to enhance their thermal conductivity. As the most thermal conductive metal on earth, silver provides a fast lane for heat transfer through the microPCMs and thus elevated their thermal conductivity. Meanwhile, different from using additives in PCMs, the external silver layer does not significantly affect the phase transition properties of the microPCMs. This type of double-shelled thermal conductive microPCMs are referred as PCM-Ag in this work. Though the PCM-Ag microcapsules are not suitable for industrial applications due to the expensiveness of silver, this research provides an alternative route to a material with both high heat capacity and high thermal conductivity.

## 7.2 Preparation of the Thermal Conductive PCM-Ag Microcapsules

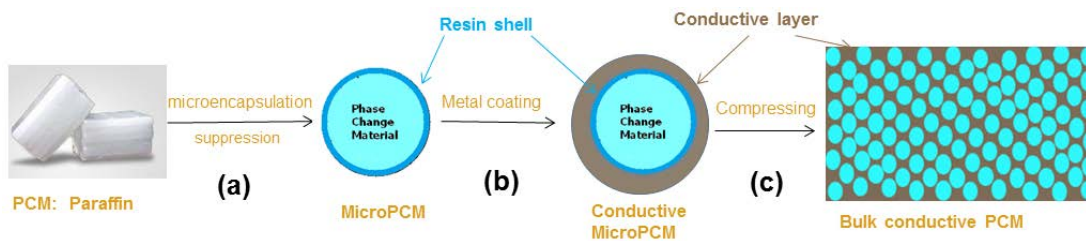
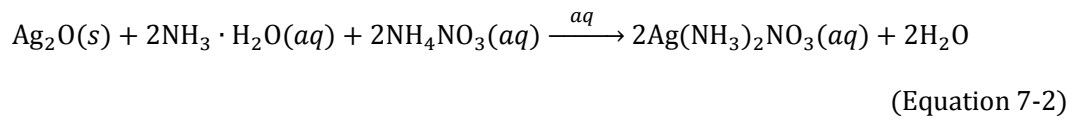
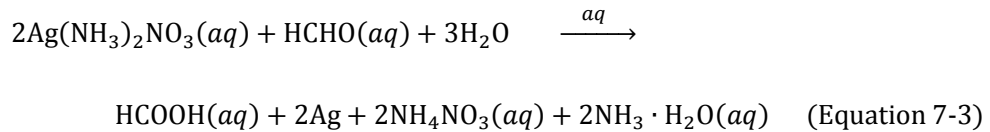


Figure 7-1. A strategy of producing thermal responsive energy storage materials. Step a): microencapsulation of paraffin in MFR shell; b): coating microPCMs with thermal conductive layer; and c): tableting of the powder of thermal conductive microPCMs to bulk TES material.

Coating of a silver layer on surface of microPCMs was performed in an aqueous solution based on so-called silver mirror reaction [223-225]. The key features of material synthesis of PCM-Ag and then the bulk thermal conductive PCMs are summarized in Figure 7-1. Typically, Tollens' reagent is produced by adding ammonia aqueous solution dropwise into 40 ml 10 wt% silver nitrite ( $\text{AgNO}_3$ ) aqueous solution while stirring, until the fluid turns back to a clear and transparent solution:



1 g of the microPCMs is then added into this solution. After 10 minutes stirring, sufficient amount of reducer such as glucose or formaldehyde solution is added into the suspension dropwise. The following chemical reaction produces a silver layer on the surface of the microPCMs:



The mixture is filtered after 10 hours reaction, and the black-to-gray powder is then washed with water and acetone and dried for future use.



Figure 7-2. Sample PCM-Ag pellets with various thickness and composition. The diameter of each cylindrical pellets is  $\frac{1}{2}$  inch.

In the final step of synthesis, the PCM-Ag microcapsule powder is further pressed with a YLJ-20TA Desktop Electric Laboratory Press to make bulk thermal conductive PCMs for further TES applications. The press was operated at room temperature, and the pressure of 1-10 MPa is applied, varying with silver contents in different samples. Figure 7-2 shows the as-produced PCM-Ag pellets.

### 7.3 Characterization of the PCM-Ag Powder and Pellets

#### 7.3.1 Morphology of the PCM-Ag Particles

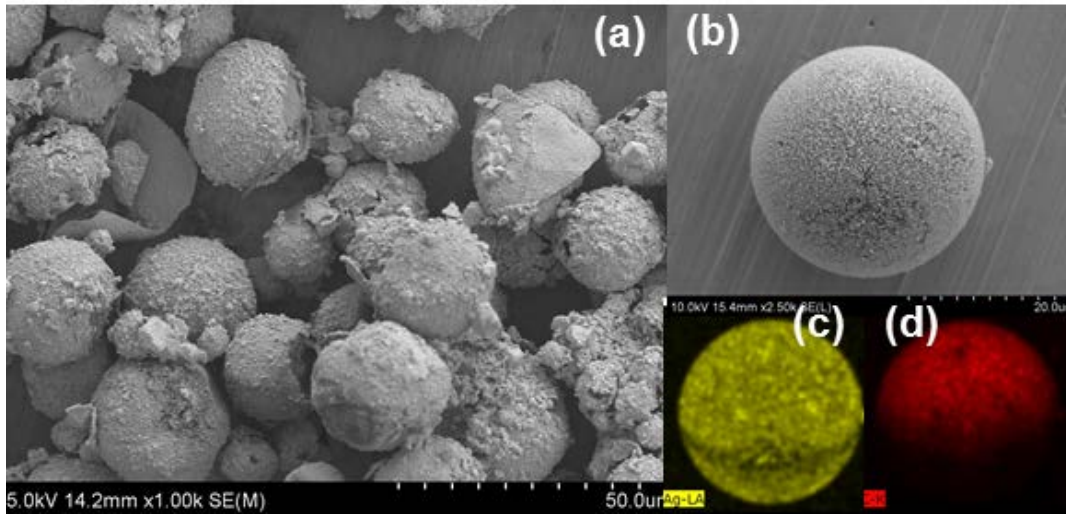


Figure 7-3. SEM images of the PCM-Ag microcapsules [67, 226]. a) and b) typical SEM images of the PCM-Ag particles with different silver ratio. c) and d) elemental (Ag and C, correspondingly) distribution in the PCM-Ag microcapsule.

SEM images with EDS of PCM-Ag microcapsules are shown in Figure 7-3. EDS shows that silver is uniformly distributed on the surface. Measured with both DSC and chemical titration, silver volume fraction in the products is as high as 45 vol%. Because of high volume fractions of metal layer, the resulting metal framework is more thermal conductive than the state-of-the-art PCM/polymer composites. Large volume fraction of silver also ensure a continuum three dimensional metal structures for heat transfer. Competitively, a high fraction

of encapsulated PCM leads to a high heat capacity of the composite. As a result, a Pareto optimized balance is needed to be found for a certain application.

### 7.3.2 Thermal Conductivity Analysis of the PCM-Ag Pellets

Typical thermal conductivity of paraffin is 0.15 W/mK in liquid state and 0.35 W/mK in solid state [195]. Typical thermal conductivity of MFR is 0.2 W/mK [136, 218]. In the thermal conductivity measurement of PCM-Ag pellets, it is found that a volume fraction of 3.4 % Ag loading increases its thermal conductivity to 1.34 W/mK, significantly larger than that without coating. For PCM-Ag pellets with a silver volume fraction of 25%, the thermal conductivity is 10.8 W/mK, much higher than the traditional PCMs. With a higher silver volume fraction of 45%, thermal conductivity can be as high as 14.6 W/mK. The results are shown in Figure 7-4.

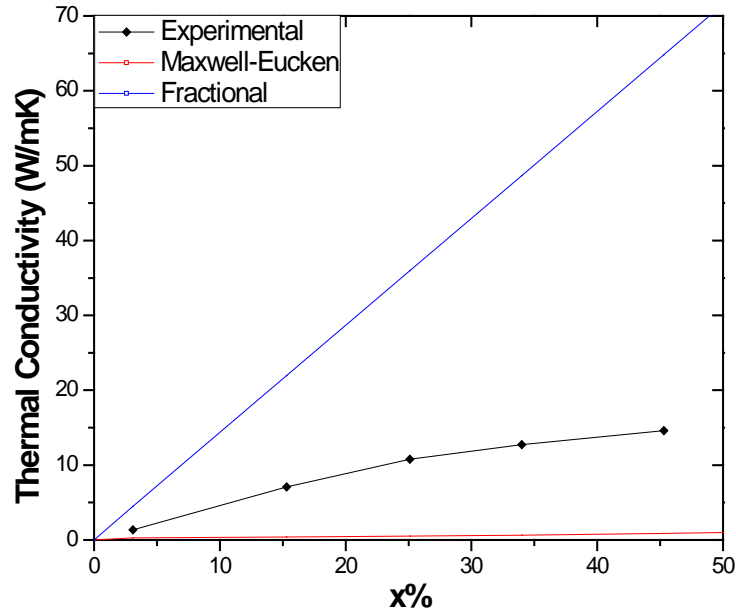


Figure 7-4. Experimental and theoretical thermal conductivities of different models of metal-PCM composites with different metal ratio.

The experimental thermal conductivity results of PCM-Ag pellets are compared with predictions based on effective media models typically used to evaluate the thermal conductivity of randomly distributed homogeneous microspheres in a continuous media. The Maxwell-Eucken model [95, 227] is shown below as

$$k_{s\_ME} = k_p \left[ \frac{1+2x(k_c-k_p)/(k_c+2k_p)}{1-x(k_c-k_p)/(k_c+2k_p)} \right] \quad (\text{Equation 7-4})$$

In this model, thermal conductive microspheres are dispersed in bulk PCMs in a volumetric ratio  $x$ , and thus no effective thermal conductive network is formed by aligning the microspheres.  $k_c$  and  $k_p$  are the thermal conductivities of the bulk continuous phase and the dispersed silver particles, correspondingly. Thermal conductivity predicted in this model is significantly lower than the experimental results.

Another simple theory to predict thermal conductivity of a composite with well-formed thermal conductive network is

$$k_{s\_f} = \frac{(1-x)k_p}{3} + \frac{xk_m}{3} \quad (\text{Equation 7-5})$$

in which interface thermal boundary resistance is assumed negligible. As shown in Figure 7-4, without considering interface resistance, thermal conductivity of the samples could be much higher than the experimental values. For example, the thermal conductivity increases from 0.25 W/mK for the pure paraffin to 10.8 W/mK with 25 vol% silver coated. The striking differences among the models and experimental result indicate that there is a different heat transfer structure in PCM-Ag pellets. The heat transfer network is partially built up in the pellets, and thermal conductivity of the pellets may further be elevated by both controlling the interface resistance either between the paraffin/MFR microPCMs and the silver shell or among the silver shells. Eliminating trapped air in the pellets during the sample preparation may also promote their thermal conductivity.

### 7.3.3 Trade-off between Heat Capacity and Thermal Conductivity

It need to be mentioned that there is a trade-off of overall latent heat capacity when enhancing the thermal conductivity by coating with silver. On one hand, the fraction of silver coating significantly contribute to thermal conductivity of PCM-Ag; on the other hand, the fraction of PCM provides latent heat capacity to the composite. The trade-off between thermal conductivity and heat capacity is shown in Figure 7-5. It is necessary to find an optimum to balance the thermal conductivity and heat capacity of PCM-Ag microcapsules for certain applications.

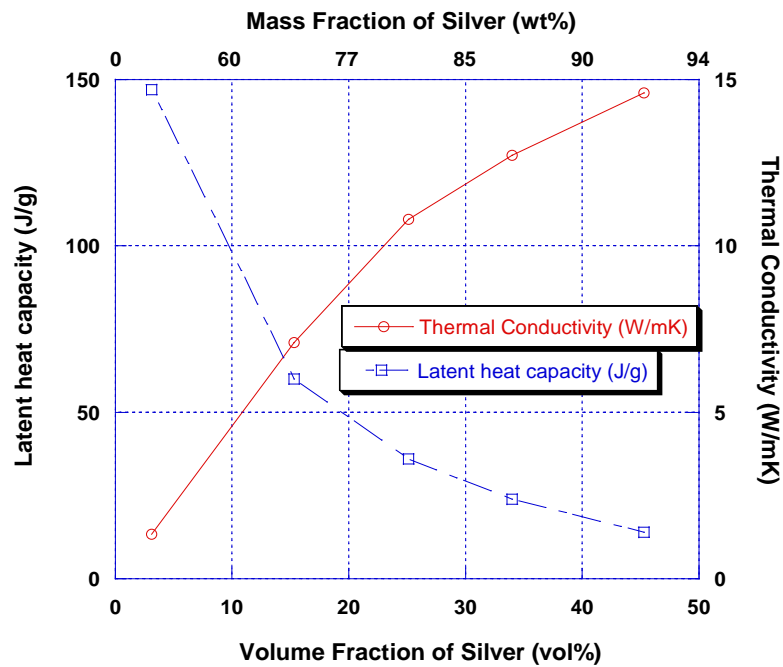


Figure 7-5. The change of thermal conductivity and heat capacity of silver-coated PCM-Ag versus the mass and volume fraction of silver.

#### **7.4 Summary**

Silver was applied as a coating layer on the surface of as-produced paraffin/NMR microPCMs to enhance their thermal conductivity. PCM-Ag microcapsules were also compressed to make bulk PCM pellets with stabled shape and structure for applications in TES. With silver coated on the microcapsules, thermal conductivity of PCM-Ag pellets is significantly larger than that of normal PCMs. Meanwhile, silver coating decreases the overall latent heat capacity of the microPCMs dramatically. It is necessary to choose proper fraction of the thermal conductive layer to balance the thermal conductivity and heat capacity of this material.

## Chapter 8. Application of MicroPCMs in Heat Transfer Fluids

### **8.1 Introduction**

Interest in engineered suspensions of micro/nanoparticles in liquids has increased in recent years, particularly in pursuing higher fluid thermal conductivity and heat capacity [91, 93-95, 219, 228-230]. For higher thermal conductivity, researchers have experimentally investigated the convective heat transfer of aqueous metal oxide or nitride nanoparticles in circular tubes and results show enhancement of the heat transfer when nanoparticles are added to the cooling fluid [18, 96, 97, 99, 101, 102]. For higher heat capacity, microPCMs can mitigate PCM leakage and potential undesirable interactions between the PCM and the base fluid [5, 8, 17, 57, 65, 91, 196, 209, 210, 229]. The main enhancement provided by PCMs is a significant increase in thermal storage density due to latent heat of PCMs [5]. However, a combination of these two advantages to enhance the heat transfer properties of a heat transfer fluid is rarely found.

In last chapters, we developed a comprehensive process to microencapsulate paraffin PCMs in MFR shell for high heat capacity and suppressed supercooling, and to further elevate the thermal conductivity of the microPCMs with a layer of silver coating on the surface of the microPCMs. In this chapter, dispersions of this type of thermal conductive microPCMs in PAO-based heat transfer fluids were produced, and thermophysical properties and heat transfer performances of the enhanced heat transfer fluid were investigated in a microchannel cold plate [67, 226].

## 8.2 Characterization of the Phase Changeable Heat Transfer Fluids

### 8.2.1 Materials

The synthesis of microPCMs and PCM-Ag microcapsules are described in Chapters 6 and 7, correspondingly. For applications in heat transfer fluids, two modifications of silver coating were attempted to improve their performance in fluids. Firstly, less silver were coated comparing with PCM-Ag microcapsules shown in Chapter 7, so as to control the average density of microPCMs and to avoid quick sedimentation due to large density difference between silver-coated PCMs and heat transfer fluids. Secondly, surface of as-synthesized paraffin/MFR microPCMs was pre-engineered and activated for different distributions of silver deposition. PCM-Ag microcapsules with both rough silver coating and smooth silver coating were synthesized, as shown in Figure 8-1.

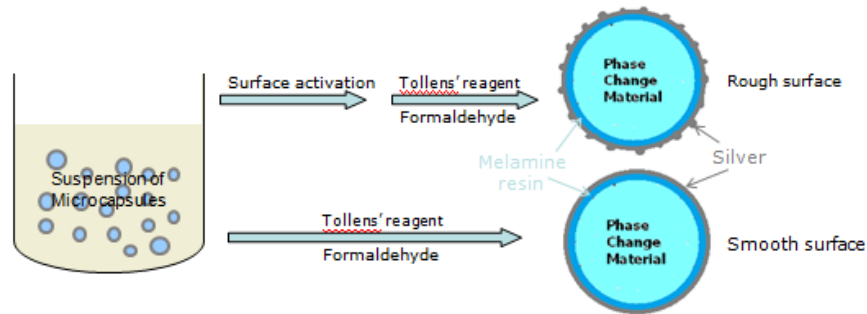


Figure 8-1. The strategy of synthesizing PCM-Ags by coating microPCMs with thin coating of silver [67].

As described in Section 7.2, coating a smooth silver layer on surface of microPCMs was performed in an aqueous solution based on the silver mirror reaction. To create a rough silver layer on the microPCMs, the MFR surface needs to be activated by stirring in diluted tin chloride solution for 10 minutes [223, 224]. After that, the same process as described in Section 7.2 was performed, using surface-activated microPCMs instead of the original ones. In a typical synthesis, 1 g of microPCMs, surface activated or not, is added into diluted Tollen's

reagent produced following Equation 7-1 and 7-2. After 10 minutes stirring, sufficient amount of reducer such as glucose or formaldehyde solution is added into the suspension dropwise. During this process, metallic silver is reduced from the solution and deposit on the surface of the microPCMs. Specifically, with surface-activated microPCMs, silver tends to deposit on the activated sites, inducing a rough silver-coated surface with non-uniform silver deposition. On the contrary, the deposition of silver on the non-activated microPCMs are uniform and smooth. The difference of the products os characterized with SEM and shown in Figure 8-2. The fluid is filtered after 10 hours reaction, and the gray powder is then washed with water and acetone and dried for future use.

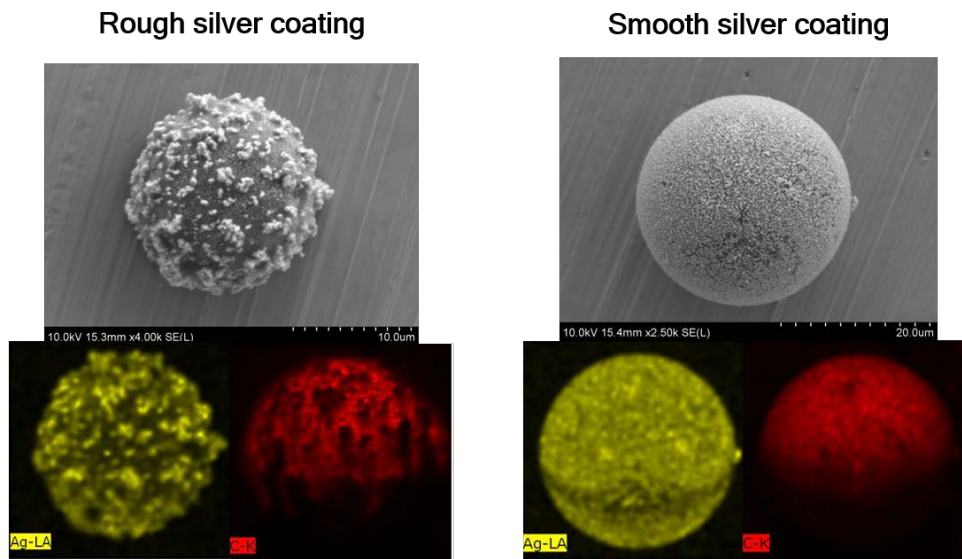


Figure 8-2. SEM and EDS of the microPCMs with rough silver coating and smooth silver coating [67]. The EDS yellow images show the distribution of silver on the surface of the above microPCM, and the red ones correspond to that of carbon.

### 8.2.2 Thermal Conductivity and Viscosity of the Heat Transfer Fluids

Thermal conductivity of the fluids with different microPCMs distributed in are shown in Table 8-1. It is interesting that the PCM-Ag microcapsules with smooth silver coating is

significantly more thermal conductive than the rough ones, even though the silver fraction of the later (3.4 vol%, in PCM-Ag2) is apparently larger than that of the smooth coated PCM-Ag3 microcapsules (2.4 vol%). Meanwhile, PCM-Ag1 and PCM-Ag2 with rough silver coating elevate viscosity of heat transfer fluids more significantly than PCM-Ag3. This phenomenon indicates that the rough coating of silver does not form a thermal conductive layer but only discrete silver clusters on the surface of microPCMs. As a result, it can be expected that heat transfer performance of the heat transfer fluid with smooth coated PCM-Ag3 is better than that of the other two PCM-Ag samples.

Table 8-1. Properties the latent functional heat transfer fluids with addition of microPCMs and PCM-Ag particles [67, 226]. Thermal Conductivity, Viscosity, and Latent Heat Capacity of the heat transfer fluids were all measured from a 20 wt% suspension of the PCMs in PAO.

Sample	Shell Material	Ag Vol %	Ag Thickness (nm)	Thermal Conductivity (W/mK)	Viscosity (cP)	Latent heat capacity (J/g)
Pure PAO	N/A	0	0	0.140	7.3	0
microPCM	Polymer	0	0	0.152	11.8	213
PCM_Ag1	Polymer Rough Ag	2.2%	73.1	0.153	13.1	165
PCM_Ag2	Polymer Rough Ag	3.4%	116.7	0.239	13.6	145
PCM_Ag3	Polymer Smooth Ag	2.4%	81.6	0.251	11.2	160

### 8.2.3 Specific Heat Capacity of the Heat Transfer Fluids

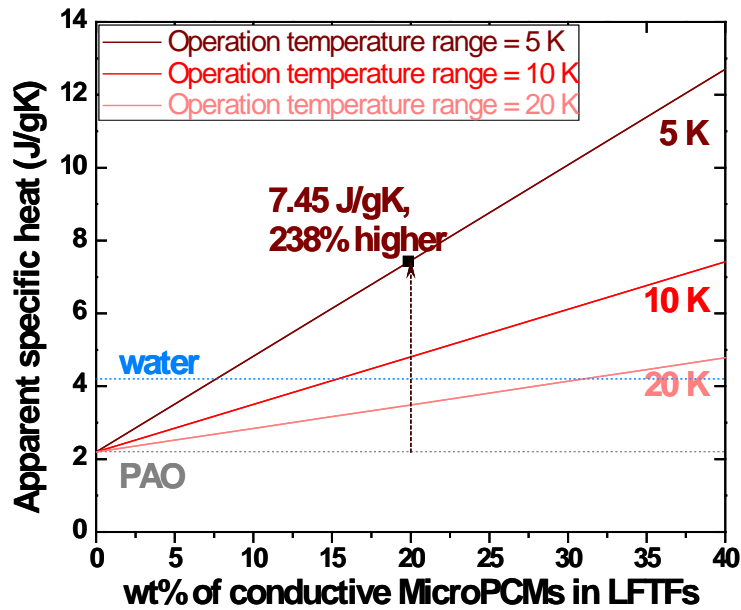


Figure 8-3. Average specific heat enhancement of the latent functional thermal fluids with addition of 20 wt% PCM-Ag3 microcapsules [67].

Based on Equation 5-3, the addition of microPCMs in heat transfer fluids induces an elevation of overall heat capacity and thus apparent specific heat of the fluids over a certain range of operation temperature. The elevations of apparent specific heat over certain temperature ranges were calculated and shown in Figure 8-3. The elevation of apparent heat capacity is proportional to the weight fraction of microPCMs and the reciprocal of operation temperature range. There is a limitation for each of the parameters. The mass fraction of the microPCMs in a fluid increases its apparent specific heat, but there is also trade-off from the increase of viscosity induced simultaneously by adding microPCMs. Apparently, this trade-off restricts the heat transfer performances of the fluid. The operation temperature range needs to be large enough so that the processes of melting and freezing can be operated cyclically. To utilize the latent heat of microPCMs, the operation temperature should cover the range from

$T_m$  to  $T_f$ , i.e., the operation temperature range  $\Delta T > \Delta T_{SC}$ . Otherwise, no phase transition happens in cycles and no latent heat is available.

Nonetheless, a significant increase of apparent specific heat has been demonstrated with the addition of PCM-Ag3 microcapsules. For example, with an operation temperature range of 5 K and a PCM-Ag3 weight ratio of 20 %, only latent heat of phase transition  $\alpha$  can be utilized, and the apparent specific heat could be increased to 7.45 J/g, 2.38 times larger than that of the base fluid PAO. Apparently, a trade-off between thermal conductivity and heat capacity occurs with the coating of Ag on the paraffin/MFR microPCMs, before which the apparent specific heat of the LFTF could be as high as 9.30 J/g with the addition of the same mass fraction of uncoated microPCMs in the same temperature range [65].

### 8.3 Fluidic and Heat Transfer Performance of the Heat Transfer Fluids

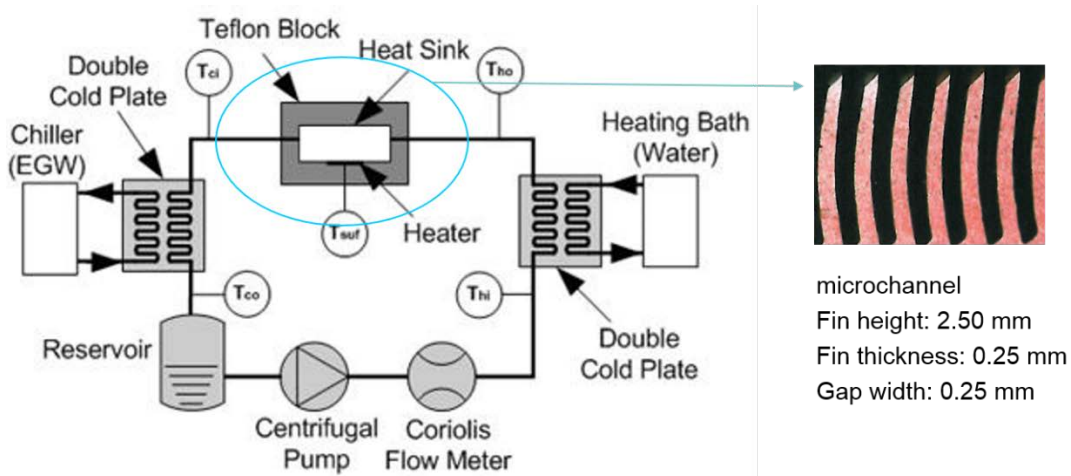


Figure 8-4. Schematic diagram (left) of the experimental set-up for heat transfer measurement and a photograph of the microchannel (right) with size [67, 226].

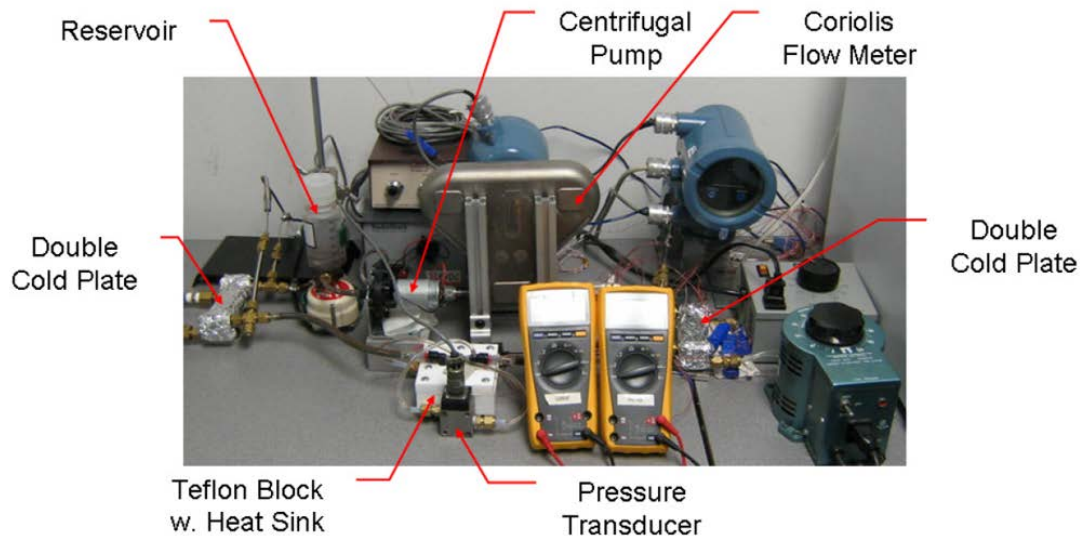


Figure 8-5. Photograph of the experimental setup for heat transfer measurement [226].

A heat transfer loop was designed and built specifically for evaluating heat transfer performance of the PCM fluids in a microchannel cold plate, and a schematic of the loop is shown in Figure 8-4. A photograph of the system is also shown in Figure 8-5. The hold-up volume of the entire system is about 80 mL. The individual components in the heat transfer loop include a reservoir tank, a centrifugal pump, a Coriolis flow meter, two heat exchangers, and a microchannel cold plate used for the test section [226]. The reservoir tank consists of a modified 120 mL polyethylene bottle, which insures the system is full of liquid and allows the fluid level to be monitored. A centrifugal pump circulates the fluid through the entire system and the flow rate is measured using a mass flow meter. The coolant is preheated before entering the test section and cooled upon leaving the microchannel using two heat exchangers, which consist of two copper cold plates with internal crisscrossed fins brazed together. Temperatures of the working fluids (50/50 aqueous ethylene glycol) in the secondary loops of these two heat exchangers are controlled by two thermal baths. The test section consists of a Microcool CP-101 microchannel cold plate and a 10 x 10 mm ceramic heater soldered to the bottom. The temperature of the heater was monitored using two T-type thermocouples attached to the

bottom of the cold plate. Two multi-meters were used to measure the voltage and current being supplied to the heater wires and the power input is adjusted using a variable transformer. The cold plate is incorporated into a milled Teflon block to reduce heat losses. Four thermocouples were placed in the system to measure the bulk temperature of the coolant after each heat exchanger and the test section. All thermocouples were calibrated in a thermal bath and the maximum deviation is  $\pm 0.2^{\circ}\text{C}$ .

### 8.3.1 Pressure Drop

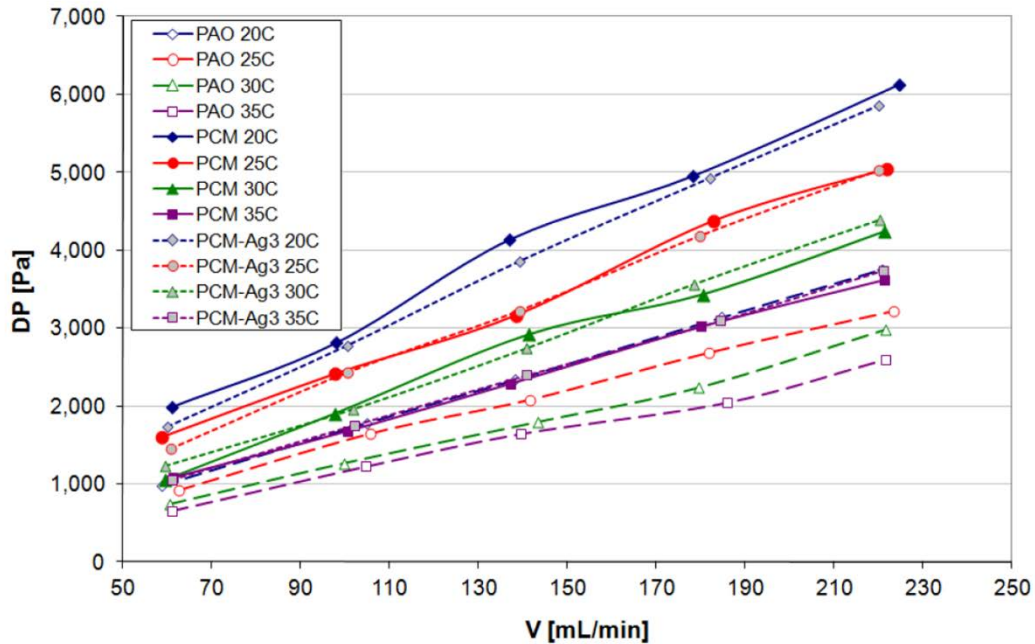


Figure 8-6. Pressure drop (Y axis) in the cold plate at different inlet temperatures versus flow rate (X axis) of the heat transfer fluids comparison of PAO, PAO with 20 wt% paraffin/MFR microPCMs (without silver coating), and PAO with 20 wt% PCM-Ag3 [67, 226].

The microchannel cold plate was tested with pure PAO, PAO suspensions containing uncoated paraffin/MFR microPCMs (labelled as PCM), and PAO suspensions containing PCM-Ag3 microcapsules (labelled as PCM-Ag3). Flow rates from 60 – 220 mL/min, heater power input from 30 – 70 W, and inlet temperatures from 20°C – 35°C were tested. Additionally,

pressure drop tests were conducted without heat input at four different fluid inlet temperatures. The results are depicted in Figure 8-6. As expected for this range of Reynolds number, the pressure drop increases linearly with flow rate. It was also found that the fluids with PCM particles have a higher viscosity than pure PAO.

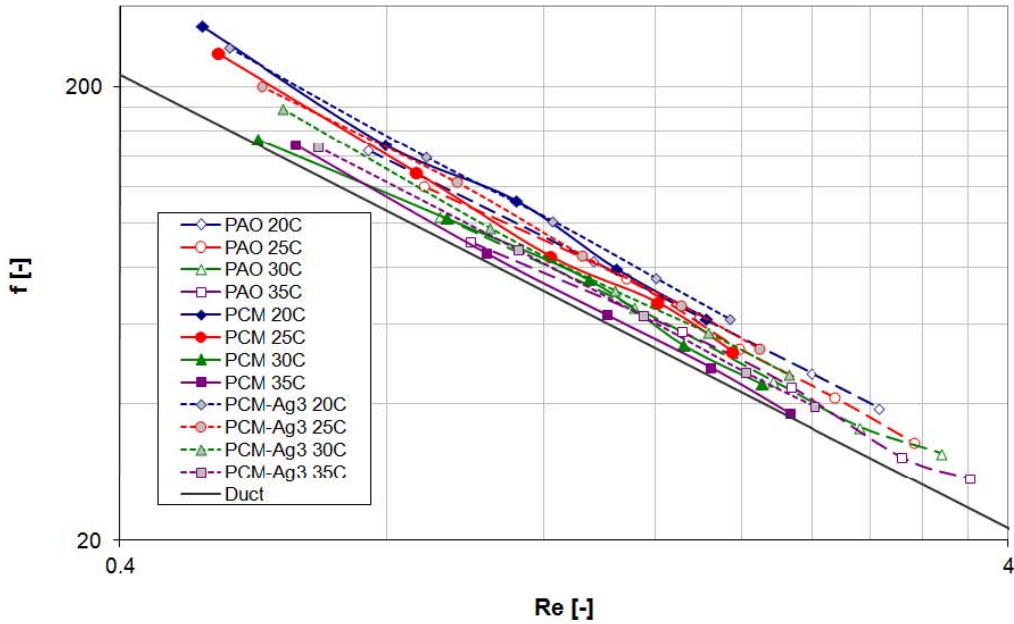


Figure 8-7. Friction factor (Y axis) versus Reynolds number (X axis) comparison of PAO, PAO with 20 wt% paraffin/MFR microPCMs (without silver coating), and PAO with 20 wt% PCM-Ag3 [67, 226].

Figure 8-7 compares the friction factor  $f$  obtained for each of the three different fluids (PAO, microPCM, and PCM-Ag3) in the experiments:

$$f = \frac{\Delta P D A_{MC}^2}{\rho L \dot{V}^2} \quad (\text{Equation 8-1})$$

where  $D$ ,  $A_{MC}$ , and  $L$  are the diameter, area, and length of the microchannel, and  $\Delta P$ ,  $\rho$ ,  $\dot{V}$  are the pressure drop, density, and volume flow rate of the flow in the microchannel, correspondingly. In addition, the results are compared with the Darcy friction factor for a rectangular duct based on the channel width/height ratio [231],  $f = \frac{84.9}{Re}$ . It can be seen that

the results for the three fluids are in good agreement with the numerical model, given the uncertainties in the viscosities of the fluids, the dimensions of the microchannel, and the increased pressure drop in the entrance and exit of the cold plate and developing regions in channels.

### 8.3.2 Heat Transfer Results

The trials with heat input were conducted over a range of flow rates and heater powers and the average heat transfer coefficients  $h$  were calculated for each power input using the equation

$$h = \frac{Q}{A_{suf}(T_{suf}-T_{in})} \quad (\text{Equation 8-2})$$

where  $Q$  is the heater power input,  $A_{suf}$  and  $T_{suf}$  is the area and average surface temperature of the heater, correspondingly, and  $T_{in}$  is the inlet temperature of the fluid. The experimental results are plotted in Figure 8-8 and Figure 8-9. For the pure PAO tests, heat transfer coefficient increases as temperature is increased, due to a slight increase in the fluid's heat capacity with temperature. However, the absorption of heat by the melting of PCMs results in a much more complex relationship of the heat transfer coefficient, the flow rate, the inlet temperature, and the heat input. The heat transfer coefficients for the PCM fluids increase as the inlet temperature is increased from 20°C to 30°C, but then decreases at higher temperature. The amount of PCM that melts in the cold plate depends on the inlet temperature, flow rate, and heat input. The greater the amount of PCM that melts in the cold plate, the higher the heat transfer coefficient becomes. However, at inlet temperatures above 30°C, a portion of the PCM has melted before entering the test section, decreasing the amount of PCM available for phase change in the cold plate, thus resulting in decreased heat transfer coefficients.

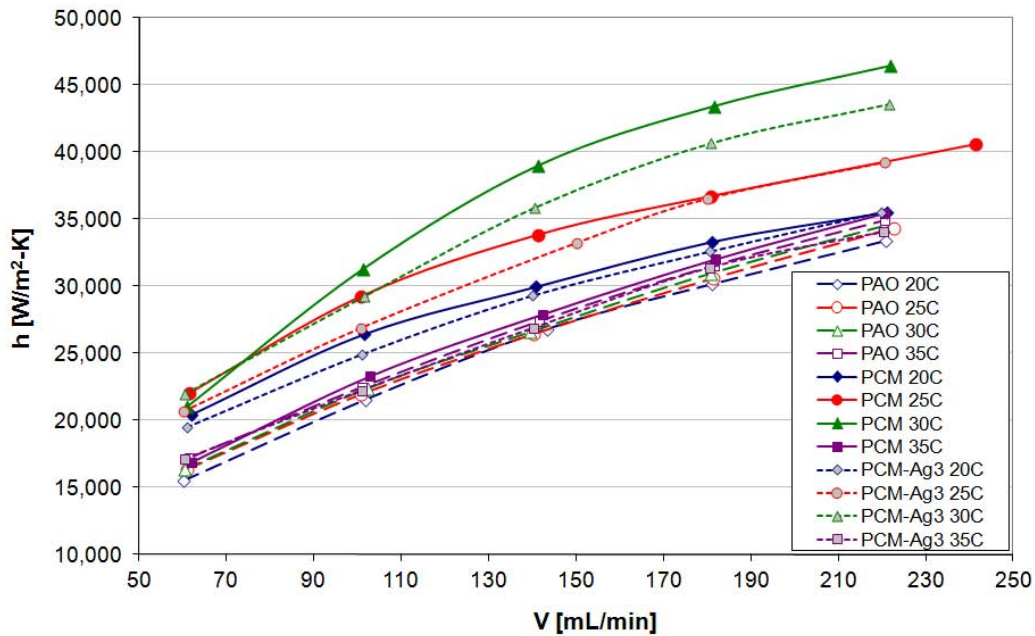


Figure 8-8. Heat transfer coefficient (Y axis) versus flow rate (X axis) of the heat transfer fluids PAO, PAO with 20 wt% paraffin/MFR microPCMs (without silver coating), and PAO with 20 wt% PCM-Ag3 at different inlet temperatures [67, 226].

The fluids containing PCM-Ag3 microcapsules had lower heat transfer coefficients than the fluid containing paraffin/MFR microPCMs, which is surprising given its higher thermal conductivity. The PCM-Ag3 microcapsules have a lower latent heat than the paraffin/MFR microPCMs, thus it is suspected that this reduction in latent heat is dominating the improvement in thermal conductivity. As described above, the latent heat is responsible for altering the temperature gradients near the heat transfer surfaces, which increases the flow of heat into the fluid.

As shown in Figure 8-9, Nusselt numbers of the PCM fluids are higher than those of the pure PAO and the PCM-Ag3 fluids, due to the higher heat transfer coefficients. The Nusselt numbers of the PCM-Ag3 fluid are actually lower than those of pure PAO because of the higher thermal conductivity of the PCM-Ag3 fluid.

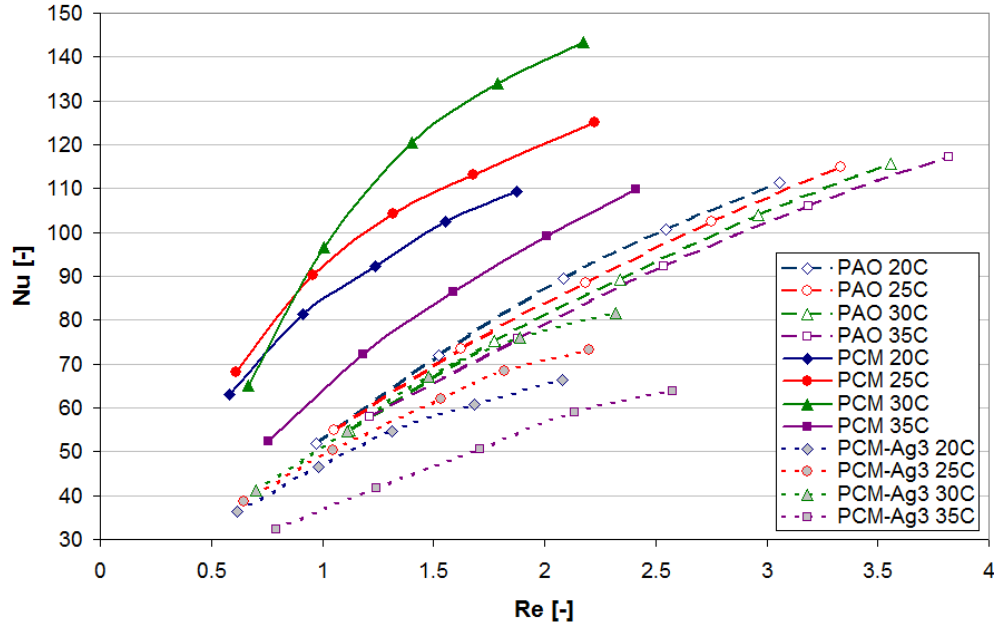


Figure 8-9. Nusselt number (Y axis) versus Reynolds number (X axis) of PAO, PAO with 20 wt% paraffin/MFR microPCMs(without silver coating), and PAO with 20 wt% PCM-Ag3 at different inlet temperatures [67, 226].

Using the equation below, the pumping power  $P$  and the thermal resistance  $R$  were also calculated in order to compare the thermal performance of pure PAO, the paraffin/MFR microPCM fluid, and the PCM-Ag3 fluid:

$$P = \dot{V} \cdot \Delta p \quad \text{(Equation 8-3)}$$

$$R = \frac{T_{max} - T_{in}}{Q} \quad \text{(Equation 8-4)}$$

where  $T_{max}$  is the maximum heater temperature. The results are plotted in Figure 8-10. It can be seen that, as expected, the pumping power of the pure PAO decreases with increasing inlet temperature, due to the viscosity of the fluids decreasing with temperature. At 30°C, thermal resistance of the PCM fluid is about 20% lower than that of the PAO over the range of flow rates tested and the heat transfer coefficient of the PCM fluid is about 36% higher than that of pure PAO. However, the advantage of this large increase in heat transfer rate is reduced by the

increase in pumping power. As can be seen in Figure 8-10, a similar result is found at other temperatures.

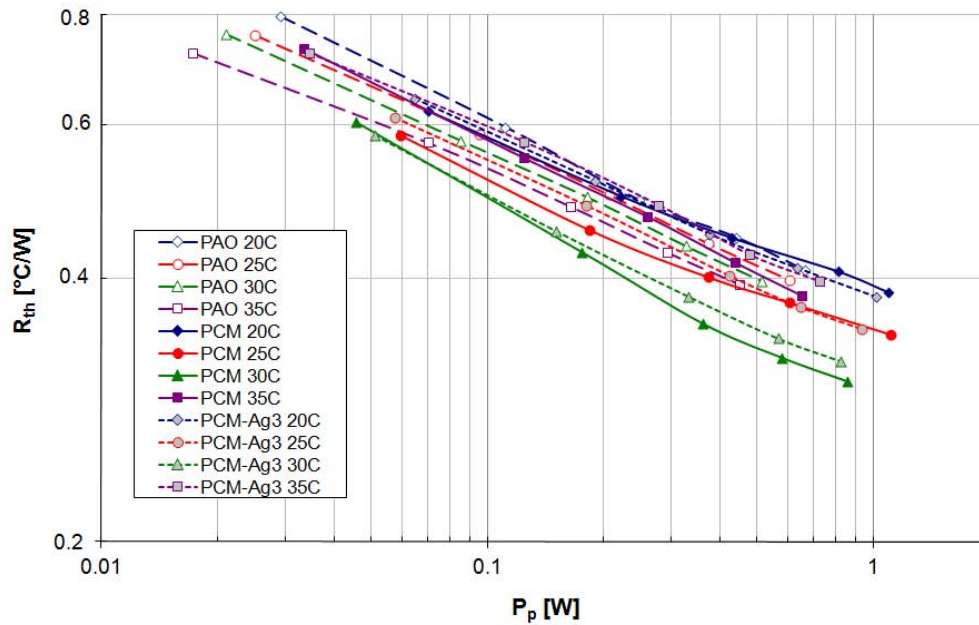


Figure 8-10. Thermal resistance comparison at different inlet temperatures of PAO, PAO with 20 wt% paraffin/MFR microPCMs (without silver coating), and PAO with 20 wt% PCM-Ag3 [226].

### 8.3.3 Stability of the Heat Transfer Fluids

To investigate the stability of the microPCM enhanced fluids, experiments were run for several hours without heat input. The tests were conducted with the PCM-Ag3 fluid for three hours. The pressure drop versus time is plotted in Figure 8-11. The pressure drops were relatively constant over the duration of the test, which indicates that no accumulation of PCM particles in the microchannel. The small pressure drop variation can be attributed to fluctuations in the room temperature and flow rate.

Another set of experiments was conducted to monitor the settling of particles in the heat transfer components over short periods of time. In these tests, the operating pump was

turned off after 5 minutes of pumping for 10 minute breaks. The results are presented in Figure 8-12. Again, the pressure drop remains relatively constant.

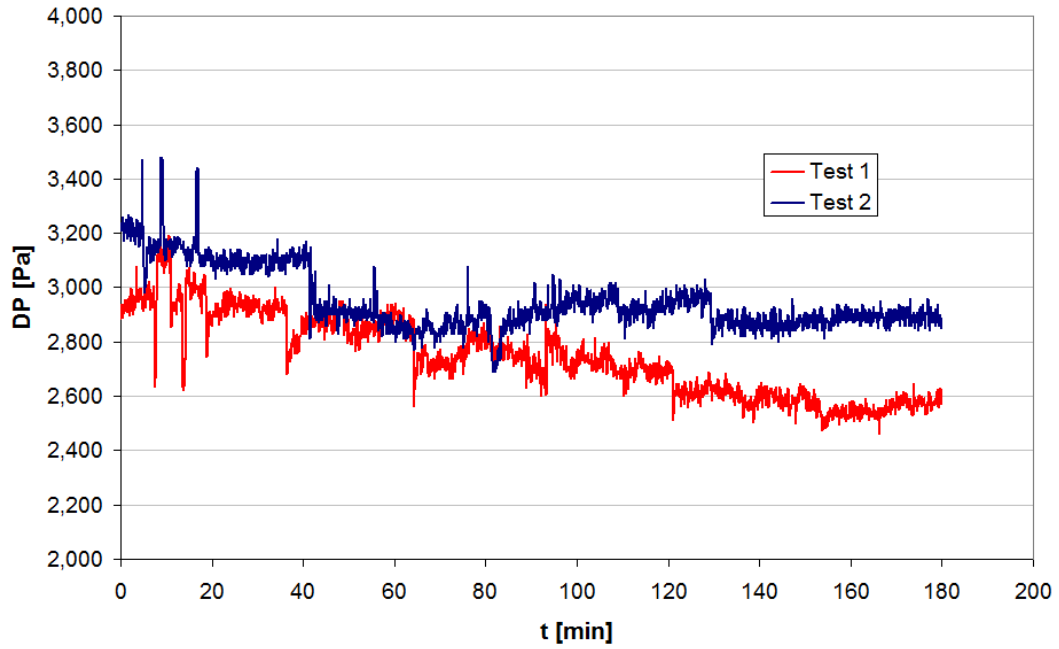


Figure 8-11. Extended duration pressure drop of a PCM-Ag3 enhanced fluid [226].

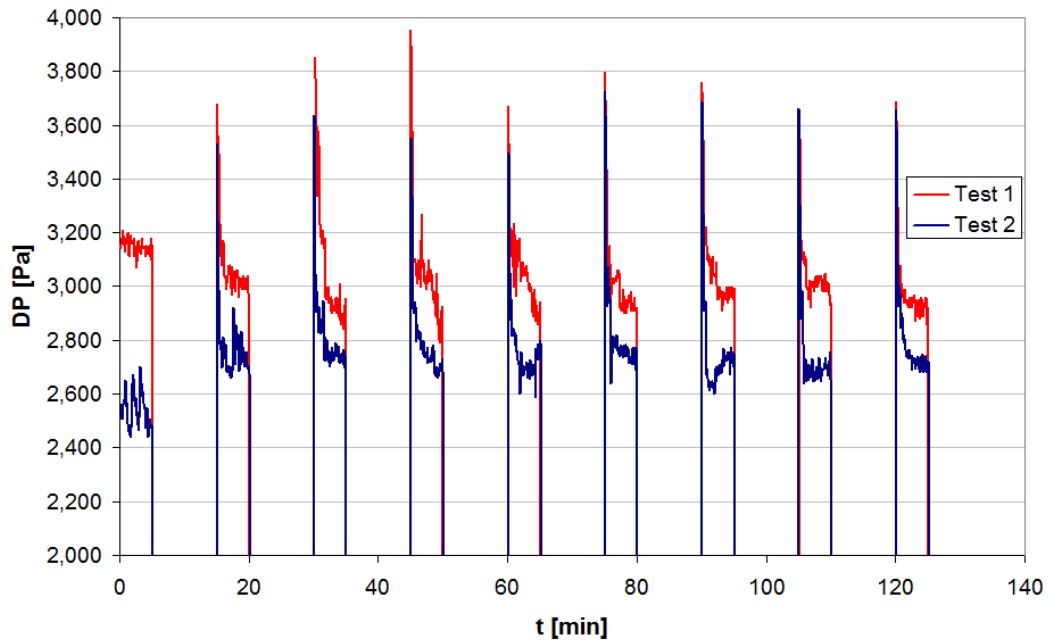


Figure 8-12. Pressure drop in idel experiments with 10 minutes break [226].

## 8.4 Uncertainty Analysis

The uncertainties in this work comprise two parts: the systematic biases and the random errors. For most of the measurements involved in this work, the systematic biases are small compared with the random errors. For example, the deviation of viscosity measured with a Brookfield DV-I prime viscometer is  $\pm 0.1$  cP. In contrast, the random error of viscosity is up to 0.6 cP and the uncertainty of this measurement is 4.4%, due to the unpredictable fluctuations during the measurement.

The uncertainties of the measured values are shown in Table 8-2. The range of the measured uncertainties is from 0.2% to 7.0%, varying from property to property. Based on these values, the uncertainties of the calculated values can be estimated using the following equations:

$$\frac{\delta h}{h} = \frac{\delta R}{R} = \sqrt{\left(\frac{\delta Q}{Q}\right)^2 + \left(-\frac{\delta L}{L}\right)^2 + \left(-\frac{\delta D}{D}\right)^2 + \left(-\frac{\delta T}{T}\right)^2} \quad (\text{Equation 8-5})$$

$$\frac{\delta Nu}{Nu} = \sqrt{\left(\frac{\delta Q}{Q}\right)^2 + \left(-\frac{\delta L}{L}\right)^2 + \left(-\frac{\delta D}{D}\right)^2 + \left(-\frac{\delta T}{T}\right)^2 + \left(-\frac{\delta k}{k}\right)^2} \quad (\text{Equation 8-6})$$

The results are shown in Table 8-2 as well.

Table 8-2. Uncertainties of the measured and calculated properties of the fluids [226].

Measured values	Uncertainty of measurement	Calculated values	Calculated Uncertainty
$\dot{Q}$	3.1%	h	4.6%
L	0.2%	Nu	8.4%
D	2.5%	R	4.6%
T	2.3%		
k	7.0%		

## 8.5 *Summary*

PCM fluids with uncoated paraffin/MFR microPCMs and silver-coated PCM-Ag3 microcapsules were synthesized and characterized, and their heat transfer performance was compared with that of pure PAO, the base fluid for the microPCM enhanced fluids. The PCM fluid with uncoated microPCMs has a 36% higher heat transfer coefficient relative to pure PAO over a range of flow rates and temperatures, when compared at the same flow rate. The thermal resistance of this PCM fluid at a given pumping power is about 20% lower than that of pure PAO. A silver-coated PCM-Ag3 fluid also shows an increased heat transfer coefficient, which is greater than that of pure PAO, but less than that of the PCM fluid. It is suspected that the reduced performance of the PCM-Ag3 fluid is due to its relatively smaller latent heat. Pumping tests conducted over several hours showed no effect of either particle accumulation or settling within the heat transfer loop. From these results, it is clear that the microPCM enhanced heat transfer fluids would provide improved performance relative to pure PAO in heat transfer applications.

## Chapter 9. Conclusions and Future Directions

### **9.1 *Conclusions of Experimental and Analytical Work***

This dissertation provides comprehensive information for the design, the synthesis, the characterization and the application of microPCMs, which have been regarded as potential advanced material for heat dissipation and thermal management. MicroPCMs based on solid-solid PCM neopentyl glycol and liquid-solid PCM n-octadecane were synthesized with wet-chemical methods utilizing colloidal systems as the reaction media. Properties of the emulsion systems as reaction media, properties of the PCMs and microPCMs, and applications of microPCMs to thermal management were carefully investigated. The conclusions reached in the course of this dissertation are summarized below:

1. A method to determine the CMC of a surfactant in a solution by measuring the thermal conductivity of the solution is developed. The minimum of thermal conductivity occurs at the CMC during the increase of surfactant concentration, which provides a simple and straightforward way to determine the value of the CMC. It was found experimentally that there is a minimum thermal conductivity occurs in the AOT/n-octane solution with an AOT loading of around 0.1 ~ 0.2 wt%. The existing theories such as effective medium theory apparently fail to explain the fact of the minimum thermal conductivity. With the hypothesis of inter-molecular low-density region and hydrogen bond network enhanced energy transfer, this phenomenon can be explained.

2. The NPG/silica microPCMs were synthesized using a modified sol-gel method. The size of these microPCMs is in the range of 0.2 - 4  $\mu\text{m}$ . It was found that the endothermic phase transition of these NPG-silica microcapsules was initiated at around 39  $^{\circ}\text{C}$  and the latent heat

was about 96.0 J/g. A large supercooling of about 43.3 °C was observed in NPG micro-particles without silica encapsulation. Encapsulated in silica, the supercooling of NPG was reduced to about 14 °C due to the heterogeneous nucleation sites provided by silica. The NPG/silica microPCMs were also added into heat transfer fluid PAO to enhance its heat capacity.

3. An in-situ polymerization method was used to synthesize paraffin/MFR microPCMs. This type of microPCMs comprising n-octadecane encapsulated in melamine-formaldehyde resin shell were synthesized in O/W emulsion. The microPCMs are 5 - 15 µm in diameter. The supercooling of these octadecane microcapsules can be as large as 13.6 °C , when the homogeneous nucleation is dominant during the melt crystallization into the thermodynamically stable triclinic phase. Supercooling suppression of the microPCMs has been accomplished by optimizing the composition and structure of the MFR shell. It is discovered that the homogeneous nucleation can be mediated by shell-induced nucleation of triclinic phase and metastable rotator phase when the shell composition and structure are optimized, without using additional nucleate agents. The effects of synthesis parameters, such as ratio of melamine to formaldehyde, pH of pre-polymer, and pH of emulsion, on the phase transition properties of the microPCMs have been investigated systemically. The optimum synthesis conditions have been identified in terms of minimizing supercooling while maintaining heat capacity.

4. Silver was applied as a coating layer on the surface of the as-produced paraffin/MFR microPCMs to enhance their thermal conductivity. The PCM-Ag microcapsules were compressed to make bulk PCMs pellets with stabled shape and structure for TES applications. With silver coated on the surface of microPCMs, thermal conductivity of PCM-Ag pellets can be as high as 14.6 W/mK, significantly larger than the thermal conductivity of normal PCMs. The disadvantage is that silver coating decreases overall latent heat capacity dramatically.

5. Adding thermally-conductive PCMs to PAO can significantly improve the fluid heat transfer properties. Paraffin/MFR microPCMs and silver-coated PCM-Ag microcapsules were added in PAO. Thermal performance of the microPCM enhanced fluids was studied in a microchannel cold plate and compared with that of pure PAO. A test loop was designed and fabricated to evaluate the synthesized PCM fluids.

The PCM fluid with uncoated microPCMs has a 36% higher heat transfer coefficient relative to pure PAO over a range of flow rates and temperatures, when compared at the same flow rate. The thermal resistance of this PCM fluid at a given pumping power is about 20% lower than that of pure PAO, despite the PCM fluid's higher viscosity. The silver-coated PCM-Ag<sub>3</sub> fluid also shows an increased heat transfer coefficient, which is greater than that of pure PAO, but less than that of the PCM fluid. It is suspected that the reduced performance of the PCM-Ag<sub>3</sub> fluid is due to its relatively smaller latent heat. It is clear that the microPCM enhanced heat transfer fluids would provide improved performance relative to pure PAO in heat transfer applications.

## **9.2 *Limitation and Future Works***

The objective of the research is to apply the colloidal systems in the fields of thermal management and water vapor recovery, by developing new colloidal-based synthesis methods, building reliable thermophysical measurement equipment, synthesizing novel materials such as microPCMs, silver-coated thermal conductive microPCMs, and the heat transfer fluids enhanced with the thermal conductive, phase changeable microcapsules, obtaining comprehensive experimental data and appropriate theoretical models of thermal and water managements, and using them to guide the applications. Although the use of microPCMs in thermal management has a brilliant future in a wide variety, the main blockade that hindering the development of this research and applications is that the detailed molecular-level

understanding of all the mechanism which are responsible for the observed change of properties remains unclear.

There are still several important clues indicating the mechanisms of heat and mass transfer in the synthesis and the products of the microPCMs, which can be drawn from numerous research projects:

1. Phase change materials, in form of both nanoparticles and microcapsules, are useful to improve the thermal conductivity and heat capacity of both bulk solid materials and heat transfer fluids simultaneously, and further increase the heat transfer efficiency. MicroPCMs have been developed and characterized in this research based on two types of PCMs, the hydrophobic paraffin and the hydrophilic polyalcohol, with promising results observed. Other combinations of PCMs, shell materials, possible nucleate agents, and base fluids are going to be explored.
2. The supercooling of the encapsulated paraffin can be suppressed by optimizing the polymeric structure of the MFR shells. Though the shell structure can be manipulated by controlling the parameters of the chemical reactions, it remains unclear how the resin is structured and how the difference structure induce heterogeneous nucleation of the encapsulated paraffin. It is meaningful to take a comprehensive investigation of the structure of the MFR for better understanding and further design of more efficient shell material as nucleate agents of encapsulated PCMs.
3. As a novel method to improve the thermal conductivity of PCMs, metal coating on the surface of the PCM microcapsules results to significant elevation of thermal conduction abilities. However, based on theoretical prediction, there are still plenty of rooms for further enhancement of thermal conductivity of the material. The main reason of thermal resistance is the interfacial resistance between the MFR shell and the

metal layer, as well as that among the metal grains in layer. In addition, in this work, the pellets of thermal conductive microPCMs were produced in air, and thus traps a certain amount of air inside, which is another reason of thermal resistance. Further research can be done to explore the surface properties of the microPCMs and origin of the interfacial resistance, and seek a proper way to eliminate it.

### **9.3 Contribution**

#### **9.3.1 Journal Papers**

1. **F. Y. Cao**, J. Ye, B. Yang. "Synthesis and characterization of solid-state phase change material microcapsules for thermal management applications". *J. Nanotechnol. Eng. Med.* 2014, 4, 041001.

2. **F. Y. Cao**, B. Yang. "Supercooling suppression of microencapsulated phase change materials by optimizing shell composition and structure". *Appl. Energ.* 2014, 113, 1512.

3. H. L. Zhu, Y. Y. Li, Z. Q. Fang, J. J. Xu, **F. Y. Cao**, J. Y. Wan, C. Preston, B. Yang, L. B. Hu. "Highly thermally conductive papers with percolative layered boron nitride nanosheets." *ACS Nano.* 2014, 8, 3606.

4. Z. H. Han, **F. Y. Cao**, Bao Yang. "Synthesis and thermal characterization of phase-changeable indium / polyalphaolefin nanofluids". *Appl. Phys. Lett.* 2008, 92, 243104.

5. **F. Y. Cao**, P. Kalinowski, J. Lawler, H. S. Lee, B. Yang. "Synthesis and heat transfer performance of phase change microcapsule enhanced thermal fluids". *Under review.*

6. **F. Y. Cao**, B. Yang. "The critical micelle concentration determined by the thermal conductivity minimum". *In preparation.*

7. **F. Y. Cao**, B. Yang. "Energy-efficient water vapor recovery using microemulsion liquid desiccants". *In preparation.*

### 9.3.2 Book Chapters

1. J. J. Xu\*, F. Y. Cao\*, B. Yang. "Phase change material particles and their application in heat transfer fluids". *Low-cost Nanomaterials*, Springer-Verlag, London, 2014, *in press*. [\*: First Authorship Shared]

### 9.3.3 Patent Applications

1. B. Yang, R. Radermacher, F. Y. Cao, B. L. Shi. "Application of microemulsion-enabled water capture and recovery technology and absorption/adsorption chiller in power plants". *US Provisional Patent Application, 61/867509, 2013*.

2. B. Yang, F. Y. Cao. "Novel phase change materials microcapsules". *US Provisional Patent Application, 61/355851, 2010*.

## Appendices

### A.1 Techniques for Characterization of Heat Transfer Fluids

#### A.1.1 The $3\omega$ – Wire Method

The  $3\omega$  -wire method was employed to measure the thermal conductivity of liquids. Most of the published thermal conductivity data on the heat transfer fluids were obtained using the hot-wire method, which measures the temperature response of the metal wire in the time domain. The  $3\omega$ -wire method is actually a combination of the  $3\omega$  method and the hot-wire method. Similar to the hot-wire method, a metal wire with a length of  $L$  and a radius of  $r$  is suspended in a liquid acts as both a heater and a thermometer [91, 92, 232, 233].

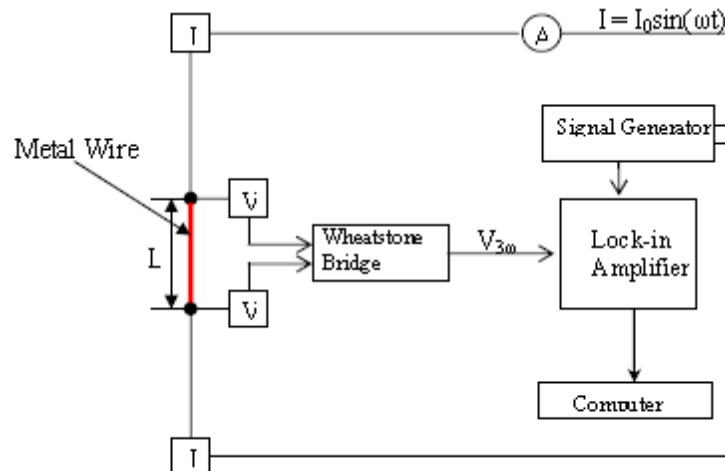


Figure A-9-1. Setup of the  $3\omega$  - wire method for thermal conductivity measurement of heat transfer fluids [167].

In the beginning, a sinusoidal AC current  $I$  at frequency  $\omega$  is passed through the metal wire:

$$I(t) = I_0 \cos(\omega t) \quad (\text{Equation A-1})$$

where  $I_0$  is the amplitude of the AC current. The current heat the metal wire, the power of which can be expressed as a superposition of DC heating source and a  $2\omega$  modulated heating source:

$$P(t) = I_0 R_E \cos^2 \omega t = \left( \frac{I_0^2 R_E}{2} \right) + \left( \frac{I_0^2 R_E \cos(2\omega t)}{2} \right) \quad (\text{Equation A-2})$$

where  $R_E$  is the resistance of the metal wire under the experimental condition which is a function of temperature. The corresponding temperature rise in the sample to be measured is also a superposition of a DC part and a  $2\omega$  modulated part, similar to the heat generation:

$$T(t) = T_{DC} + T_{2\omega} \cos(2\omega t + \varphi) \quad (\text{Equation A-3})$$

in which  $T_{2\omega}$  is the amplitude of the AC temperature rise and  $\varphi$  is the phase shift induced by heating the thermal mass of the sample. Because of the temperature, the resistance of the wire has also a  $2\omega$  component:

$$R_E(t) = R_{E0} [1 + C (T_{DC} + T_{2\omega} \cos(2\omega t + \varphi))] \quad (\text{Equation A-4})$$

where  $C$  is the temperature coefficient of resistance for the metal wire,  $R_{E0}$  is the reference heater resistance at a reference temperature  $T_0$ . Thus, the voltage applied over the metal wire is

$$\begin{aligned} V(t) &= I(t) R_E(t) \\ &= I_0 R_{E0} (1 + C_n T_{DC}) \cos(\omega t) + \frac{I_0 R_{E0} C_n T_{2\omega}}{2} \cos(\omega t + \varphi) + \frac{I_0 R_{E0} C_n T_{2\omega}}{2} \cos(3\omega t + \varphi) \end{aligned} \quad (\text{Equation A-5})$$

in which the voltage contains the voltage drop due to the DC resistance of the wire at  $1\omega$ , and two new components proportional to the temperature rise in the wire at  $1\omega$  and  $3\omega$ , respectively. With applying a lock-in amplifier, the  $3\omega$  term of the voltage can extracted and used to deduce the temperature rise amplitude at  $2\omega$ :

$$T_{2\omega} = \frac{2V_{3\omega}}{CI_0R_{E0}} \quad (\text{Equation A-6})$$

Meanwhile, the frequency dependent temperature rise  $T_{2\omega}$  can be approximated[234] based on

$$T_{2\omega} = \frac{P}{2\pi L k_f} \left[ \frac{1}{2} \ln \left( \frac{\alpha_f}{r^2} \right) - \frac{1}{2} \ln \omega + \eta - 2i \right] \quad (\text{Equation A-7})$$

in which  $P$  is the applied electric power,  $L$  is the length of the metal wire,  $\alpha_f$  and  $k_f$  are the thermal diffusivity and thermal conductivity of the fluids, correspondingly, the later can be calculated by

$$k_f = -\frac{P}{4\pi L} \left( \frac{\partial T_{2\omega}}{\partial \ln \omega} \right)^{-1} \quad (\text{Equation A-8})$$

The  $3\omega$  -wire method has several advantages over the traditional hot-wire transient method. It has little effect to the fluid system, and the temperature oscillation of this method can be kept as small as less than 1K, compared to about 5K for the hot-wire method. Meanwhile, the background noises such as temperature variation have much less influence on the measurements due to the use of the lock-in technique. These advantages make the  $3\omega$ -wire method ideally suited for measuring the thermal conductivity of heat transfer fluids.

### **A.1.2 Differential Scanning Calorimetry**

The DSC determines the temperature and heat flow associated with material transitions as a function of time and temperature. It also provides quantitative and qualitative data endothermic and exothermic processes of materials during physical transitions that caused by phase transition, chemical reaction, and other heat-related changes. The information is helpful for identifying processing and end-use performance [235].

In DSC analysis, the sample is placed in an aluminum pan, and the sample pan and an empty reference pan are placed on small platforms within the DSC chamber. Thermocouple

sensors lie below the pans, as shown in Figure A-2. DSC measurements can be made in two ways: by measuring the electrical energy provided to heaters below the pans necessary to maintain the two pans at the same temperature (power compensation), or by measuring the heat flow (differential temperature) as a function of sample temperature (heat flux) [236]. The DSC ultimately outputs the differential heat flow (heat/time) between your material and the empty reference pan. Heat capacity may be determined by taking the ratio of heat flow to heating rate.

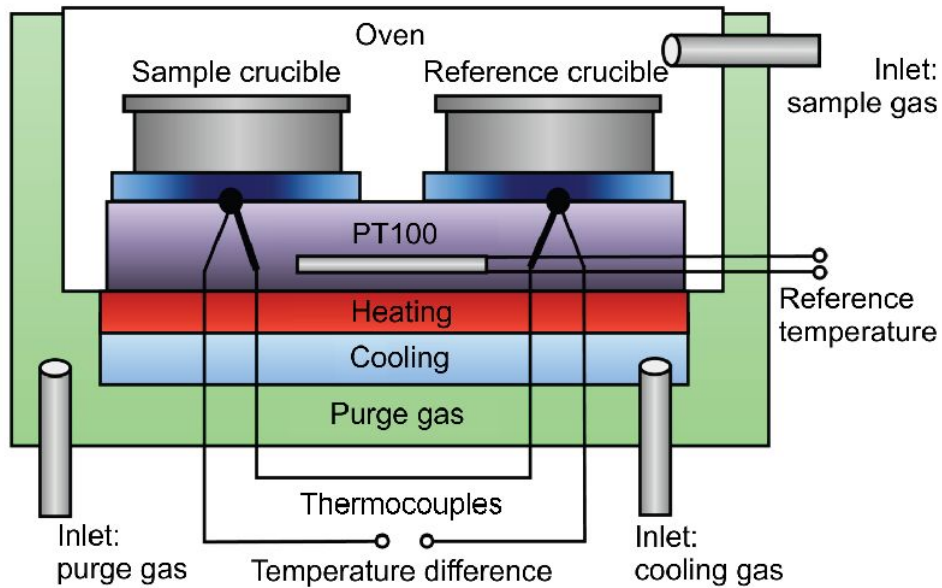


Figure A-9-2. Scheme of the setup of a DSC cell [236].

## A.2 Theories of Thermal Conductivity

### A.2.1 Effective Medium Theory (EMT): the Maxwell Model

Effective thermal conductivity of composites or nanofluids,  $k_{EMT}$ , are dependent only on the thermal conductivity of base fluids,  $k_f$ , the thermal conductivity of dispersed particles,  $k_p$ , and the volumetric fraction of particles,  $\phi$ , and can be expressed as

$$k_{EMT} = f(k_f, k_p, \phi) \quad \text{(Equation A-9)}$$

An empirical version of this equation is given as [237]

$$k_{EMT}^n = (1 - \phi)k_f^n + \phi k_p^n, \quad -1 \leq n \leq 1 \quad (\text{Equation A-10})$$

Maxwell investigated the conduction of liquid suspensions analytically by considering a very dilute suspension containing spherical particles and ignoring the interactions among particles [238]. If the radius of spherical particles are identical, and can be denoted as  $r_p$ , in a temperature field  $T$  and temperature gradient  $G_T$ , the governing equation for the steady-state condition is the Laplace equation:

$$\nabla^2 T(\mathbf{r}) = 0 \quad (\text{Equation A-11})$$

By introducing a large sphere of radius  $R_0$ , within which all the solid spherical particles are included in this large sphere, so that from a point  $r \gg R_0$ , the sphere with radius  $R_0$  is considered as a system with an effective thermal conductivity  $k_{EMT}$  embedded in a matrix or base fluid with a thermal conductivity of  $k_f$ . Solving the Laplace equation with the boundary conditions of

$$T(r)|_{r \rightarrow R_0^-} = T(r)|_{r \rightarrow R_0^+} \quad (\text{Equation A-12})$$

$$k_{EMT} \frac{\partial T(r)}{\partial r} \Big|_{r \rightarrow R_0^-} = k_{EMT} \frac{\partial T(r)}{\partial r} \Big|_{r \rightarrow R_0^+} \quad (\text{Equation A-13})$$

the temperature field outside the sphere  $R_0$  is then expressed as

$$T(r) = \left( \frac{k_{EMT} - k_f}{2k_f + k_{EMT}} \frac{r_0^3}{r^3} - 1 \right) \mathbf{G}_T \cdot \mathbf{r} \quad (\text{Equation A-14})$$

At the same time, the temperature field  $T(r)$  can also be viewed as all the spherical solid particles with radius  $r_p$  being embedded in the matrix with a thermal conductivity of  $k_f$ . Using the superposition principle, the following equation can be derived:

$$T(r) = \left( \frac{k_p - k_f}{2k_f + k_p} \frac{\phi r_0^3}{r^3} - 1 \right) \mathbf{G}_T \cdot \mathbf{r} \quad (\text{Equation A-15})$$

Equating Equation A-14 and A-15, the effective thermal conductivity for suspensions of spherical particles can be obtained:

$$k_{EMT} = \frac{k_p + 2k_f + 2\phi(k_p - k_f)}{k_p + 2k_f - \phi(k_p - k_f)} k_f \quad (\text{Equation A-16})$$

### A.2.2 Hashin-Shtrikman (H-S) Model

For nanocomposite and heat transfer fluids filled with irregularly shaped nanoparticles, fitting of the experimental results was found to be more challenging. While Equation A-16 works for the nanocomposite where the filler remained spherical and uniformly distributed, the thermal conductive nanoparticles may change the effective shape, the aspect ratio, and the volume fraction in different part of the nanocomposite or fluids. The percolation concentration was reported to strongly depend on the shape and the aspect ratio of the particles [239]. Fitting with Equation A-10, this may result in  $n > 1$ , which is outside the expected range. A more general model by Hashin and Shtrikman to estimate the lower and upper bounds of the thermal conductivity of heat transfer fluids and nanocomposite with irregular shaped particles [240]:

$$k_f \left( 1 + \frac{3\phi(k_p - k_f)}{3k_f + (1 - \phi)(k_p - k_f)} \right) < k < k_p \left( 1 - \frac{3(1 - \phi)(k_p - k_f)}{3k_p - \phi(k_p - k_f)} \right) \quad (\text{Equation A-17})$$

where the lower bound is for well-dispersed and isolated nanoparticles in the matrix, and the upper limit represents the thermal conductivity for a perfectly networked structure of the filler in the matrix [241].

## Bibliography

- [1] Vazquez, S., Lukic, S. M., Galvan, E., Franquelo, L. G., and Carrasco, J. M., 2010, "Energy Storage Systems for Transport and Grid Applications," *Industrial Electronics, IEEE Transactions on*, 57(12), pp. 3881-3895.
- [2] Eyer, J., and Corey, G., 2010, "Energy storage for the electricity grid: Benefits and market potential assessment guide," Sandia National Laboratories.
- [3] Kintner-Meyer, M., Balducci, P., Colella, W., Elizondo, M., Jin, C., Nguyen, T., Viswanathan, V., and Zhang, Y., 2012, "National assessment of energy storage for grid balancing and arbitrage: Phase 1, WECC," US Department of Energy, Tech. Rep. DE-AC05-76RL01830.
- [4] Lane, G. A., 1968, *Solar Heat Storage: Latent Heat Materials*, CRC Press, Boca Raton, FL.
- [5] Farid, M. M., Khudhair, A. M., Razack, S. A. K., and Al-Hallaj, S., 2004, "A review on phase change energy storage: materials and applications," *Energy Conversion and Management*, 45(9-10), pp. 1597-1615.
- [6] Hasnain, S. M., 1998, "Review on sustainable thermal energy storage technologies, part I: Heat storage materials and techniques," *Energy Conversion and Management*, 39(11), pp. 1127-1138.
- [7] Paksoy, H. O., 2007, "Thermal Energy Storage for Sustainable Energy Consumption - Fundamentals, Case Studies and Design," *NATO Science Series II*, Springer, Dordrecht, Netherlands.
- [8] Oró, E., de Gracia, A., Castell, A., Farid, M. M., and Cabeza, L. F., 2012, "Review on phase change materials (PCMs) for cold thermal energy storage applications," *Appl. Energy*, 99(0), pp. 513-533.
- [9] Zhang, P., Ma, Z. W., and Wang, R. Z., 2010, "An overview of phase change material slurries: MPCs and CHS," *Renewable and Sustainable Energy Reviews*, 14(2), pp. 598-614.

- [10] Zalba, B., Marín, J. M., Cabeza, L. F., and Mehling, H., 2003, "Review on thermal energy storage with phase change: materials, heat transfer analysis and applications," *Applied Thermal Engineering*, 23(3), pp. 251-283.
- [11] Li, G., Hwang, Y., and Rademacher, R., 2012, "Review of cold storage materials for air conditioning application," *international journal of refrigeration*, 35(8), pp. 2053-2077.
- [12] Li, G., 2013, "Review of thermal energy storage technologies and experimental investigation of adsorption thermal energy storage for residential application."
- [13] Fan, L., and Khodadadi, J. M., 2011, "Thermal conductivity enhancement of phase change materials for thermal energy storage: A review," *Renewable and Sustainable Energy Reviews*, 15(1), pp. 24-46.
- [14] Lafdi, K., Mesalhy, O., and Elgafy, A., 2008, "Graphite foams infiltrated with phase change materials as alternative materials for space and terrestrial thermal energy storage applications," *Carbon*, 46(1), pp. 159-168.
- [15] Sanusi, O., Warzoha, R., and Fleischer, A. S., 2011, "Energy storage and solidification of paraffin phase change material embedded with graphite nanofibers," *International Journal of Heat and Mass Transfer*, 54(19–20), pp. 4429-4436.
- [16] Marín, J. M., Zalba, B., Cabeza, L. F., and Mehling, H., 2005, "Improvement of a thermal energy storage using plates with paraffin–graphite composite," *International Journal of Heat and Mass Transfer*, 48(12), pp. 2561-2570.
- [17] Mondal, S., 2008, "Phase change materials for smart textiles - An overview," *Applied Thermal Engineering*, 28(11-12), pp. 1536-1550.
- [18] Chen, H., Yang, W., He, Y., Ding, W., Zhang, L., Tan, C., Lapkin, A. A., and Bavykin, D. V., 2008, "Heat transfer and flow behaviour of aqueous suspensions of titanate nanotubes (nanofluids)," *Powder Technology*, 183(1), pp. 63-72.
- [19] Baetens, R., Jelle, B. P., and Gustavsen, A., 2010, "Phase change materials for building applications: A state-of-the-art review," *Energy and Buildings*, 42(9), pp. 1361-1368.

- [20] Wang, X., Guo, Q., Zhong, Y., Wei, X., and Liu, L., 2013, "Heat transfer enhancement of neopentyl glycol using compressed expanded natural graphite for thermal energy storage," *Renewable Energy*, 51(0), pp. 241-246.
- [21] ~200 BC, Rites of Zhou (Zhou Li), China.
- [22] McGuffey, O. S., 1947, "METHOD OF MAKING HOLDOVER," U.S. Patent 2416015.
- [23] Skogsberg, K., and Nordell, B., 2001, "The Sundsvall hospital snow storage," *Cold Regions Science and Technology*, 32(1), pp. 63-70.
- [24] Sterling, F. W., and Crooker, H. L., 1928, U.S. Patent 1656366.
- [25] Hogan, G. L., 1949, U.S. Patent 2289425.
- [26] Shepherd, J. C., 1958, "REFRIGERANT ARTICLE AND COMPOSITION," U.S. Patent 2853305.
- [27] Mavleos, M. G., and Desy, J. J., 1965, "LITHIUM HYDRIDE BODY HEATING DEVICE," U.S. Patent 3182653.
- [28] Cot-Gores, J., Castell, A., and Cabeza, L. F., 2012, "Thermochemical energy storage and conversion: A-state-of-the-art review of the experimental research under practical conditions," *Renewable and Sustainable Energy Reviews*, 16(7), pp. 5207-5224.
- [29] Ding, Y., and Riffat, S. B., 2012, "Thermochemical energy storage technologies for building applications: a state-of-the-art review," *International Journal of Low-Carbon Technologies*.
- [30] Mohammad, A. T., Bin Mat, S., Sulaiman, M. Y., Sopian, K., and Al-abidi, A. A., 2013, "Survey of hybrid liquid desiccant air conditioning systems," *Renew. Sust. Energ. Rev.*, 20, pp. 186-200.
- [31] Chua, K. J., Chou, S. K., Yang, W. M., and Yan, J., 2013, "Achieving better energy-efficient air conditioning - A review of technologies and strategies," *Appl. Energy*, 104, pp. 87-104.

- [32] Badami, M., Portoraro, A., and Ruscica, G., 2012, "Analysis of trigeneration plants: engine with liquid desiccant cooling and micro gas turbine with absorption chiller," *International Journal of Energy Research*, 36(5), pp. 579-589.
- [33] Enteria, N., and Mizutani, K., 2011, "The role of the thermally activated desiccant cooling technologies in the issue of energy and environment," *Renew. Sust. Energ. Rev.*, 15(4), pp. 2095-2122.
- [34] Badami, M., and Portoraro, A., 2009, "Performance analysis of an innovative small-scale trigeneration plant with liquid desiccant cooling system," *Energy and Buildings*, 41(11), pp. 1195-1204.
- [35] Lowenstein, A., 2008, "Review of Liquid Desiccant Technology for HVAC Applications," *HVAC&R Research*, 14(6), pp. 819-839.
- [36] Jain, S., and Bansal, P. K., 2007, "Performance analysis of liquid desiccant dehumidification systems," *Int. J. Refrig.-Rev. Int. Froid*, 30(5), pp. 861-872.
- [37] Yao, Y., 2010, "Using power ultrasound for the regeneration of dehumidizers in desiccant air-conditioning systems: A review of prospective studies and unexplored issues," *Renew. Sust. Energ. Rev.*, 14(7), pp. 1860-1873.
- [38] Gandhidasan, P., 2003, "Parametric analysis of natural gas dehydration by a triethylene glycol solution," *Energy Sources*, 25(3), pp. 189-201.
- [39] Yamagishi, Y., Sugeno, T., Ishige, T., Takeuchi, H., and Pyatenko, A. T., "An evaluation of microencapsulated PCM for use in cold energy transportation medium," *Proc. Energy Conversion Engineering Conference, 1996. IECEC 96., Proceedings of the 31st Intersociety*, pp. 2077-2083 vol.2073.
- [40] Yamagishi, Y., Takeuchi, H., Pyatenko, A. T., and Kayukawa, N., 1999, "Characteristics of microencapsulated PCM slurry as a heat-transfer fluid," *Aiche J.*, 45(4), pp. 696-707.
- [41] Fan, Y. F., Zhang, X. X., Wang, X. C., Li, J., and Zhu, Q. B., 2004, "Super-cooling prevention of microencapsulated phase change material," *Thermochimica Acta*, 413(1-2), pp. 1-6.

- [42] Lee, W.-m., 2004, "Microcapsule containing phase change material and article having same," US Patent Application 10/611417
- [43] Gschwander, S., Schossig, P., and Henning, H. M., 2005, "Micro-encapsulated paraffin in phase-change slurries," *Sol. Energy Mater. Sol. Cells*, 89(2-3), pp. 307-315.
- [44] Alvarado, J. L., Marsh, C., Sohn, C., Phetteplace, G., and Newell, T., 2007, "Thermal performance of microencapsulated phase change material slurry in turbulent flow under constant heat flux," *International Journal of Heat and Mass Transfer*, 50(9-10), pp. 1938-1952.
- [45] Xuan, Y. M., Huang, Y., and Li, Q., 2009, "Experimental investigation on thermal conductivity and specific heat capacity of magnetic microencapsulated phase change material suspension," *Chem. Phys. Lett.*, 479(4-6), pp. 264-269.
- [46] Fu, D., Su, Y., Xie, B., Zhu, H., Liu, G., and Wang, D., 2011, "Phase change materials of n-alkane-containing microcapsules: observation of coexistence of ordered and rotator phases," *Physical Chemistry Chemical Physics*, 13(6), pp. 2021-2026.
- [47] Fu, D. S., Liu, Y. F., Liu, G. M., Su, Y. L., and Wang, D. J., 2011, "Confined crystallization of binary n-alkane mixtures: stabilization of a new rotator phase by enhanced surface freezing and weakened intermolecular interactions," *Physical Chemistry Chemical Physics*, 13(33), pp. 15031-15036.
- [48] Zhao, C. Y., and Zhang, G. H., 2011, "Review on microencapsulated phase change materials (MEPCMs): Fabrication, characterization and applications," *Renewable and Sustainable Energy Reviews*, 15(8), pp. 3813-3832.
- [49] Prakash, J., Garg, H. P., and Datta, G., 1985, "A SOLAR WATER HEATER WITH A BUILT-IN LATENT-HEAT STORAGE," *Energy Conversion and Management*, 25(1), pp. 51-56.
- [50] Buddhi, D., Sawhney, R. L., Sehgal, P. N., and Bansal, N. K., 1987, "A SIMPLIFICATION OF THE DIFFERENTIAL THERMAL-ANALYSIS METHOD TO DETERMINE THE LATENT-HEAT OF FUSION OF PHASE-CHANGE MATERIALS," *Journal of Physics D-Applied Physics*, 20(12), pp. 1601-1605.

- [51] Shaikh, S., and Lafdi, K., 2010, "C/C composite, carbon nanotube and paraffin wax hybrid systems for the thermal control of pulsed power in electronics," *Carbon*, 48(3), pp. 813-824.
- [52] Han, Z. H., Yang, B., Qi, Y., and Cumings, J., 2011, "Synthesis of low-melting-point metallic nanoparticles with an ultrasonic nanoemulsion method," *Ultrasonics*, 51(4), pp. 485-488.
- [53] Han, Z. H., Cao, F. Y., and Yang, B., 2008, "Synthesis and thermal characterization of phase-changeable indium/polyalphaolefin nanofluids," *Applied Physics Letters*, 92(24), pp. 243104-243103.
- [54] Hawlader, M. N. A., Uddin, M. S., and Zhu, H. J., 2000, "PREPARATION AND EVALUATION OF A NOVEL SOLAR STORAGE MATERIAL: MICROENCAPSULATED PARAFFIN," *International Journal of Solar Energy*, 20(4), pp. 227-238.
- [55] Sarier, N., and Onder, E., 2007, "The manufacture of microencapsulated phase change materials suitable for the design of thermally enhanced fabrics," *Thermochimica Acta*, 452(2), pp. 149-160.
- [56] O'Sullivan, M., and Vincent, B., 2010, "Aqueous dispersions of silica shell/water-core microcapsules," *Journal of Colloid and Interface Science*, 343(1), pp. 31-35.
- [57] Delgado, M., Lazaro, A., Mazo, J., and Zalba, B., 2012, "Review on phase change material emulsions and microencapsulated phase change material slurries: Materials, heat transfer studies and applications," *Renew. Sust. Energ. Rev.*, 16(1), pp. 253-273.
- [58] Jamekhorshid, A., Sadrameli, S. M., and Farid, M., 2014, "A review of microencapsulation methods of phase change materials (PCMs) as a thermal energy storage (TES) medium," *Renewable and Sustainable Energy Reviews*, 31(0), pp. 531-542.
- [59] Zhang, Y. P., Lin, K. P., Yang, R., Di, H. F., and Jiang, Y., 2006, "Preparation, thermal performance and application of shape-stabilized PCM in energy efficient buildings," *Energy and Buildings*, 38(10), pp. 1262-1269.

- [60] Fang, G., Chen, Z., and Li, H., 2010, "Synthesis and properties of microencapsulated paraffin composites with SiO<sub>2</sub> shell as thermal energy storage materials," *Chemical Engineering Journal*, 163(1–2), pp. 154-159.
- [61] Su, J.-F., Wang, X.-Y., Wang, S.-B., Zhao, Y.-H., and Huang, Z., 2012, "Fabrication and properties of microencapsulated-paraffin/gypsum-matrix building materials for thermal energy storage," *Energy Conversion and Management*, 55, pp. 101-107.
- [62] Zhang, H., and Wang, X., 2009, "Fabrication and performances of microencapsulated phase change materials based on n-octadecane core and resorcinol-modified melamine–formaldehyde shell," *Colloids and Surfaces A: Physicochemical and Engineering Aspects*, 332(2–3), pp. 129-138.
- [63] Tseng, Y. H., Fang, M. H., Tsai, P. S., and Yang, Y. M., 2005, "Preparation of microencapsulated phase-change materials (MCPCMs) by means of interfacial polycondensation," *J. Microencapsul.*, 22(1), pp. 37-46.
- [64] Hawlader, M. N. A., Uddin, M. S., and Khin, M. M., 2003, "Microencapsulated PCM thermal-energy storage system," *Appl. Energy*, 74(1–2), pp. 195-202.
- [65] Cao, F. Y., and Yang, B., 2014, "Supercooling suppression of microencapsulated phase change materials by optimizing shell composition and structure," *Appl. Energy*, 113, pp. 1512-1518.
- [66] Cao, F., Ye, J., and Yang, B., 2014, "Synthesis and Characterization of Solid-State Phase Change Material Microcapsules for Thermal Management Applications," *Journal of Nanotechnology in Engineering and Medicine*, 4(4), pp. 041001-041001.
- [67] Cao, F., Kalinowski, P., Lawler, J., Lee, H. S., and Yang, B., 2014, "Synthesis and Heat Transfer Performance of Phase Change Microcapsule Enhanced Thermal Fluids " Submitted.
- [68] Giraud, S., Bourbigot, S., Rochery, M., Vroman, I., Tighzert, L., and Delobel, R., 2002, "Microencapsulation of phosphate: application to flame retarded coated cotton," *Polymer Degradation and Stability*, 77(2), pp. 285-297.

- [69] Giraud, S., Bourbigot, S., Rochery, M., Vroman, I., Tighzert, L., Delobel, R., and Poutch, F., 2005, "Flame retarded polyurea with microencapsulated ammonium phosphate for textile coating," *Polymer degradation and stability*, 88(1), pp. 106-113.
- [70] Onder, E., Sarier, N., and Cimen, E., 2008, "Encapsulation of phase change materials by complex coacervation to improve thermal performances of woven fabrics," *Thermochimica Acta*, 467(1–2), pp. 63-72.
- [71] Hawes, D. W., Feldman, D., and Banu, D., 1993, "Latent heat storage in building materials," *Energy and Buildings*, 20(1), pp. 77-86.
- [72] Neeper, D. A., 2000, "Thermal dynamics of wallboard with latent heat storage," *Solar Energy*, 68(5), pp. 393-403.
- [73] Chen, Z., Cao, L., Shan, F., and Fang, G., 2013, "Preparation and characteristics of microencapsulated stearic acid as composite thermal energy storage material in buildings," *Energy and Buildings*, 62(0), pp. 469-474.
- [74] Tyagi, V. V., Kaushik, S. C., Tyagi, S. K., and Akiyama, T., 2011, "Development of phase change materials based microencapsulated technology for buildings: A review," *Renewable and Sustainable Energy Reviews*, 15(2), pp. 1373-1391.
- [75] Rao, Y., Lin, G., Luo, Y., Chen, S., and Wang, L., 2007, "Preparation and thermal properties of microencapsulated phase change material for enhancing fluid flow heat transfer," *Heat Transfer—Asian Research*, 36(1), pp. 28-37.
- [76] Dammal, F., and Stephan, P., 2012, "Heat Transfer to Suspensions of Microencapsulated Phase Change Material Flowing Through Minichannels," *Journal of Heat Transfer-Transactions of the Asme*, 134(2).
- [77] Rao, Y., Dammal, F., Stephan, P., and Lin, G., 2007, "Convective heat transfer characteristics of microencapsulated phase change material suspensions in minichannels," *Heat and Mass Transfer*, 44(2), pp. 175-186.

- [78] Eastman, J. A., Phillpot, S., Choi, S., and Keblinski, P., 2004, "Thermal transport in nanofluids 1," *Annu. Rev. Mater. Res.*, 34, pp. 219-246.
- [79] Keblinski, P., Eastman, J. A., and Cahill, D. G., 2005, "Nanofluids for thermal transport," *Materials Today*, 8(6), pp. 36-44.
- [80] Inaba, H., 2000, "New challenge in advanced thermal energy transportation using functionally thermal fluids," *International Journal of Thermal Sciences*, 39(9-11), pp. 991-1003.
- [81] Ruckenstein, E., and Djikaev, Y. S., 2005, "Recent developments in the kinetic theory of nucleation," *Advances in Colloid and Interface Science*, 118(1-3), pp. 51-72.
- [82] Sun, G., and Zhang, Z., 2002, "Mechanical strength of microcapsules made of different wall materials," *Int. J. Pharm.*, 242(1-2), pp. 307-311.
- [83] Zhang, H., Wang, X., and Wu, D., 2010, "Silica encapsulation of n-octadecane via sol-gel process: A novel microencapsulated phase-change material with enhanced thermal conductivity and performance," *Journal of Colloid and Interface Science*, 343(1), pp. 246-255.
- [84] Chang, C. C., Tsai, Y. L., Chiu, J. J., and Chen, H., 2009, "Preparation of phase change materials microcapsules by using PMMA network-silica hybrid shell via sol-gel process," *J. Appl. Polym. Sci.*, 112(3), pp. 1850-1857.
- [85] Wang, L.-Y., Tsai, P.-S., and Yang, Y.-M., 2006, "Preparation of silica microspheres encapsulating phase-change material by sol-gel method in O/W emulsion," *J. Microencapsul.*, 23(1), pp. 3-14.
- [86] Sirota, E. B., 1998, "Supercooling, nucleation, rotator phases, and surface crystallization of n-alkane melts," *Langmuir*, 14(11), pp. 3133-3136.
- [87] Alvarado, J. L., Marsh, C., Sohn, C., Vilceus, M., Hock, V., Phetteplace, G., and Newell, T., 2006, "Characterization of supercooling suppression of microencapsulated phase change material by using DSC," *J Therm Anal Calorim*, 86(2), pp. 505-509.

- [88] Zhang, X. X., Fan, Y. F., Tao, X. M., and Yick, K. L., 2005, "Crystallization and prevention of supercooling of microencapsulated n-alkanes," *Journal of Colloid and Interface Science*, 281(2), pp. 299-306.
- [89] Khodadadi, J. M., Fan, L., and Babaei, H., 2013, "Thermal conductivity enhancement of nanostructure-based colloidal suspensions utilized as phase change materials for thermal energy storage: A review," *Renewable and Sustainable Energy Reviews*, 24(0), pp. 418-444.
- [90] Xu, J., Yang, B., and Hammouda, B., 2011, "Thermal conductivity and viscosity of self-assembled alcohol/polyalphaolefin nanoemulsion fluids," *Nanoscale Res Lett*, 6(1), pp. 1-6.
- [91] Han, Z. H., and Yang, B., 2008, "Thermophysical characteristics of water-in-FC72 nanoemulsion fluids," *Applied Physics Letters*, 92(1), pp. 013118-013113.
- [92] Yang, B., and Han, Z. H., 2006, "Thermal conductivity enhancement in water-in-FC72 nanoemulsion fluids," *Applied Physics Letters*, 88(26), pp. 261914-261913.
- [93] Buongiorno, J., Venerus, D. C., Prabhat, N., McKrell, T., Townsend, J., Christianson, R., Tolmachev, Y. V., Keblinski, P., Hu, L. W., Alvarado, J. L., Bang, I. C., Bishnoi, S. W., Bonetti, M., Botz, F., Cecere, A., Chang, Y., Chen, G., Chen, H. S., Chung, S. J., Chyu, M. K., Das, S. K., Di Paola, R., Ding, Y. L., Dubois, F., Dzido, G., Eapen, J., Escher, W., Funfschilling, D., Galand, Q., Gao, J. W., Gharagozloo, P. E., Goodson, K. E., Gutierrez, J. G., Hong, H. P., Horton, M., Hwang, K. S., Iorio, C. S., Jang, S. P., Jarzebski, A. B., Jiang, Y. R., Jin, L. W., Kabelac, S., Kamath, A., Kedzierski, M. A., Kieng, L. G., Kim, C., Kim, J. H., Kim, S., Lee, S. H., Leong, K. C., Manna, I., Michel, B., Ni, R., Patel, H. E., Philip, J., Poulikakos, D., Reynaud, C., Savino, R., Singh, P. K., Song, P. X., Sundararajan, T., Timofeeva, E., Tritcak, T., Turanov, A. N., Van Vaerenbergh, S., Wen, D. S., Witharana, S., Yang, C., Yeh, W. H., Zhao, X. Z., and Zhou, S. Q., 2009, "A benchmark study on the thermal conductivity of nanofluids," *Journal of Applied Physics*, 106(9), p. 094312.
- [94] Fan, J., and Wang, L. Q., 2011, "Review of heat conduction in nanofluids," *Journal Of Heat Transfer-Transactions Of The Asme*, 133, pp. 040801/040801-040814.

- [95] Wang, X.-Q., and Mujumdar, A. S., 2008, "A review on nanofluids - part I: theoretical and numerical investigations," *Brazilian Journal of Chemical Engineering*, 25, pp. 613-630.
- [96] Heris, S. Z., Esfahany, M. N., and Etemad, S. G., 2007, "Experimental investigation of convective heat transfer of Al<sub>2</sub>O<sub>3</sub>/water nanofluid in circular tube," *International Journal of Heat and Fluid Flow*, 28(2), pp. 203-210.
- [97] Chein, R., and Chuang, J., 2007, "Experimental microchannel heat sink performance studies using nanofluids," *International Journal of Thermal Sciences*, 46(1), pp. 57-66.
- [98] Kim, S. H., Choi, S. R., and Kim, D., 2006, "Thermal Conductivity of Metal-Oxide Nanofluids: Particle Size Dependence and Effect of Laser Irradiation," *Journal of Heat Transfer*, 129(3), pp. 298-307.
- [99] Heris, S. Z., Etemad, S. G., and Esfahany, A. N., 2006, "Experimental investigation of oxide nanofluids laminar flow convective heat transfer," *International Communications in Heat and Mass Transfer*, 33(4), pp. 529-535.
- [100] Assael, M. J., Metaxa, I. N., Arvanitidis, J., Christofilos, D., and Lioutas, C., 2005, "Thermal Conductivity Enhancement in Aqueous Suspensions of Carbon Multi-Walled and Double-Walled Nanotubes in the Presence of Two Different Dispersants," *Int J Thermophys*, 26(3), pp. 647-664.
- [101] Wen, D. S., and Ding, Y. L., 2004, "Experimental investigation into convective heat transfer of nanofluids at the entrance region under laminar flow conditions," *International Journal of Heat and Mass Transfer*, 47(24), pp. 5181-5188.
- [102] Xuan, Y., and Li, Q., 2003, "Investigation on Convective Heat Transfer and Flow Features of Nanofluids," *Journal of Heat Transfer*, 125(1), pp. 151-155.
- [103] McClements, D. J., 2012, "Nanoemulsions versus microemulsions: terminology, differences, and similarities," *Soft Matter*, 8(6), pp. 1719-1729.
- [104] Fanun, M., 2008, "Microemulsions: Properties and Applications," CRC Press, Boca Raton, FL.

- [105] Moulik, S. P., and Rakshit, A. K., 2006, "Physicochemistry and Applications of Microemulsions," *Journal of Surface Science and Technology*, 22(3/4), p. 159.
- [106] Sjoblom, J., Lindberg, R., and Friberg, S. E., 1996, "Microemulsions - Phase equilibria characterization, structures, applications and chemical reactions," *Advances in Colloid and Interface Science*, 65, pp. 125-287.
- [107] Ruckenstein, E., 1996, "Microemulsions, Macroemulsions, and the Bancroft Rule," *Langmuir*, 12(26), pp. 6351-6353.
- [108] Nagarajan, R., 2011, "Amphiphilic Surfactants and Amphiphilic Polymers: Principles of Molecular Assembly," *Amphiphiles: Molecular Assembly and Applications*, American Chemical Society, pp. 1-22.
- [109] Solans, C., Izquierdo, P., Nolla, J., Azemar, N., and Garcia-Celma, M. J., 2005, "Nanoemulsions," *Curr. Opin. Colloid Interface Sci.*, 10(3-4), pp. 102-110.
- [110] Rosen, M. J., Mathias, J. H., and Davenport, L., 1999, "Aberrant aggregation behavior in cationic gemini surfactants investigated by surface tension, interfacial tension, and fluorescence methods," *Langmuir*, 15(21), pp. 7340-7346.
- [111] Binks, B. P., 1993, "EMULSION-TYPE BELOW AND ABOVE THE CMC IN AOT MICROEMULSION SYSTEMS," *Colloids and Surfaces a-Physicochemical and Engineering Aspects*, 71(2), pp. 167-172.
- [112] Lindman, B., and Wennerström, H., 1980, "Micelles," *Micelles*, Springer Berlin Heidelberg, pp. 1-83.
- [113] Chattopadhyay, A., and London, E., 1984, "Fluorimetric determination of critical micelle concentration avoiding interference from detergent charge," *Analytical Biochemistry*, 139(2), pp. 408-412.
- [114] Chatterjee, A., Moulik, S. P., Sanyal, S. K., Mishra, B. K., and Puri, P. M., 2001, "Thermodynamics of micelle formation of ionic surfactants: A critical assessment for sodium dodecyl sulfate, cetyl pyridinium chloride and dioctyl sulfosuccinate (Na salt) by

- microcalorimetric, conductometric, and tensiometric measurements," *Journal of Physical Chemistry B*, 105(51), pp. 12823-12831.
- [115] Mukerjee, P., and Mysels, K. J., 1971, "Critical micelle concentrations of aqueous surfactant systems," DTIC Document.
- [116] Turro, N. J., and Yekta, A., 1978, "Luminescent probes for detergent solutions. A simple procedure for determination of the mean aggregation number of micelles," *Journal of the American Chemical Society*, 100(18), pp. 5951-5952.
- [117] Griffin, W. C., 1949, "CLASSIFICATION OF SURFACE-ACTIVE AGENTS BY "HLB", " *Journal of Cosmetic Science*, 1(5), pp. 311-326.
- [118] Rosen, M. J., and Kunjappu, J. T., 2012, *Surfactants and interfacial phenomena*, John Wiley & Sons.
- [119] Langevin, D., 1988, "Microemulsions," *Accounts of Chemical Research*, 21(7), pp. 255-260.
- [120] BECHER, P., 2001, *Emulsions: Theory and Practice*, OXFORD UNIVERSITY PRESS.
- [121] Tadros, T., Izquierdo, P., Esquena, J., and Solans, C., 2004, "Formation and stability of nano-emulsions," *Advances in Colloid and Interface Science*, 108–109(0), pp. 303-318.
- [122] Kumar, P., and Mittal, K. L., 1999, *Handbook of microemulsion science and technology*, New York: Marcel Dekker.
- [123] Mitchell, D. J., and Ninham, B. W., 1981, "Micelles, vesicles and microemulsions," *Journal of the Chemical Society, Faraday Transactions 2: Molecular and Chemical Physics*, 77(4), pp. 601-629.
- [124] Winsor, P. A., 1948, "Hydrotropy, solubilisation and related emulsification processes," *Transactions of the Faraday Society*, 44(0), pp. 376-398.
- [125] Cosgrove, T., 2010, *Colloid science: principles, methods and applications*, John Wiley & Sons.

- [126] McClements, D. J., 1999, Food emulsions: Principles, practices and techniques, CRC press.
- [127] Chen, Z., Cao, L., Fang, G., and Shan, F., 2013, "Synthesis and characterization of microencapsulated paraffin microcapsules as shape-stabilized thermal energy storage materials," *Nanoscale and Microscale Thermophysical Engineering*, 17(2), pp. 112-123.
- [128] Sumiga, B., Knez, E., Vrtacnik, M., Savec, V. F., Staresinic, M., and Boh, B., 2011, "Production of Melamine-Formaldehyde PCM Microcapsules with Ammonia Scavenger used for Residual Formaldehyde Reduction," *Acta Chimica Slovenica*, 58(1), pp. 14-25.
- [129] Palanikkumaran, M., Gupta, K. K., Agrawal, A. K., and Jassal, M., 2010, "Effect of emulsion preparation method on microencapsulation of n- octadecane using melamine-formaldehyde pre-polymers," *Indian Journal of Fibre & Textile Research*, 35(2), pp. 101-106.
- [130] Erkan, G., Sariisik, M., and Pazarlioglu, N. K., 2010, "The Microencapsulation of Terbinafine via In Situ Polymerization of Melamine-Formaldehyde and Their Application to Cotton Fabric," *J. Appl. Polym. Sci.*, 118(6), pp. 3707-3714.
- [131] Palanikkumaran, M., Gupta, K. K., Agrawal, A. K., and Jassal, M., 2009, "Highly Stable Hexamethylolmelamine Microcapsules Containing n-Octadecane Prepared by In Situ Encapsulation," *J. Appl. Polym. Sci.*, 114(5), pp. 2997-3002.
- [132] Shin, Y., Yoo, D. I., and Son, K., 2005, "Development of thermoregulating textile materials with microencapsulated phase change materials (PCM). II. Preparation and application of PCM microcapsules," *J. Appl. Polym. Sci.*, 96(6), pp. 2005-2010.
- [133] Sun, G., and Zhang, Z., 2002, "Mechanical strength of microcapsules made of different wall materials," *Int. J. Pharm.*, 242(1-2), pp. 307-311.
- [134] Lee, H. Y., Lee, S. J., Cheong, I. W., and Kim, J. H., 2002, "Microencapsulation of fragrant oil via in situ polymerization: effects of pH and melamine-formaldehyde molar ratio," *J. Microencapsul.*, 19(5), pp. 559-569.
- [135] Jahromi, S., 1999, "Storage stability of melamine-formaldehyde resin solutions, 1. The mechanism of instability," *Macromolecular Chemistry and Physics*, 200(10), pp. 2230-2239.

- [136] Kumar, A., and Katiyar, V., 1990, "MODELING AND EXPERIMENTAL INVESTIGATION OF MELAMINE FORMALDEHYDE POLYMERIZATION," *Macromolecules*, 23(16), pp. 3729-3736.
- [137] Hong, K., and Park, S., 1999, "Melamine resin microcapsules containing fragrant oil: synthesis and characterization," *Materials Chemistry and Physics*, 58(2), pp. 128-131.
- [138] Liang, C., Lingling, X., Hongbo, S., and Zhibin, Z., 2009, "Microencapsulation of butyl stearate as a phase change material by interfacial polycondensation in a polyurea system," *Energy Conversion and Management*, 50(3), pp. 723-729.
- [139] Cho, J.-S., Kwon, A., and Cho, C.-G., 2002, "Microencapsulation of octadecane as a phase-change material by interfacial polymerization in an emulsion system," *Colloid Polym Sci*, 280(3), pp. 260-266.
- [140] Zhang, X.-x., Tao, X.-m., Yick, K.-l., and Wang, X.-c., 2004, "Structure and thermal stability of microencapsulated phase-change materials," *Colloid Polym Sci*, 282(4), pp. 330-336.
- [141] Zhang, X. X., Fan, Y. F., Tao, X. M., and Yick, K. L., 2004, "Fabrication and properties of microcapsules and nanocapsules containing n-octadecane," *Materials Chemistry and Physics*, 88(2-3), pp. 300-307.
- [142] Song, Q., Li, Y., Xing, J., Hu, J., and Marcus, Y., 2007, "Thermal stability of composite phase change material microcapsules incorporated with silver nano-particles," *Polymer*, 48(11), pp. 3317-3323.
- [143] Boh, B., Knez, E., and Staresinic, M., 2005, "Microencapsulation of higher hydrocarbon phase change materials by in situ polymerization," *J. Microencapsul.*, 22(7), pp. 715-735.
- [144] Su, J., Wang, L., and Ren, L., 2006, "Fabrication and thermal properties of microPCMs: Used melamine - formaldehyde resin as shell material," *J. Appl. Polym. Sci.*, 101(3), pp. 1522-1528.

- [145] Salaun, F., Devaux, E., Bourbigot, S., and Rumeau, P., 2009, "Influence of process parameters on microcapsules loaded with n-hexadecane prepared by in situ polymerization," *Chemical Engineering Journal*, 155(1-2), pp. 457-465.
- [146] Long, Y., York, D., Zhang, Z., and Preece, J. A., 2009, "Microcapsules with low content of formaldehyde: preparation and characterization," *Journal of Materials Chemistry*, 19(37), pp. 6882-6887.
- [147] Hadjieva, M., Stoykov, R., and Filipova, T., 2000, "Composite salt-hydrate concrete system for building energy storage," *Renewable Energy*, 19(1-2), pp. 111-115.
- [148] Ryu, H. W., Woo, S. W., Shin, B. C., and Kim, S. D., 1992, "Prevention of supercooling and stabilization of inorganic salt hydrates as latent heat storage materials," *Sol. Energy Mater. Sol. Cells*, 27(2), pp. 161-172.
- [149] Sandnes, B., and Rekstad, J., 2006, "Supercooling salt hydrates: Stored enthalpy as a function of temperature," *Solar Energy*, 80(5), pp. 616-625.
- [150] Avrami, M., 1939, "Kinetics of phase change. I General theory," *The Journal of Chemical Physics*, 7, p. 1103.
- [151] Xie, B., Liu, G., Jiang, S., Zhao, Y., and Wang, D., 2008, "Crystallization Behaviors of n-Octadecane in Confined Space: Crossover of Rotator Phase from Transient to Metastable Induced by Surface Freezing," *Journal of Physical Chemistry B*, 112(42), pp. 13310-13315.
- [152] Ji, H., Sellan, D. P., Pettes, M. T., Kong, X., Ji, J., Shi, L., and Ruoff, R. S., 2014, "Enhanced thermal conductivity of phase change materials with ultrathin-graphite foams for thermal energy storage," *Energy & Environmental Science*, 7(3), pp. 1185-1192.
- [153] Balikowski, J., and Mollendorf, J., 2007, "Performance of phase change materials in a horizontal annulus of a double-pipe heat exchanger in a water-circulating loop," *Journal of heat transfer*, 129(3), pp. 265-272.

- [154] Griffiths, P. W., and Eames, P. C., 2007, "Performance of chilled ceiling panels using phase change material slurries as the heat transport medium," *Applied Thermal Engineering*, 27(10), pp. 1756-1760.
- [155] Gschwander, S., Schossig, P., and Henning, H. M., 2005, "Micro-encapsulated paraffin in phase-change slurries," *Sol. Energy Mater. Sol. Cells*, 89(2-3), pp. 307-315.
- [156] Mehling, H., and Cabeza, L. F., 2008, "Heat and cold storage with PCM," *Hand book*, Publisher Springer, Germany.
- [157] Davis, D. A., Hart, R. L., Work, D. E., and Virgallito, D. R., 2004, "Macrocapsules containing microencapsulated phase change materials," *Google Patents*.
- [158] Castellón, C., Medrano, M., Roca, J., Cabeza, L. F., Navarro, M. E., Fernández, A. I., Lázaro, A., and Zalba, B., 2010, "Effect of microencapsulated phase change material in sandwich panels," *Renewable Energy*, 35(10), pp. 2370-2374.
- [159] Kotlarchyk, M., Huang, J. S., and Chen, S. H., 1985, "Structure of AOT reversed micelles determined by small-angle neutron scattering," *The Journal of Physical Chemistry*, 89(20), pp. 4382-4386.
- [160] Griffiths, P. C., Whatton, M. L., Abbott, R. J., Kwan, W., Pitt, A. R., Howe, A. M., King, S. M., and Heenan, R. K., 1999, "Small-Angle Neutron Scattering and Fluorescence Studies of Mixed Surfactants with Dodecyl Tails," *Journal of Colloid and Interface Science*, 215(1), pp. 114-123.
- [161] Mears, S. J., Cosgrove, T., Obey, T., Thompson, L., and Howell, I., 1998, "Dynamic Light Scattering and Small-Angle Neutron Scattering Studies on the Poly(ethylene oxide)/Sodium Dodecyl Sulfate/Polystyrene Latex System," *Langmuir*, 14(18), pp. 4997-5003.
- [162] Hirai, M., Hirai, R. K., Iwase, H., Arai, S., Mitsuya, S., Takeda, T., Seto, H., and Nagao, M., 1999, "Dynamics of w/o AOT microemulsions studied by neutron spin echo," *Journal of Physics and Chemistry of Solids*, 60(8-9), pp. 1359-1361.

- [163] Hammouda, B., 2010, "SANS from polymers—review of the recent literature," *Journal of Macromolecular Science*, Part C: Polymer Reviews, 50(1), pp. 14-39.
- [164] Hammouda, B. K., S.; Glinka, C.J., 1993, "Small angle neutron scattering at the National Institute of Standards and Technology " *Journal of Research of NIST*, 98(1), pp. 31-46.
- [165] Marszalek, J., Pojman, J. A., and Page, K. A., 2008, "Neutron scattering study of the structural change induced by photopolymerization of AOT/D<sub>2</sub>O/dodecyl acrylate inverse microemulsions," *Langmuir*, 24(23), pp. 13694-13700.
- [166] Pu, H., and Jiang, F., 2005, "Towards high sedimentation stability: magnetorheological fluids based on CNT/Fe<sub>3</sub>O<sub>4</sub> nanocomposites," *Nanotechnology*, 16(9), p. 1486.
- [167] Han, Z., 2008, "Nanofluids with enhanced thermal transport properties."
- [168] Sastry, N., Thummar, A., and Punjabi, S., 2013, "Mixed Micelles of Trisiloxane Based Silicone and Hydrocarbon Surfactants Systems in Aqueous Media: Dilute Aqueous Solution Phase Diagrams, Surface Tension Isotherms, Dilute Solution Viscosities, Critical Micelle Concentrations and Application of Regular Solution Theory," *J Surfact Deterg*, 16(6), pp. 829-840.
- [169] Cao, F., and Yang, B., 2014, "The critical micelle concentration determined by the thermal conductivity minimum," Submitted.
- [170] Williams, R., Phillips, J., and Mysels, K., 1955, "The critical micelle concentration of sodium lauryl sulphate at 25 C," *Transactions of the Faraday Society*, 51, pp. 728-737.
- [171] Pérez-Rodríguez, M., Prieto, G., Rega, C., Varela, L. M., Sarmiento, F., and Mosquera, V., 1998, "A comparative study of the determination of the critical micelle concentration by conductivity and dielectric constant measurements," *Langmuir*, 14(16), pp. 4422-4426.
- [172] Dominguez, A., Fernandez, A., Gonzalez, N., Iglesias, E., and Montenegro, L., 1997, "Determination of critical micelle concentration of some surfactants by three techniques," *Journal of Chemical Education*, 74(10), p. 1227.

- [173] Wang, X.-j., Li, X., and Yang, S., 2009, "Influence of pH and SDBS on the Stability and Thermal Conductivity of Nanofluids," *Energy & Fuels*, 23(5), pp. 2684-2689.
- [174] Xie, H., Yu, W., Li, Y., and Chen, L., 2011, "Discussion on the thermal conductivity enhancement of nanofluids," *Nanoscale Res Lett*, 6(1), pp. 1-12.
- [175] Assael, M. J., Chen, C. F., Metaxa, I., and Wakeham, W. A., 2004, "Thermal Conductivity of Suspensions of Carbon Nanotubes in Water," *Int J Thermophys*, 25(4), pp. 971-985.
- [176] Seifert, G., Patzlaff, T., and Graener, H., 2002, "Size Dependent Ultrafast Cooling of Water Droplets in Microemulsions by Picosecond Infrared Spectroscopy," *Physical Review Letters*, 88(14), p. 147402.
- [177] Deàk, J. C., Pang, Y., Sechler, T. D., Wang, Z., and Dlott, D. D., 2004, "Vibrational Energy Transfer Across a Reverse Micelle Surfactant Layer," *Science*, 306(5695), pp. 473-476.
- [178] Sigma-Aldrich, <http://www.sigmaaldrich.com/>.
- [179] Hammouda, B., 2010, "A new Guinier-Porod model," *Journal of Applied Crystallography*, 43(4), pp. 716-719.
- [180] Xu, J., Yang, B., and Hammouda, B., "Thermophysical properties and pool boiling characteristics of water in polyalphaolefin nanoemulsion fluids," *Proc. Proceedings of ASME Micro/Nanoscale Heat and Mass Transfer International Conference 2012: ASME*.
- [181] Nan, C.-W., Birringer, R., Clarke, D. R., and Gleiter, H., 1997, "Effective thermal conductivity of particulate composites with interfacial thermal resistance," *Journal of Applied Physics*, 81(10), pp. 6692-6699.
- [182] Sarmiento, F., del Rio, J. M., Prieto, G., Attwood, D., Jones, M. N., and Mosquera, V., 1995, "Thermodynamics of Micelle Formation of Chlorhexidine Digluconate," *The Journal of Physical Chemistry*, 99(49), pp. 17628-17631.
- [183] Phillips, J. N., 1955, "The energetics of micelle formation," *Transactions of the Faraday Society*, 51(0), pp. 561-569.

- [184] Matijevic, E., and Pethica, B. A., 1958, "The heats of micelle formation of sodium dodecyl sulphate," *Transactions of the Faraday Society*, 54(0), pp. 587-592.
- [185] Chattopadhyay, S., Uysal, A., Stripe, B., Ha, Y.-g., Marks, T. J., Karapetrova, E. A., and Dutta, P., 2010, "How Water Meets a Very Hydrophobic Surface," *Physical Review Letters*, 105(3), p. 037803.
- [186] Mezger, M., Reichert, H., Ocko, B. M., Daillant, J., and Dosch, H., 2011, "Comment on "How Water Meets a Very Hydrophobic Surface"," *Physical Review Letters*, 107(24), p. 249801.
- [187] Cringus, D., Bakulin, A., Lindner, J., Vöhringer, P., Pshenichnikov, M. S., and Wiersma, D. A., 2007, "Ultrafast Energy Transfer in Water–AOT Reverse Micelles," *The Journal of Physical Chemistry B*, 111(51), pp. 14193-14207.
- [188] Levinger, N. E., 2002, "Water in Confinement," *Science*, 298(5599), pp. 1722-1723.
- [189] Schoen, P. A. E., Michel, B., Curioni, A., and Poulikakos, D., 2009, "Hydrogen-bond enhanced thermal energy transport at functionalized, hydrophobic and hydrophilic silica–water interfaces," *Chem. Phys. Lett.*, 476(4–6), pp. 271-276.
- [190] Hu, M., Michel, B., and Poulikakos, D., 2011, "Surface functionalization mechanisms of enhancing heat transfer at solid-liquid interfaces," *Journal of Heat Transfer*, 133, pp. 082401-082401.
- [191] Hu, M., Goicochea, J. V., Michel, B., and Poulikakos, D., 2009, "Water Nanoconfinement Induced Thermal Enhancement at Hydrophilic Quartz Interfaces," *Nano Letters*, 10(1), pp. 279-285.
- [192] Chandra, D., Chellappa, R., and Chien, W. M., 2005, "Thermodynamic assessment of binary solid-state thermal storage materials," *Journal of Physics and Chemistry of Solids*, 66(2-4), pp. 235-240.
- [193] Wang, X. W., Lu, E. R., Lin, W. X., Liu, T., Shi, Z. S., Tang, R. S., and Wang, C. Z., 2000, "Heat storage performance of the binary systems neopentyl glycol/pentaerythritol and neopentyl

- glycol/trihydroxy methyl-aminomethane as solid-solid phase change materials," *Energy Conversion and Management*, 41(2), pp. 129-134.
- [194] Zhang, Z.-Y., and Xu, Y.-P., 2001, "Measurement of the Thermal Conductivities of Pentaerythritol, 1,1,1-Tris(hydroxymethyl)ethane, and Their Mixture in the Temperature Range from 20 °C to 200 °C," *Journal of Chemical & Engineering Data*, 46(4), pp. 888-890.
- [195] Sharma, S. D., Kitano, H., and Sagara, K., 2004, "Phase change materials for low temperature solar thermal applications," *Res. Rep. Fac. Eng. Mie Univ*, 29, pp. 31-64.
- [196] Zhao, C. Y., and Zhang, G. H., 2011, "Review on microencapsulated phase change materials (MEPCMs): Fabrication, characterization and applications," *Renew. Sust. Energ. Rev.*, 15(8), pp. 3813-3832.
- [197] Wang, J.-X., Wang, Z.-H., Chen, J.-F., and Yun, J., 2008, "Direct encapsulation of water-soluble drug into silica microcapsules for sustained release applications," *Materials Research Bulletin*, 43(12), pp. 3374-3381.
- [198] Almeida, R. M., and Pantano, C. G., 1990, "STRUCTURAL INVESTIGATION OF SILICA-GEL FILMS BY INFRARED-SPECTROSCOPY," *Journal of Applied Physics*, 68(8), pp. 4225-4232.
- [199] "NIST Chemistry WebBook," <http://webbook.nist.gov/>.
- [200] CHEN, H.-s., SUN, Z.-y., and SHAO, J.-c., 2011, "Investigation on FT-IR Spectroscopy for Eight Different Sources of SiO<sub>2</sub> [J]," *Bulletin of the Chinese Ceramic Society*, 4, p. 040.
- [201] Ibrahim, M., Alaam, M., El-Haes, H., Jalbout, A. F., and Leon, A. d., 2006, "Analysis of the structure and vibrational spectra of glucose and fructose," *Ecletica quimica*, 31(3), pp. 15-21.
- [202] Griffiths, P. R., and De Haseth, J. A., 2007, *Fourier transform infrared spectrometry*, John Wiley & Sons.
- [203] Divi, S., Chellappa, R., and Chandra, D., 2006, "Heat capacity measurement of organic thermal energy storage materials," *Journal of Chemical Thermodynamics*, 38(11), pp. 1312-1326.

- [204] Santiso, E., and Firoozabadi, A., 2006, "Curvature dependency of surface tension in multicomponent systems," *Aiche J.*, 52(1), pp. 311-322.
- [205] Gibout, S., Jamil, A., Kousksou, T., Zeraoui, Y., and Castaing-Lasvignottes, J., 2007, "Experimental determination of the nucleation probability in emulsions," *Thermochimica Acta*, 454(1), pp. 57-63.
- [206] Cao, F., and Yang, B., 2014, "Supercooling suppression of microencapsulated phase change materials by optimizing shell composition and structure," *Appl. Energy*, 113(0), pp. 1512-1518.
- [207] 2002, "Synfluid PAO Databook," Chevron Phillips Chemical Company LP.
- [208] Diaconu, B. M., Varga, S., and Oliveira, A. C., 2010, "Experimental assessment of heat storage properties and heat transfer characteristics of a phase change material slurry for air conditioning applications," *Appl. Energy*, 87(2), pp. 620-628.
- [209] Mehling, H., and Cabeza, L. F., 2008, *Heat and Cold Storage with PCM: An up to Date Introduction into Basics and Applications*, Springer, Berlin, Germany.
- [210] Xu, B., and Li, Z., 2013, "Paraffin/diatomite composite phase change material incorporated cement-based composite for thermal energy storage," *Appl. Energy*, 105(0), pp. 229-237.
- [211] Kalinowski, P., Lawler, J., Yang, B., and Cao, F., "Heat Transfer Performance of a Phase Change Microcapsule Fluid," *Proc. ASME 2012 3rd Micro/Nanoscale Heat and Mass Transfer International Conference*, ASME, pp. MNHMT2012-75190.
- [212] Chen, Z.-H., Yu, F., Zeng, X.-R., and Zhang, Z.-G., 2012, "Preparation, characterization and thermal properties of nanocapsules containing phase change material n-dodecanol by miniemulsion polymerization with polymerizable emulsifier," *Appl. Energy*, 91(1), pp. 7-12.
- [213] Rao, Z., Wang, S., and Peng, F., 2012, "Self diffusion of the nano-encapsulated phase change materials: A molecular dynamics study," *Appl. Energy*, 100(0), pp. 303-308.
- [214] Kraack, H., Sirota, E. B., and Deutsch, M., 2000, "Measurements of homogeneous nucleation in normal-alkanes," *J. Chem. Phys.*, 112(15), pp. 6873-6885.

- [215] Yang, R., Xu, H., and Zhang, Y. P., 2003, "Preparation, physical property and thermal physical property of phase change microcapsule slurry and phase change emulsion," *Sol. Energy Mater. Sol. Cells*, 80(4), pp. 405-416.
- [216] Shulkin, A., and Stöver, H. D. H., 2002, "Polymer microcapsules by interfacial polyaddition between styrene-maleic anhydride copolymers and amines," *Journal of Membrane Science*, 209(2), pp. 421-432.
- [217] Ocko, B., Wu, X., Sirota, E., Sinha, S., Gang, O., and Deutsch, M., 1997, "Surface freezing in chain molecules: Normal alkanes," *Physical Review E*, 55(3), p. 3164.
- [218] Coullerez, G., Leonard, D., Lundmark, S., and Mathieu, H. J., 2000, "XPS and ToF-SIMS study of freeze-dried and thermally cured melamine-formaldehyde resins of different molar ratios," *Surface and Interface Analysis*, 29(7), pp. 431-443.
- [219] He, P., and Qiao, R., 2008, "Self-consistent fluctuating hydrodynamics simulations of thermal transport in nanoparticle suspensions," *Journal of Applied Physics*, 103, p. 094305.
- [220] Sirota, E. B., and Herhold, A. B., 2000, "Transient rotator phase induced nucleation in n-alkane melts," *Polymer*, 41(25), pp. 8781-8789.
- [221] Wu, X. Z., Ocko, B. M., Sirota, E. B., Sinha, S. K., Deutsch, M., Cao, B. H., and Kim, M. W., 1993, "SURFACE-TENSION MEASUREMENTS OF SURFACE FREEZING IN LIQUID NORMAL-ALKANES," *Science*, 261(5124), pp. 1018-1021.
- [222] Luo, W.-j., Yang, W., Jiang, S., Feng, J.-m., and Yang, M.-b., 2007, "Microencapsulation of decabromodiphenyl ether by in situ polymerization: Preparation and characterization," *Polymer Degradation and Stability*, 92(7), pp. 1359-1364.
- [223] Xu, C., Zhou, R., Chen, H., Hou, X., Liu, G., and Liu, Y., 2014, "Silver-coated glass fibers prepared by a simple electroless plating technique," *J Mater Sci: Mater Electron*, pp. 1-5.
- [224] Bao, Y., Lai, C., Zhu, Z., Fong, H., and Jiang, C., 2013, "SERS-active silver nanoparticles on electrospun nanofibers facilitated via oxygen plasma etching," *RSC Advances*, 3(23), pp. 8998-9004.

- [225] Montazer, M., Alimohammadi, F., Shamei, A., and Rahimi, M. K., 2012, "In situ synthesis of nano silver on cotton using Tollens' reagent," *Carbohydrate Polymers*, 87(2), pp. 1706-1712.
- [226] Kalinowski, P., Lawler, J., Yang, B., and Cao, F., "Heat Transfer Performance of a Phase Change Microcapsule Fluid," *Proc. ASME 2012 Third International Conference on Micro/Nanoscale Heat and Mass Transfer*, American Society of Mechanical Engineers, pp. 235-243.
- [227] Wang, J., Carson, J. K., North, M. F., and Cleland, D. J., 2006, "A new approach to modelling the effective thermal conductivity of heterogeneous materials," *International Journal of Heat and Mass Transfer*, 49(17-18), pp. 3075-3083.
- [228] Wang, J. J., Zheng, R. T., Gao, J. W., and Chen, G., 2012, "Heat conduction mechanisms in nanofluids and suspensions," *Nano Today*, 7, pp. 124-136.
- [229] Han, Z. H., Cao, F. Y., and Yang, B., 2008, "Synthesis and thermal characterization of phase-changeable indium/polyalphaolefin nanofluids," *Applied Physics Letters*, 92(24), pp. -.
- [230] Fan, J., and Wang, L. Q., 2010, "Constructal design of nanofluids," *International Journal Of Heat And Mass Transfer*, 53, pp. 4238-4247.
- [231] Lundgren, T. S., Sparrow, E. M., and Starr, J. B., 1964, "Pressure Drop Due to the Entrance Region in Ducts of Arbitrary Cross Section," *Journal of Fluids Engineering*, 86(3), pp. 620-626.
- [232] Dames, C., 2013, "Measuring the thermal conductivity of thin films: 3 omega and related electrothermal methods," *Annual Review of Heat Transfer*, 16(16).
- [233] Wang, H., and Sen, M., 2009, "Analysis of the 3-omega method for thermal conductivity measurement," *International Journal of Heat and Mass Transfer*, 52(7), pp. 2102-2109.
- [234] Cahill, D. G., 1990, "Thermal conductivity measurement from 30 to 750 K: the 3 $\omega$  method," *Review of Scientific Instruments*, 61(2), pp. 802-808.
- [235] Höhne, G., Hemminger, W., and Flammersheim, H.-J., 2003, *Differential scanning calorimetry*, Springer.

- [236] Freire, E., 1995, "Differential scanning calorimetry," Protein stability and folding, Springer, pp. 191-218.
- [237] Nielsen, L. E., 1973, "Thermal conductivity of particulate - filled polymers," J. Appl. Polym. Sci., 17(12), pp. 3819-3820.
- [238] Maxwell, J. C., 1881, A treatise on electricity and magnetism, Clarendon press.
- [239] Vikas, S., and Vikas, T., 2010, "The role of straining and morphology in thermal conductivity of a set of Si-Ge superlattices and biomimetic Si-Ge nanocomposites," Journal of Physics D: Applied Physics, 43(13), p. 135401.
- [240] Hashin, Z., and Shtrikman, S., 1962, "A variational approach to the theory of the effective magnetic permeability of multiphase materials," Journal of applied Physics, 33(10), pp. 3125-3131.
- [241] Keblinski, P., Prasher, R., and Eapen, J., 2008, "Thermal conductance of nanofluids: is the controversy over?," J Nanopart Res, 10(7), pp. 1089-1097.